Report –

ESTIMATES OF LAND SUBSIDENCE IN GMA 15 BASED ON GROUND SURFACE ELEVATION DATA AND MODEL RESULTS

Estimated Land Subsidence* (feet)

Prepared For:

Calhoun County GCD
Coastal Bend GCD
Coastal Plains GCD
Pecan Valley GCD
Refugio GCD
Texana GCD
Victoria County GCD

Prepared By:

GEOSCIENCE & ENGINEERING SOLUTIONS
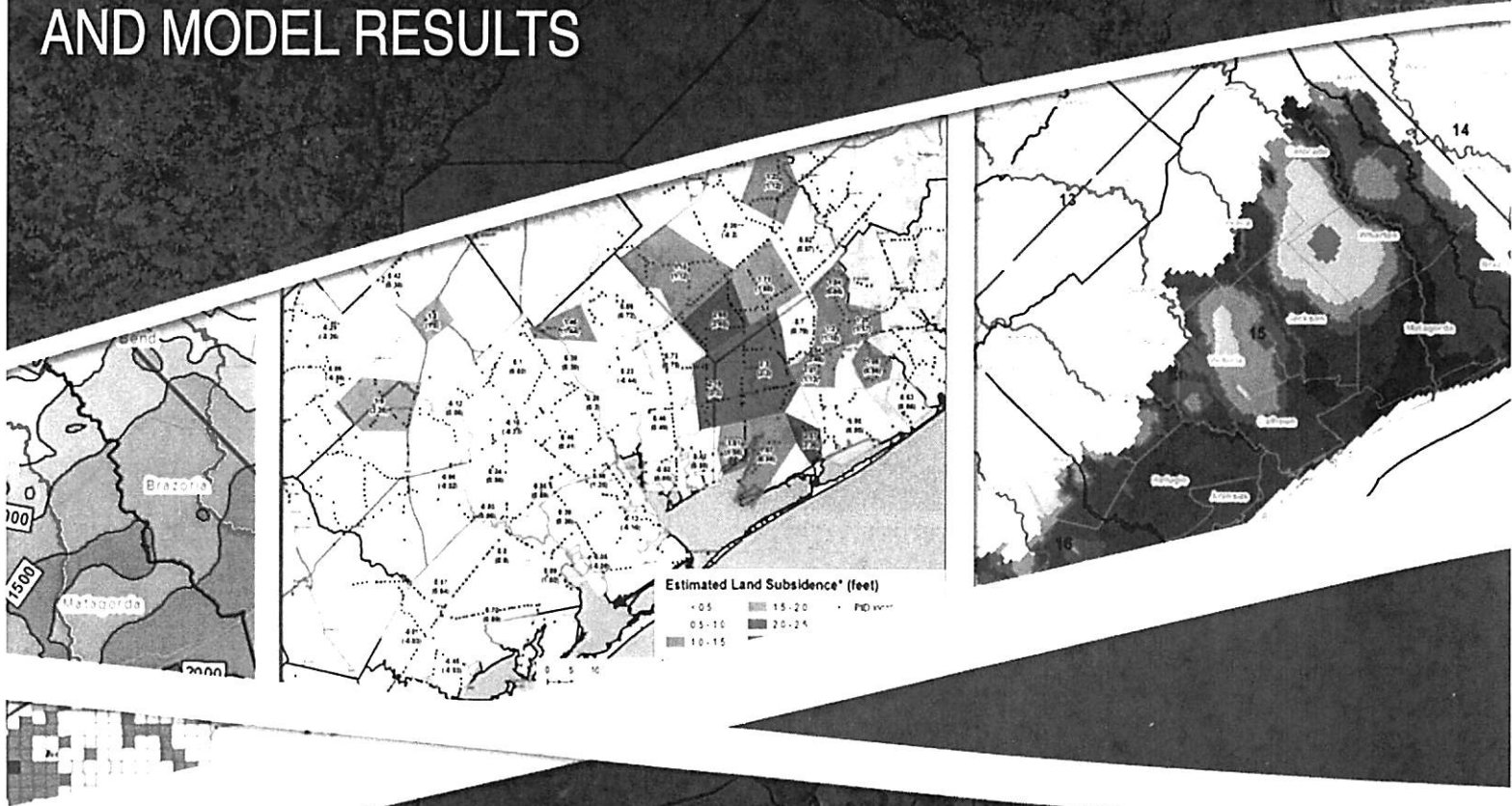
Steven Young, PhD, PE, PG

February 2016

ESTIMATES OF LAND SUBSIDENCE IN GMA 15 BASED ON GROUND SURFACE ELEVATION DATA AND MODEL RESULTS

Prepared for:

Calhoun County GCD
Coastal Bend GCD
Coastal Plains GCD
Pecan Valley GCD
Refugio GCD
Texana GCD
Victoria County GCD

Prepared by:

INTERA
GEOSCIENCE & ENGINEERING SOLUTIONS

1812 Centre Creek Drive Suite 300
Austin, Texas 78754
Steven C. Young

February 2016

EXECUTIVE SUMMARY

Land-surface subsidence is caused both by natural compression of subsurface earth materials and anthropogenic withdrawals of subsurface fluids, gases, and minerals (groundwater, oil, gas, sulfur, and salt). Land subsidence is a potentially important issue associated with the management of groundwater along the Gulf Coast. This report addresses a wide range of issues associated with land subsidence along the Texas Gulf Coast, with an emphasis on hydrogeological conditions in Groundwater Management Area (GMA) 15. The report accomplishes the following five goals.

1.) <u>Describe the physics and mechanics associated with land subsidence.</u> The report explains the concepts and terminology associated with the physics and mechanics that can cause land subsidence as a result of groundwater pumping. These concepts are used to explain the equations used by the groundwater code MODFLOW to simulate land subsidence. The report overviews the development and application of the Houston Area Groundwater Model (HAGM) and the Lower Colorado River Basin (LCRB) model to predict land subsidence in GMA 14 and 15, with an emphasis on the former model.

2.) <u>Conduct a literature review of land subsidence reports in GMA 15.</u> The report summarizes the land subsidence data by county from state water reports, and from several reports that address subsidence along the Texas Gulf Coast. Key limitations of these studies are the lack of locations with repeated measurements of ground surface elevation, and a lack of ground surface elevations measured after 1973. Despite these limitations, the literature review provides ample evidence that land subsidence has occurred across most of the counties within GMA 15. Prior to 1973, very few areas in GMA 15 had land subsidence greater than one foot, and no areas had more than two feet of land subsidence. The literature review also provides considerable data that tie oil and gas production to land subsidence. Where such land subsidence has occurred, the areal extent of the land subsidence appears to be limited to the footprint of the oil field and therefore typically affects only a few square miles.

3.) <u>Estimate historical land subsidence in seven counties in GMA 15.</u> The report presents ground surface elevation data from National Geodectic Survey (NGS) benchmarks called Permanent Identifiers (PIDs), old topographic maps, and LIght and raDAR (LIDAR) data from seven counties in GMA 15. The PID data provide ground surface elevations at 1,700 point locations prior to 1950. The topographic maps cover approximately 2,150 square miles and were constructed between 1950 and 1960. To extract point location data from the topographic maps, the maps were digitized and converted to Geographic Information System (GIS) files. The LIDAR data cover approximately 2,500 square miles and were collected after 2006. The joint analysis of these three data sets support the following conclusions:

   ▪ The LIDAR and PID data indicate that DeWitt, Jackson, Matagorda, Refugio, Victoria, and Wharton counties have experienced at least 2 ft of land subsidence, and Calhoun County has experienced at least 1.5 ft of land subsidence.

Estimates of Land Subsidence in GMA 15
Based on Ground Surface Elevation Data
and Models   ES-i   February 3, 2016

INTERA

- The LIDAR and topographic map data indicate that Calhoun, DeWitt, Jackson, Matagorda, Refugio, Victoria, and Wharton counties have experienced at least 2 ft of land subsidence since 1950.

- A joint analysis of the PID data, topographic map data, and LIDAR data indicates that more than two feet of average subsidence has occurred across about 100 square miles covering southwest Wharton, southeast Jackson, and northwest Matagorda counties.

4.) <u>Develop and Apply an Approach for Performing Scoping Calculations for Land Subsidence.</u> An approach was developed to perform scoping calculations for how much land subsidence will occur in response to drawdowns in the aquifers. The approach was based on solving equations similar to those used by the groundwater code MODFLOW and is defined below.

$$\Delta b = \Delta d * \alpha_{eff} * C_t$$

Where:

Δb = Amount that the aquifer thickness has compacted

Δd = Amount of drawdown in the aquifer since predevelopment

α_{eff} = Effective compressibility coefficient for clays in the aquifer

C_t = Total thickness of the clay units in the aquifer

The approach was used to predict existing and future land subsidence at 14 sites in GMA 15. To solve the equation, drawdown was extracted from a GMA 15 groundwater availability model run. Clay thicknesses were extracted from clay thickness maps developed using a Texas Water Development Board (TWDB) lithologic database. The value for the effective compressibility was based on research performed by the United States Geological Survey (USGS) in the Houston area. For the 14 sites in GMA 15, the calculated land subsidence ranges from 0.1 foot to 3.2 ft from 1940 to 2000. The predicted land subsidence values from the scoping calculations at the 14 locations were compared to the calculated land subsidence values for 2006 based on field measured data (PID data, topographic map data, and LIDAR data). The scoping calculations are consistent and in agreement with the field measured values.

5.) <u>Review of options for monitoring subsidence.</u> The report describes the different types of land surface monitoring that have occurred over time in the Harris-Galveston region. Over the last few decades, borehole extensometers have provided excellent subsidence data, but high cost prohibits their extensive use. Similarly, releveling of survey benchmarks is a reliable but an expensive approach. The most cost-efficient approach being used in the Harris-Galveston area is use of mobile global positioning stations referred to as Port-A-Measure (PAM) units. A PAM unit includes a trailer, its own power supply, and a cellular phone. The PAM units use dual-frequency, full-wavelength GPS instruments (with geodetic antennas) to collect data that provide daily land subsidence measurements with a vertical accuracy of "plus or minus" one centimeter.

Estimates of Land Subsidence in GMA 15
Based on Ground Surface Elevation Data
and Models   ES-ii   February 3, 2016

≋INTERA

TABLE OF CONTENTS

Estimates of Land Subsidence in GMA 15
Based on Ground Surface Elevation Data
and Models   i   February 3, 2016

LIST OF TABLES

Estimates of Land Subsidence in GMA 15
Based on Ground Surface Elevation Data
and Models   ii   February 3, 2016

LIST OF FIGURES

Estimates of Land Subsidence in GMA 15
Based on Ground Surface Elevation Data
and Models   iii   February 3, 2016

Estimates of Land Subsidence in GMA 15
Based on Ground Surface Elevation Data
and Models   iv   February 3, 2016

LIST OF APPENDICES

Estimates of Land Subsidence in GMA 15
Based on Ground Surface Elevation Data
and Models   v   February 3, 2016

ACRONYMS AND ABBREVIATIONS

AFY   acre-feet per year

cm   centimeter(s)

CORS   Continuously Operating Reference Stations

CV   coefficient of variation

DEM   Digital Elevation Model

DFC   Desired Future Condition

ft   feet

ft^{-1} per foot

GAM   Groundwater Availability Model

GCD   Groundwater Conservation District

GIS   Geographic Information System

GMA   Groundwater Management Area

GPS   Global Positioning System

HAGM   Houston Area Groundwater Model (HAGM)

HGSD   Harris-Galveston Subsidence District

IBS   Interbed-Storage

INTERA   INTERA Incorporated

km   kilometer

LCRB   Lower Colorado River Basin

LIDAR   LIght and raDAR

LSWP   Lower Colorado River Authority – San Antonio Water Project

m   meter(s)

$mm\ yr^{-1}$ millimeters per year

N   Newtons

NGS   National Geodetic Survey

NOAA   National Oceanic and Atmospheric Administration

NOS   National Ocean Service

Estimates of Land Subsidence in GMA 15
Based on Ground Surface Elevation Data
and Models   vi   February 3, 2016

ACRONYMS AND ABBREVIATIONS (CONT.)

PAM	Port-A-Measure
PIDS	Permanent Identifiers
SUB	Subsidence (package)
ton/ft^2	ton per foot squared
TNRIS	Texas Natural Resource Information System
TWDB	Texas Water Development Board
USCGS	United States Coast and Geodetic Survey
USGS	United States Geological Survey

Estimates of Land Subsidence in GMA 15
Based on Ground Surface Elevation Data
and Models   vii   February 3, 2016

1.0   INTRODUCTION

Along the Texas Gulf Coast Aquifer, land subsidence is a potentially important issue associated with the management of groundwater. In Harris County, the pumping of groundwater has caused the land surface to subside more than three feet across most of the county and more than nine feet across the southeast part of the county. To help prevent land subsidence in the Gulf Coast, the Houston-Galveston Subsidence District was created in 1975, and the Fort Bend Subsidence District was created in 1989. Both of these districts have conducted hydrogeological studies, including extensive groundwater and subsidence monitoring. Information from these studies has been used to develop groundwater availability models (GAMs) for Groundwater Management Area (GMA) 14 (Kasmarek, 2012; Kasmarek and Robinson, 2004) that have the capability to simulate land subsidence in response to groundwater pumping.

1.1   Background Information

Figure 1-1 shows the groundwater conservation districts (GCDs) and subsidence districts that manage groundwater resources along the Texas Gulf Coast. For the purpose of regional joint planning, these entities are grouped into three GMAs: GMA 14, GMA 15, and GMA 16, which are located in the northern, central, and southern region of the Texas Gulf Coast, respectively.

In summer 2014, the Texas Water Development Board (TWDB) began development of a GAM for both GMA 15 and GMA 16. Based on the information presented by the TWDB in a stakeholder forum in June 2014 (Ridgeway and Goswami, 2014), the GAM will be developed in two phases. The first phase is the development of a conceptual model for the groundwater flow system. The second phase is the development of a computer flow model based on the conceptual groundwater flow system. Reports associated with both phases will be available for review and comment by the public.

During the June 2014 stakeholder meeting, the TWDB requested hydrogeologic data and feedback from stakeholders. Because of a lack of land subsidence data in GMA 15, several GCDs hired INTERA Incorporated (INTERA) to assemble historical measurements of ground surface elevations and to estimate land subsidence based on changes in the ground surface elevation over time. These GCDs are the Calhoun County GCD, Coastal Bend GCD, Coastal Plains GCD, Pecan Valley GCD, Texana GCD, Refugio GCD, and Victoria County GCD.

In April 2015, INTERA presented results (see Appendix A) of their analysis of ground surface elevation data to the TWDB. In June 2015, INTERA provided the TWDB with the data used to develop the presentation, except for the information from the Texas Natural Resources Information System (TNRIS). The TWDB said that they would acquire the TNRIS information directly from TNRIS.

INTERA

1.2   Report Objectives

This report documents the April 2015 meeting with the TWDB. The report includes the supporting data, data sources and analyses performed to develop the information and figures associated with the TWDB meeting presentation included as Appendix A. In addition, the report provides a conceptual framework for the aquifer conditions and geotechnical processes that are responsible for land subsidence. Specific report objectives are to:

- Describe the physics and mechanics associated with land subsidence.

- Conduct a literature review of land subsidence reports in GMA 15.

- Develop historical ground surface elevation data using the National Geodectic Survey (NGS) network of Permanent Identifiers (PIDS), old topographic maps, and LIght and raDAR (LIDAR) surveys for selected counties in GMA 15.

- Develop estimates of land subsidence based on changes in measured ground surface elevation over time for selected counties in GMA 15.

- Review and discuss approaches for modeling land subsidence.

- Develop an approach for performing scoping calculations to estimate land subsidence.

Administrative Boundaries - Gulf Coast

- Groundwater Conservation District (GCD)
- Groundwater Management Area (GMA)
- County Boundary

| 0 | 25 | 50 | 100 |
Miles
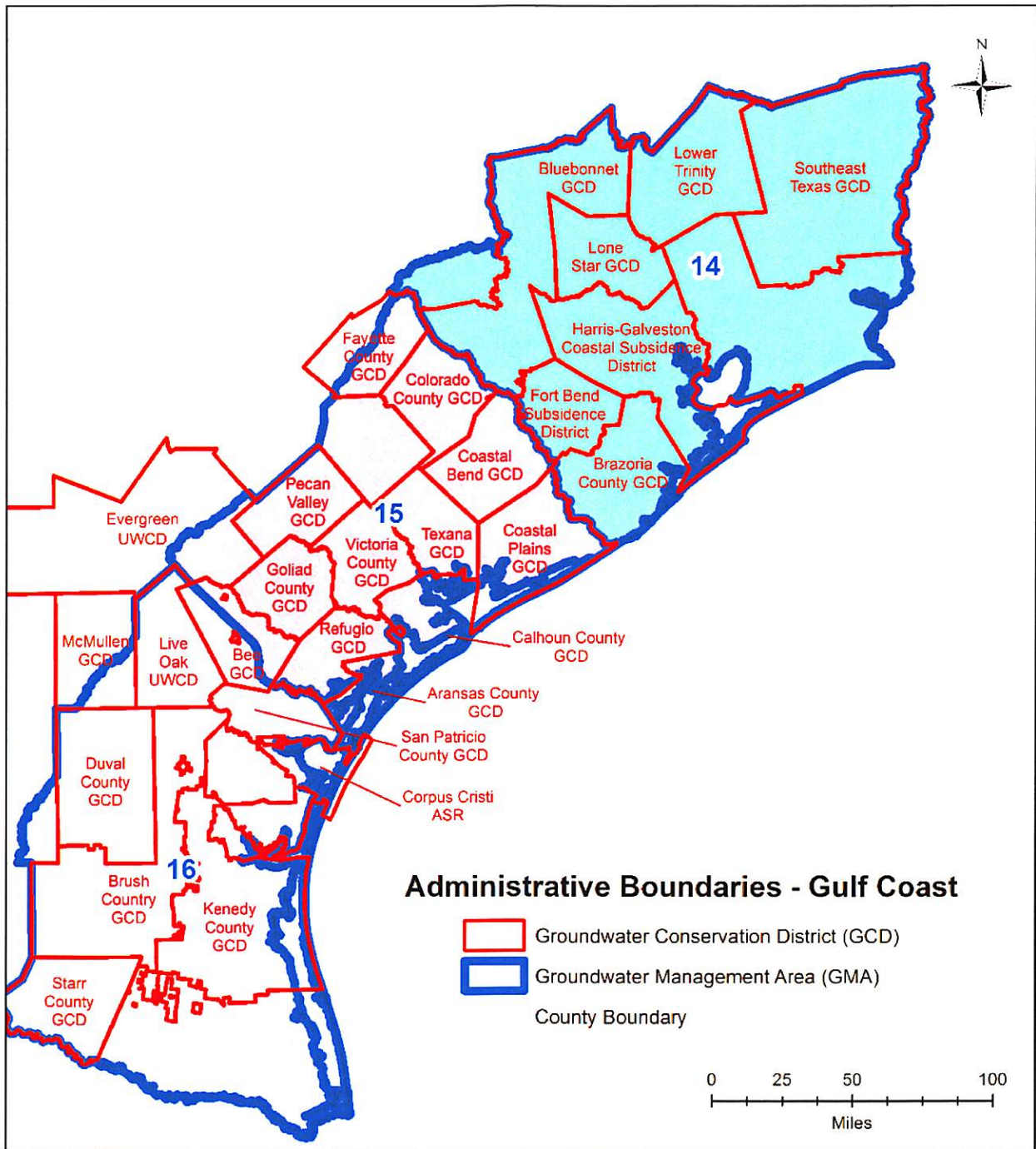
Figure 1-1   Location of Groundwater Conservation Districts, Subsidence Districts, and Groundwater Management Zones in the Texas Gulf Coast

2.0 CONCEPTS AND TERMINOLOGY

Land-surface subsidence is the lowering or sinking of the land surface in response to removal of subsurface support. Land-surface subsidence is caused both by natural compression of subsurface earth materials and anthropogenic withdrawals of subsurface fluids, gases, and minerals (groundwater, oil, gas, sulfur, and salt). To familiarize the reader with these processes, this section introduces terms and concepts important to understanding land subsidence.

2.1 Effective Stress

Karl Terzaghi (1925; Terzaghi and Peck, 1967) developed the theory for one-dimensional consolidation of clays that has served as the basis for the mathematical equations describing most practical soil mechanics and land subsidence problems for the past half century. This theory commonly is used to estimate the magnitude and rate of settlement or compaction that will occur in aquifers under a given change in load (stress). The change in load can be caused by adding weight on the ground, such as the construction of a large building, or by reducing fluid pore-pressure in an aquifer, such as by pumping groundwater. According to the theory, compaction results from the release of pore water from the stressed deposit. The most compressible deposits are composed primarily of clays, and the least compressible deposits are composed primarily of sand.

In developing his consolidation theory in 1925, Terzaghi introduced the basic principle of effective stress, σ_{eff}, which is defined in **Equation 2-1**.

$$\sigma_{eff} = \sigma_{total} - h_{pore} \qquad \text{(Eq. 2-1)}$$

Where:

σ_{eff} = Effective stress or intergranular stress (effective stress, or pressure, at the grain-to-grain contact points in a deposit)

σ_{total} = Total stress on the deposit (geostatic pressure on the deposit caused by the weight of the overlying water and subsurface material above a deposit)

h_{pore} = Pore-fluid pressure (hydraulic head in the interstitial pores of a deposit)

Figure 2-1 illustrates how the effective stress changes in a clayey aquifer after being pumped. The figure shows the thickness of the clayey aquifer before and after pumping. Before and after pumping, the total stress, or geostatic pressure, on the clayey aquifer is the same. In response to the pore-fluid pressure in the interstitial pores being reduced by pumping, the effective stress on the clay particles in the clayey aquifer has been increased by the same amount of pressure that that pore-fluid has been decreased. For both situations, before and after pumping, the total stress on the clayey aquifer from above is balanced by the pore-fluid pressure and effective stress on the clay particles in the clayey aquifer.

The increase in the effective stress on the clay particles caused by the depressurization of groundwater in the aquifer causes the clay grains to reorient and shift position, which in turn leads to consolidation of the

aquifer. The result of the change in aquifer volume is manifested as subsidence of the land surface as shown in Figure 2-1.

2.2   Compressibility

In 1925, O.E. Meinzer (Meinzer and Hard, 1925) recognized that a confined aquifer (the Dakota Sandstone) was compressed when the hydraulic head was decreased. He stated that the overburden pressure of all deposits above the confined Dakota Aquifer was supported partly by the fluid pressure at the top of the Dakota and partly by the sandstone itself (grain-to-grain load).

This concept of both the fluid and the deposits in an aquifer supporting the overlying weight of the material above is equivalent to the research being performed by Terzaghi (1925) in the same year. During his study of the Dakota Aquifer at Ellendale, North Dakota, Meinzer deduced that the stress that was borne by the grain-to-grain load in the Dakota Aquifer had increased about 50 percent because of the decline of hydraulic head caused by pumping.

Meinzer formulated his concept of effective stress in 1928 in a classic paper (Meinzer, 1928), which discusses the compressibility and elasticity of artesian aquifers in detail. He cited evidence for compressibility and elasticity derived from laboratory tests and from field evidence for confined aquifers and for large artesian basins, notably the Dakota artesian basin. He concluded:

> "...aquifers are apparently all more or less compressible and elastic though they differ widely in the degree and relative importance of these properties. In general the properties of compressibility and elasticity are of the most consequence in aquifers that have low permeability, slow recharge, and high head. In many aquifers these properties are evidently important in supplying water not only by permanent reduction of storage but also by temporary reduction that is replenished when the wells are shut down or during the season of minimum use."

An important consideration regarding how depressurization will affect the compressibility of the aquifer is the distribution of clays and sands within the aquifer. Clays are orders of magnitude more susceptible to compression than sands (Freeze and Cherry, 1979; Domenico and Schwartz, 1990). In fact, the difference between clays and sands is so large that the compressibility of the sands is sometimes ignored in the calculation of land subsidence.

The large difference in compressibility between sands and clays occurs because sands and clays have dissimilar shaped grains and dissimilar grain-to-grain geometry. Whereas sand grains are round-like structures, clay grains are flat-like structures. The difference in shape between sands and clays affects how they consolidate in response to increased effective stress. **Figure 2-2** is a schematic showing how sand grains mechanically compress differently than clay grains. Mechanical compression occurs as a result of slippage and rotation that change the position and orientation of individual grains and does not involve

the actual compression of the individual grains. Because of the plate-like shape, clay grains can pack closer together than sand grains. After compaction, the porosity in sands typically ranges between 0.25 and 0.4, whereas the porosity of clays typically ranges between 0.05 and 0.1 (Revil and others, 2002). At the time of their deposition, clays typically have higher porosities than sands. Therefore, the potential reduction in porosity caused by compressibility from the time of deposition to consolidation is significantly greater for clays than for sands. This is because of the compressibility of clay versus sand.

The compressibility coefficient, α, is a measure of how easily a unit volume of substance can be changed by pressure or, in other words, how easily the density of a substance can be changed by pressure. **Equation 2-2** is a mathematical expression that defines the compressibility coefficient.

$$\alpha = (dv / V) * (1/dp) \hspace{4cm} \text{(Eq. 2-2)}$$

Where:

α = compressibility coefficient
dp = change in pressure (or hydraulic head)
dv = change in volume of sample
V = total volume of sample

To illustrate a calculation of the compressibility coefficient, field data gathered by the United States Geological Survey (USGS) from their field tests at Seabrook, Texas will be used. Gabrysch (1975) reports that from 1964 to 1973, the average change in hydraulic head in the aquifer is 59 feet (ft), the total thickness of the clay in the aquifer is 799 ft, and the measured land subsidence is 1.2 ft. Application of Equation 2-2 produces a compressibility coefficient of 0.0000255 per foot (ft^{-1}) (0.000025 = [1.2 ft /799 ft]*[1/59 ft]). In Standard International units using Newtons (N) as a unit of force, and meters (m) as a unit of distance, the compressibility coefficient of 2.55×10^{-5} ft^{-1} is equivalent to 8.52×10^{-9} m^2/N.

Figure 2-3 shows two pictures of consolidometers, which are used to measure compressibility coefficients of soil samples in the laboratory. Consolidometers provide the means for both applying different pressures on a soil sample, as well as measuring the change of a sample's density at each pressure. As the applied pressure increases, the soil sample should become denser. An important aspect of the consolidometer testing is to allow sufficient time for water to drain from the sample at each of the different pressures so that the soil sample can reach its full consolidation. A standard display of the testing results is to represent changes in density as changes in void space. As the density increases, the void space decreases. A plot of void ratio versus pressure is called a consolidation curve.

Figure 2-4 through **Figure 2-7** are consolidation curves from a consolidometer test performed by the USGS (Gabrysch and Bonnet, 1975) on clay samples obtained at different depths in Seabrook, Texas. The compressibility coefficient, α, is calculated from the slope of the consolidation curve. The variable results and slopes are caused by differences in the sample properties such as sand and clays percentages, types

of clays, depth of burial, consolidation by differences in the sampling, preparation, and testing of the sample. Despite differences among aquifers, consolidation curves for aquifer deposits should have flatter slopes at lower stresses and the steeper slopes at higher stresses. In Figures 2-4 through 2-7, the flatter slopes occur for stresses less than 1 ton per foot squared (ton/ft^2) and steeper slopes occur for stresses greater than 20 ton/ft^2. The stress where the transition occurs between the flatter slopes at lower stresses and the steeper slopes at higher stresses is called the "preconsolidation stress."

2.3   Preconsolidation Stress

If the aquifer had once been under greater stress than it is currently, then the aquifer is considered over consolidated. In principal, preconsolidation stress, σ_{pre}, represents the maximum overburden stress that an aquifer has sustained in the past. Holzer (1981) identified various natural mechanisms that can result in an over consolidated condition in alluvial basins; these mechanisms include removal of overburden by erosion or melting or glaciers, prehistoric ground-water-level declines, desiccation, and diagenesis.

Arthur Casagrande was the first to develop a systemic procedure for determining the preconsolidation stress from a consolidation curve, such as the ones shown in Figures 2-4 through 2.-7. **Figure 2-8** explains the graphical technique developed by Casagrande (1936) to calculate preconsolidation stress. With regard to simulating land subsidence, the preconsolidation stress is typically used to mark where two important changes occur with the compressibility coefficient. One change is with the magnitude of the compressibility coefficient: at stresses less than the preconsolidation stress, the magnitude of the compressibility coefficient is significantly less than for stresses greater than the preconsolidation stress. A second change is with the nature of the consolidation: at stresses less than the preconsolidation stress, the compressibility is reversible but is irreversible at stresses higher than the preconsolidation stress. Reversible consolidation means that, if stress is removed from an aquifer, the aquifer will rebound and return to the ground surface elevation that existed prior to the reversible consolidation. Irreversible consolidation means that the consolidation is permanent.

Hanson (1989) and Hanson and Benedict (1994) state that an accurate estimate of the preconsolidation stress is one of the most important requirements for successful simulation of aquifer-system compaction. In the context of aquifer systems, preconsolidation stress is often not estimated from consolidation curves but rather historical water levels. Often, the preconsolidation stress is represented by the estimates of the lowest groundwater level (hydraulic head), but only after sufficient time is allowed for fluid pressures to equilibrate throughout the aquifer system (Riley, 1969). Under ideal conditions of pressure equilibration for a confined aquifer system where the total stress applied by the overburden is constant, the previous lowest hydraulic head may be taken as a first-order approximation of the preconsolidation stress.
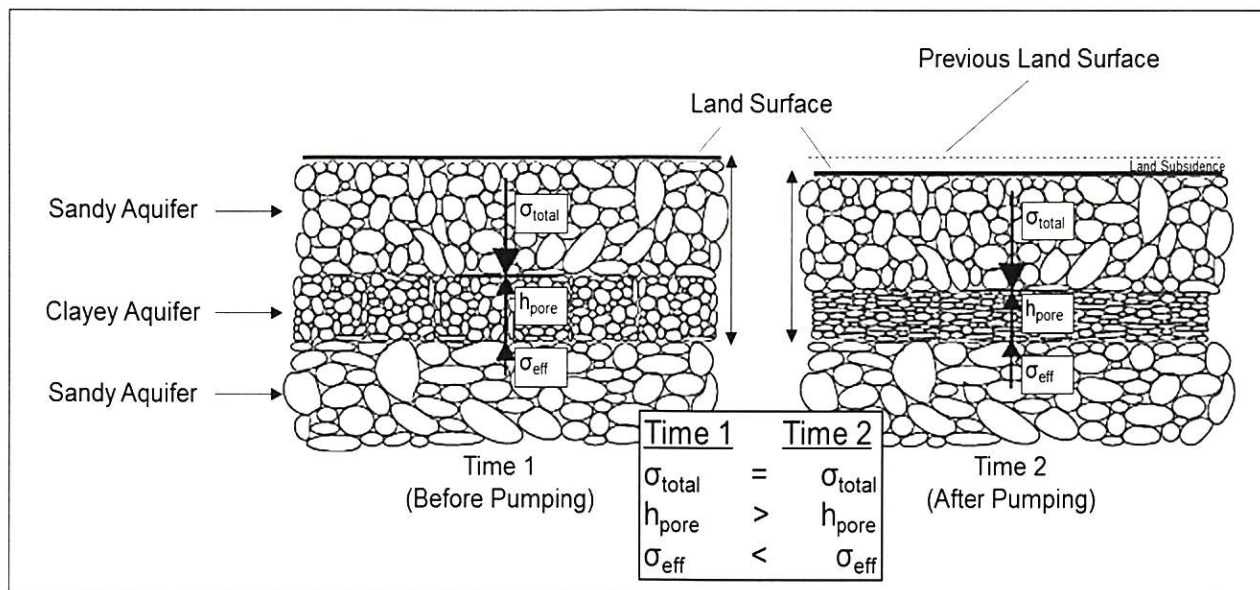
Figure 2-1   Schematic showing increases in effective stress on clay particles in a fine-grained aquifer after pumping and the resulting consolidation of the fine-grained aquifer that causes land subsidence
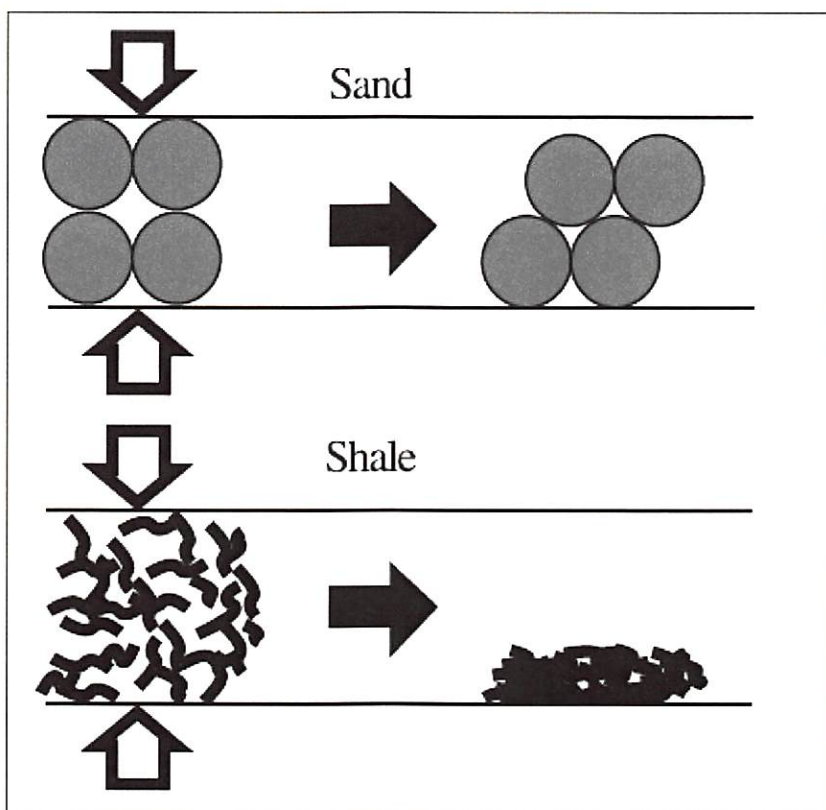
Figure 2-2   Schematic showing the reorientation and shifting of sand grains and shale comprised of clay particles associated with compaction caused by increased effective stress on the grain-grain contacts

Estimates of Land Subsidence in GMA 15
Based on Ground Surface Elevation Data
and Models   15   February 3, 2016
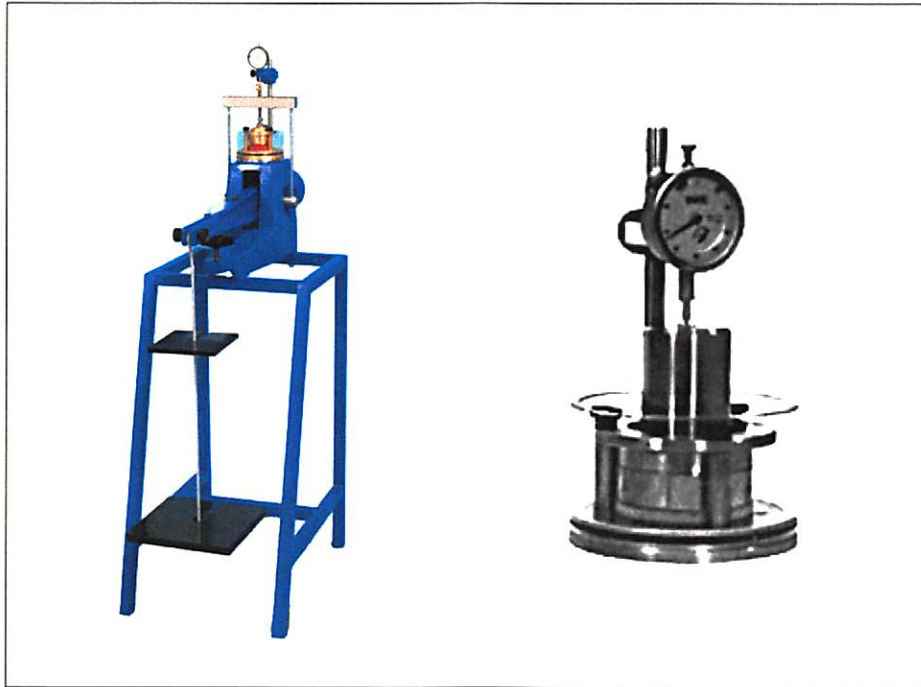
Figure 2-3   Pictures of consolidometers used to perform compressibility tests on soil samples
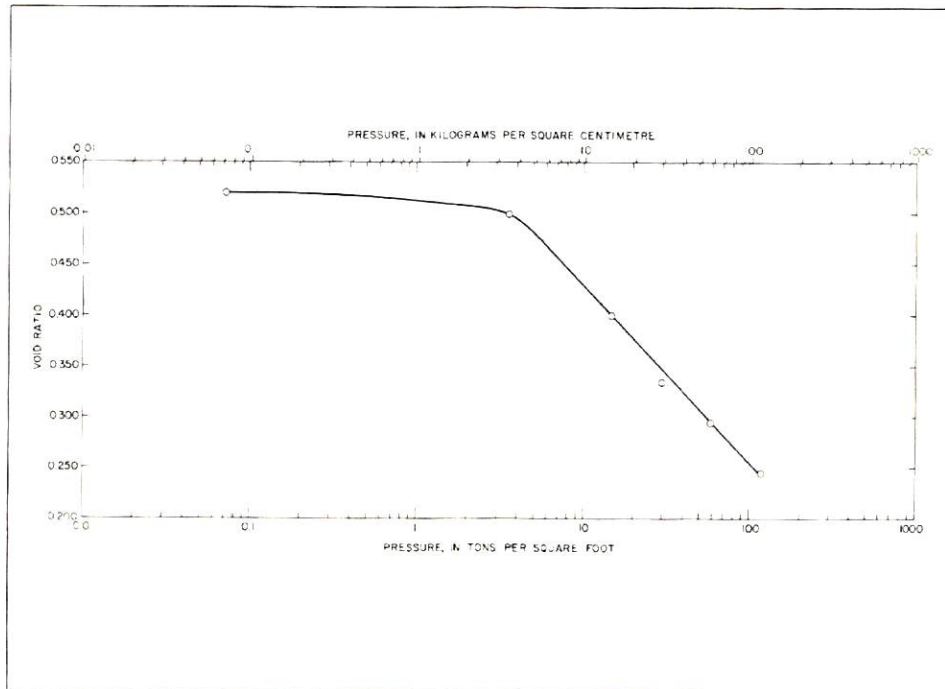
Figure 2-4   Relation between void ratio and applied pressure for clay sample from a depth of 979 ft (298m), well LJ 65-32-627 (USGS, 1975)
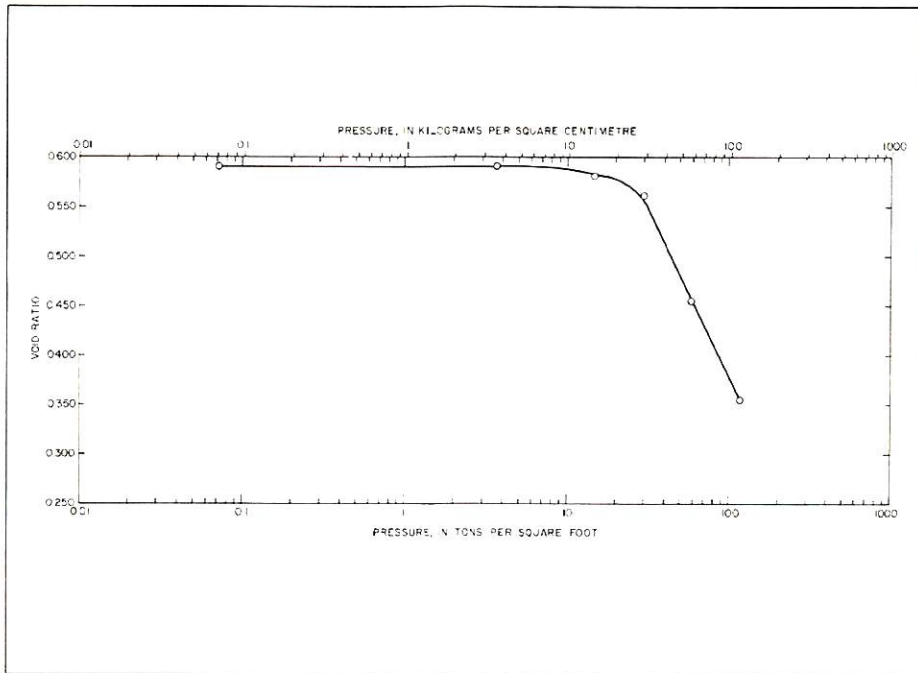
Figure 2-5   Relation between void ratio and applied pressure for clay sample from a depth of 1,023 ft (312m), well LJ 65-32-627 (USGS, 1975)
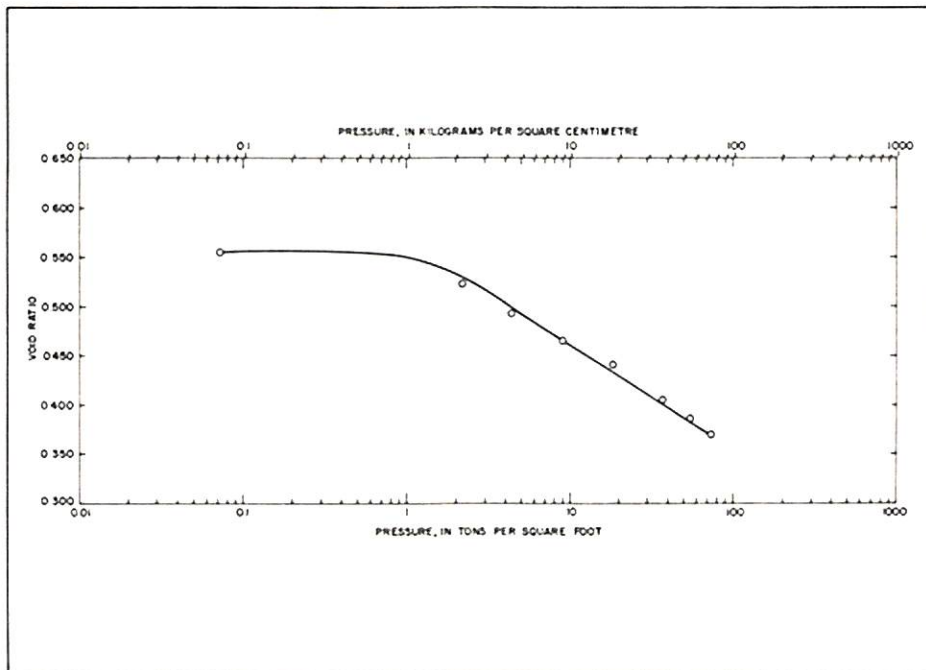
Figure 2-6   Relation between void ratio and applied pressure for clay sample from a depth of 1,059 ft (323m), well LJ 65-32-627 (USGS, 1975)

Estimates of Land Subsidence in GMA 15
Based on Ground Surface Elevation Data
and Models   17   February 3, 2016
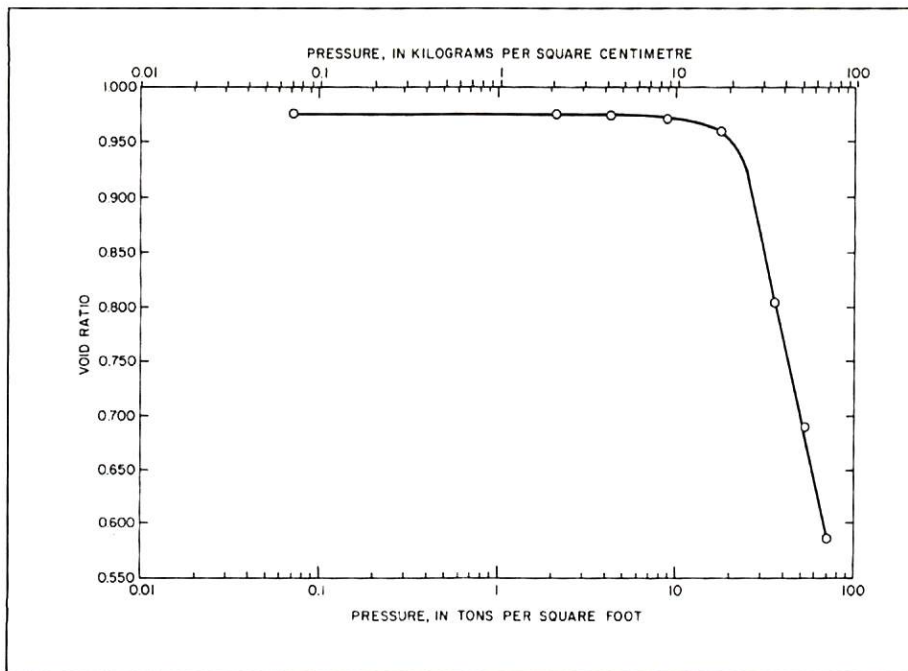
Figure 2-7   Relation between void ratio and applied pressure for clay sample from a depth of 1,250 ft (381m), well LJ 65-32-627 (USGS, 1975)
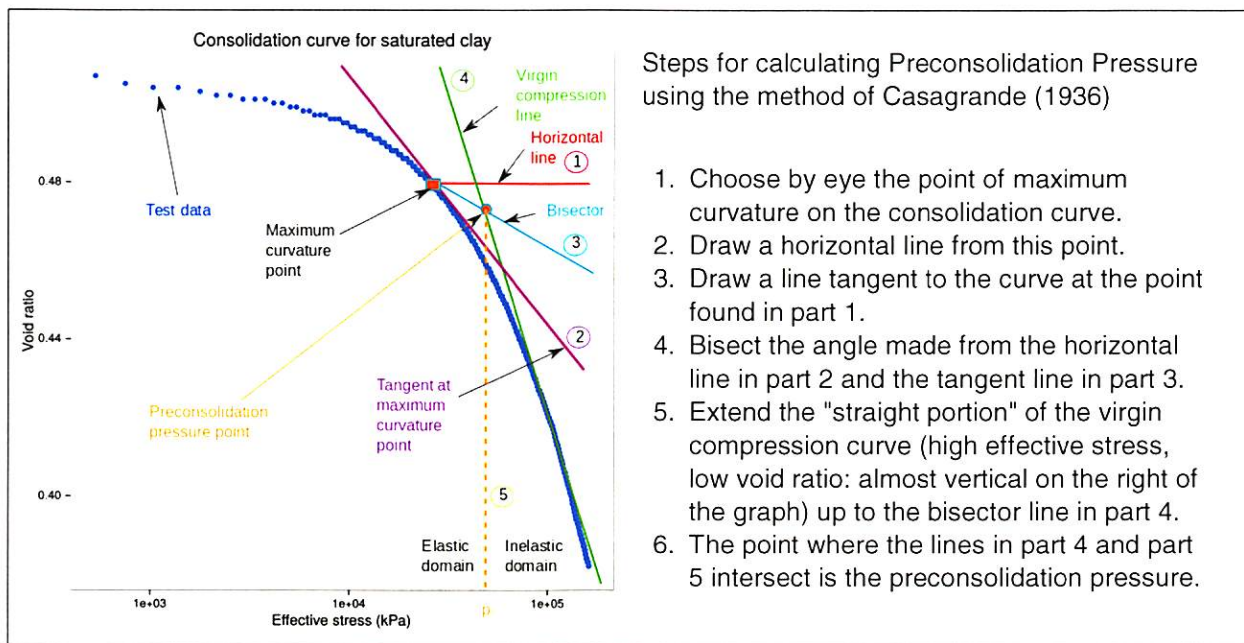
Figure 2-8   Consolidation Curve of void ratio versus Effective Stress that has been Analyzed using the Graphic Approach by Casagrande (1936) to estimate Preconsolidation Pressure (figure from https://en.wikipedia.org/wiki/File:Consol_curve_plain.svg)

3.0 SIMULATED LAND SUBSIDENCE FROM GROUNDWATER PUMPING

The purpose of this section is twofold. One purpose is to provide an overview of the modeling of land subsidence that has occurred in the Texas Gulf Coast. The second purpose is to provide data and results from groundwater models that may be useful to GCDs in GAM 15 to estimate land subsidence.

The section begins with a description of the algorithms used by MODFLOW (McDonald and Harbaugh, 1988) to simulate land subsidence. MODFLOW is the code used by the TWDB for developing GAMs. The previous GAMs developed for GMA 14, 15, and 16 are MODFLOW-based models, and the updated GAM for GMAs 15 and 16 will be a MODFLOW-based model. The section concludes by discussing the key aquifer properties used by the MODFLOW-based models to simulate land subsidence and presenting the simulated land subsidence for the Gulf Coast.

3.1 Capability of MODFLOW to Simulate Land Subsidence

MODFLOW is a groundwater flow code that was developed by the USGS for modeling groundwater in three dimensions. The code has been continually enhanced and expanded by the USGS. The code is the most widely used groundwater code in the United States and is the preferred code for many state and federal agencies. All of the GAMs developed by the TWDB have been built using the MODFLOW code. Among MODFLOW's attractive features is a modular structure that allows it to be modified easily and adapted for a particular application. The first major release of MODFLOW was by McDonald and Harbaugh (1988). To provide MODFLOW with the capability to simulate land subsidence, the USGS developed the Interbed-Storage (IBS) package in 1991 and the Subsidence (SUB) package in 2003. These two packages are described below.

3.1.1 Interbed-Storage Package

The IBS package is based on the principle of effective stress developed by Terzaghi (1925) to calculate land subsidence and was verified using the one-dimensional compaction model developed by Helm (1975). The IBS package calculates storage and compaction changes based on a single or multiple "interbeds" that exists in an aquifer. The term "interbeds" refers to a low permeable deposit (or bed) within a relatively permeable aquifer. **Figure 3-1** is a schematic of interbeds in an aquifer. Leake and Prudic (1991) assume that interbeds are:

- of significantly lower hydraulic conductivity than the surrounding sediments considered to be aquifer material, yet porous and permeable enough to accept or release water in response to head changes in adjacent aquifer material;

- of insufficient lateral extent to be considered a confining bed that separates adjacent aquifers;

- of relatively small thickness in comparison to lateral extent; and

- primarily composed of compressible clay and silt beds from which water flows vertically to adjacent coarse-grained beds.

The IBS package does not support the explicit inclusion of multiple interbeds into an aquifer. Rather, the modeler is required to represent more than a single interbed in an aquifer by using composite values for specific storage, which is developed from the compressibility of the individual interbeds. Leake and Prudic (1991) provide an equation to calculate a composite value for specific storage based on the individual thicknesses and compressibility coefficients of the interbeds.

The IBS package uses **Equation 3-1** to predict land-surface subsidence.

$$\Delta b_A = - \Delta h * \alpha * b \hspace{4cm} \text{(Eq. 3-1)}$$

Where:

Δb_A = Amount that the aquifer thickness has compacted or expanded

Δh = Change in hydraulic head in the aquifer

α = Aquifer compressibility coefficient (calculated from one or more interbeds)

b = Total thickness of the interbed(s)

The IBS requires a modeler to input an elastic (reversible) compressibility coefficient, an inelastic (irreversible) aquifer compressibility coefficient, and a preconsolidation stress for each aquifer. The preconsolidation input is expressed as a hydraulic head. For conditions where the aquifer stress (hydraulic head) is lower than the preconsolidation stress, the IBS package uses the elastic (reversible) compressibility coefficient. For conditions where the aquifer stress (hydraulic head) is greater than the preconsolidation stress, the IBS package uses the inelastic (irreversible) compressibility coefficient.

To demonstrate an application of Equation 3-1, a hypothetical situation is considered. The situation involves 100 ft of drawdown that occurred in an aquifer with 300 ft of clay interbed after the preconsolidation stress has been exceeded. Using an inelastic aquifer compressibility 4×10^{-5} ft^{-1}, the calculated land subsidence is 1.2 ft (100 ft $\cdot$ 4 x 10^{-5} ft^{-1} $\cdot$ 300 ft).

3.1.2 Subsidence Package

The SUB package (Hoffman and others, 2003) improves upon the IBS package (Leake and Prudic, 1991) by providing an option to simulate the delayed dewatering of the thicker fine-grained interbeds in addition to instantaneous dewatering of the relatively thin fine-grained interbeds. A limitation of the IBS package is that it assumes that the drainage from the consolidating interbeds occurs instantaneously and, therefore, is fully realized at the end of every model time step. If the time-delay option is not used in the SUB package, the SUB package will provide identical results to the IBS package.

In aquifers with thick clay layers or clays with low vertical conductivity, the assumption of instantaneous consolidation in response to a reduction in effective stress may not be valid because aquifer compaction is time-dependent. Aquifer compaction does not occur instantaneously with a drop in the hydraulic head because time is required for the groundwater to drain from the clay beds. **Figure 3-2** is a schematic illustrating the drainage of the clay beds into permeable sand beds. Factors that affect the time to reach ultimate compaction include the thickness and hydraulic conductivity of the clay beds. If the expansion of

water is considered small compared to the compressibility of the aquifer matrix, then **Equation 3-2** can be used to estimate the time required for the clays to reach ultimate compaction:

$$\tau \left[\frac{\alpha \left(\frac{b_0}{2} \right)^2}{K_v} \right]$$

(Eq. 3-2)

Where:

τ = Time constant of interbed (day)
α = Specific inelastic storage of interbed (ft^{-1});
b_0 = Thickness of the interbed (ft); and
K_v = Vertical hydraulic conductivity of the interbed.

The time constant, τ, is the time required for 93% of the excess pore pressure to dissipate following an instantaneous change in the pore pressure at the boundaries of the interbed. The upper limit of τ should be compared with the length of the time steps used by MODFLOW to evaluate the validity of the assumption that all of the excess pore pressure is dissipated. If this assumption is not valid, the model results may overestimate storage changes and compaction in early time and underestimate those quantities in later time.

Table 3-1 provides the calculated values of τ for interbeds of different thicknesses and hydraulic conductivities for an assumed value for α of 4.0 x 10^{-5} ft^{-1}, which is a typical value used for the Chicot Aquifer by Kasmarek and Strom (2002) and Kasmarek and Robinson (2004). The vertical hydraulic conductivity values for the clay layers are based on values used to simulate vertical consolidation in the Houston area by McClelland (McClelland Engineering, 1979). Based on the ranges of times in Table 3-1, the instantaneous assumption appears reasonable only for clay lens less than 20 ft thick if the maximum time steps of 365 days are used. Given that numerous clay thicknesses greater than 20 ft have been identified in both GMA 14 and GMA 15 (Young and others, 2010; Young and others, 2012), use of the SUB package with delayed drainage is recommended for modeling land subsidence with a maximum time step of 365 days.

Table 3-1   Calculation of the Time Constant τ (days) for the Interbeds of Various Thickness and Vertical Hydraulic Conductivity

Thickness of Clay Lens	Vertical Hydraulic Conductivity of Clay Lens (ft/day)		
	0.001	0.0001	0.00001
20	4	40	400
40	16	160	1600
60	36	360	3600
80	64	640	6400

3.2   Modeling Land Subsidence in the Texas Gulf Coast Using MODFLOW

This subsection summarizes several of the major hydrogeological studies performed by the USGS and the Harris-Galveston Subsidence District (HGSD) to characterize land subsidence and overviews two MODFLOW-based groundwater models that have been used to simulate land subsidence in the Harris-Galveston area. One of these models is the Houston Area Groundwater Model (HAGM), which was developed by the USGS for the HGSD and currently is the GAM for GMA 14. The other model is the Lower Colorado River Basin (LCRB), which was developed by the Lower Colorado River Authority – San Antonio Water Project (LSWP).

3.2.1   Characterization of Land Subsidence in the Harris-Galveston Region

Since the mid-1950s, the USGS and cooperating agencies have placed an emphasis on collecting and analyzing groundwater-elevation data in the Harris-Galveston Region because of concerns about land subsidence. A historical review of these activities is discussed by Gabrysch (1982), Gabrysch and Coplin (1990), and Gabrysch and Neighbors (2000, 2005). **Figure 3-3** shows a map of land subsidence estimated to have occurred from 1906 to 2000. The map of land subsidence is based on the analysis and integration of many different data sets, which include the following:

- Numerous topographic maps dating back to 1915

- Eight USGS 7.5-minute topographic quadrangles

- 2001 LIDAR data from Harris County

- Repeated ground elevation line and benchmark surveys by the United States Coast and Geodetic Survey (USCGS) and the NGS.

- Data from 13 extensometers at 11 sites, six of which are designed to measure land subsidence

Figure 3-4 illustrates pumping from 1890 to 2004 that has occurred in the Harris-Galveston area shown in **Figure 3-5**. As the population of the area increased and industrialization occurred, groundwater pumping reached about 90 million gallons per day, or 100,818 acre-feet per year (AFY), by 1930 and was somewhat

stable through the years of the Great Depression. From 1935 to 1950, pumping increased dramatically from 100,800 AFY to 336,100 AFY as industrialization occurred in the area bordering Galveston Bay, the population of the area grew dramatically, and irrigation also increased in the area west of Houston. In 1953–1954, Lake Houston was constructed and began providing a supply of surface water, which resulted in a reduction of the rate of growth of groundwater usage from 1950 to 1960. Since the establishment of the HGSD, groundwater usage has decreased in the continuing effort to address land surface subsidence. Surface water usage has increased and is planned to continue increasing in the future as the demand for water in Harris, Galveston, Fort Bend, and Montgomery counties increases.

From the late 1960s to the early 1980s, the USGS performed several detailed investigations in the Harris County region to develop improved methods for measuring and modeling land subsidence (Gabrysch, 1969; Gabrysch and Bonnet, 1975; Gabrysch and Bonnet, 1976a,b; Gabrysch, 1982). The investigations concluded that the following information is required to estimate the impact of groundwater withdrawal on subsidence: (1) the amount of compressible material (i.e., the thickness and frequency of clay material); (2) the change in the aquifer stress (i.e., the amount of drawdown caused by pumping); and (3) the degree of compressibility of the aquifer material (i.e., compressibility coefficient of the clay layers).

Maps of clay thicknesses in the Chicot and Evangeline aquifers used in the development of GAMs for GMA 14 (Kasmarek and Robinson, 2004; and Kasmarek, 2014) are shown in **Figure 3-6** and **Figure 3-7**, respectively. The clay thicknesses are thickest near the coast and thinnest near the aquifer outcrop. In the Harris-Galveston area, clay thicknesses for the Chicot and Evangeline aquifers typically exceed 700 ft and 1,000 ft, respectively. These clay thickness maps are primarily based on Gabrysch (1982) and Strom and others (2003 a,b,c), who relied on interpretations of geophysical logs.

Most of the USGS investigations on measuring the compressibility of clay involved the ten locations shown in **Figure 3-8**. At these sites, the USGS performed the laboratory and field tests necessary to measure the distribution of clay thicknesses, the compressibility of clays, and the groundwater level change to evaluate approaches for simulating land subsidence over time. Compressibility coefficients determined from consolidometer tests on cores have only been used with limited success in predicting subsidence (Gabrysch, 1982). Some of the problems associated with obtaining representative measurements from cores include obtaining undisturbed samples and accounting for spatial variability in the properties of the different and numerous clay beds. Experience has shown that the best method of estimating aquifer compressibility values at the regional scale is to analyze field data where measurements of land-surface subsidence can be compared with measured changes in the hydraulic head field over time (Gabrysch, 1982).

Table 3-2 summarizes compressibility coefficients from ten different sites in the Harris-Galveston region shown in Figure 3-8. The locations for several of these sites are provided in Figure 2.4. The compressibility coefficients range from 7×10^{-6} ft^{-1} to 4×10^{-5} ft^{-1}. Among the various factors that could contribute to this different unit compaction of clays are the age of the sediments, the depth of burial, and the pumping

history. By noting the locations of the different sites, Gabrysch (1982) observed that clays at locations equidistant from the coast generally have comparable specific-unit compaction values and that the greater specific-unit compactions occur closer to the coast.

Table 3-2   Average Specific-Unit Compaction in the Harris-Galveston Region (Gabrysch, 1982)

Site	Period	Average Stress Change		Clay Thickness		Measured Subsidence		Compaction Coefficient (ft^{-1})	
		(Head, ft of water)	(Pacals, N/m^2)	Ft	m	ft	m	ft^{-1}	m^2/N
Addicks	1906-78	316	944,504	730	223	2.5	0.77	1.1 x 10^{-5}	3.7 x 10^{-9}
Baytown	1906-78	273	815,980	1,000	305	8.7	2.66	3.2 x 10^{-5}	1.1 x 10^{-8}
Clear Lake	1906-78	221	660,555	590	180	5.2	1.59	4.0 x 10^{-5}	1.3 x 10^{-8}
Houston-Northeast	1906-78	358	1,070,040	1,020	311	5.5	1.67	1.5 x 10^{-5}	5.0 x 10^{-9}
Johnson Space Center	1906-78	366	1,093,951	915	279	4.0	1.22	1.2 x 10^{-5}	4.0 x 10^{-9}
Lake Houston	1906-78	216	645,611	1,300	396	2.8	0.86	1.0 x 10^{-5}	3.3 x 10^{-9}
Moses Lake	1906-78	110	328,783	500	152	2.1	0.64	3.8 x 10^{-5}	1.3 x 10^{-8}
Pasadena	1906-78	342	1,022,217	1,140	347	9.0	2.73	2.3 x 10^{-5}	7.7 x 10^{-9}
Seabrook	1906-78	198	591,810	800	244	3.8	1.16	2.4 x 10^{-5}	8.0 x 10^{-9}
Sheldon	1906-64	186	555,942	1,270	387	1.7	0.52	7.2 x 10^{-6}	2.4 x 10^{-9}

3.2.2   Simulated Land Subsidence from the Houston Area Groundwater Model

The HAGM is a MODFLOW-based groundwater model that uses the SUB package (Hoffman and others, 2003) to predict land subsidence. The HAGM model includes all of the counties in GMA 14 and the most eastern counties in GMA 15. It has four model layers, which represent the Chicot Aquifer, the Evangeline Aquifer, the Burkeville Confining Layer, and the Jasper Aquifer.

Figure 3-9 compares the measured and simulated land subsidence simulated by the HAGM. In Harris County and adjacent counties, where the main area of subsidence has been measured, the 1891–2000 simulated subsidence matches closely with the 1906–2000 measured subsidence. As much as 10 ft of subsidence has occurred in southeastern Harris County near the northern end of Galveston Bay. A total of 474 sites located in Harris and surrounding counties were used to evaluate simulated subsidence relative to measured subsidence. After numerous iterative trial-and-error transient model simulations, the final land-surface subsidence root-mean-square error was 0.37 ft.

A result shown in Figure 3-9 that is relevant to GMA 15 is that the HAGM predicts over a foot of land subsidence in Matagorda, Wharton, and Jackson counties in GMA 14. The maximum simulated land subsidence is about 3.5 ft and occurs in southwest Wharton County.

Two key aquifer parameters for calculating land subsidence are the preconsolidation stress and the compressibility coefficient for clays. In the HAGM, the elastic compressibility coefficient was assumed to be one one-hundredth of the inelastic coefficient. Also, the preconsolidation stress was defined in terms of total drawdown that has occurred since pumping began in 1890. The HAGM includes different and uncorrelated aquifer properties for the Chicot and the Evangeline aquifers. **Figure 3-10** and **Figure 3-11** show the spatial distribution of preconsolidation drawdown for the Chicot and the Evangeline aquifers. For cumulative drawdown less than the preconsolidation drawdown, the elastic compressibility coefficient was used to calculate the land subsidence according to **Equation 3-1**. For cumulative drawdown greater than the preconsolidation drawdown, the inelastic compressibility coefficient was used to calculate the land subsidence according to **Equation 3-1**. **Figure 3-12** and **Figure 3-13** show the spatial distribution of the inelastic storage coefficient for the Chicot and Evangeline aquifers, respectively.

The inelastic storage coefficient is related to the compressibility coefficient by the addition of the effects of expansion of water as expressed by **Equation 3-3**. The expansion of water is typically more than 10 times less than aquifer compressibility and is represented by porosity multiplied by the elasticity coefficient of water, which is about $3\text{x }10^{-7}$ ft^{-1}. For the purpose of this report, the values in Figure 3-12 and Figure 3-13 provide an acceptable map of the spatial distribution of the aquifer compressibility coefficients.

$$S_s = (\alpha + \theta * \beta) \hspace{5cm} \text{(Eq. 3-3)}$$

Where:

α = aquifer compressibility coefficient
β = elasticity coefficient of water
θ = aquifer porosity

The spatial distribution of preconsolidation stress is similar for the Chicot and Evangeline aquifers. The range in drawdown is between 0 and 160 ft of drawdown, with most of the aquifers having a value between 80 and 100 ft. For both aquifers, there is a strong correlation with the lower drawdown values occurring farthest away from the shoreline and the higher drawdown values occurring closest to shoreline.

With regard to the inelastic storage coefficients, the Evangeline aquifer has values considerably lower than the Chicot Aquifer. For the Chicot Aquifer, inelastic storage coefficients range between $1\text{x }10^{-7}$ ft^{-1} to $1\text{x }10^{-2}$ ft^{-1}, with most of the aquifer having values between 3×10^{-5} ft^{-1} to $1\text{x }10^{-4}$ ft^{-1}. For the Evangeline Aquifer, inelastic storage coefficients range between $1\text{x }10^{-7}$ ft^{-1} to 3×10^{-5} ft^{-1} with most of the aquifer having values between $3\text{x }10^{-6}$ ft^{-1} to $1\text{x }10^{-5}$ ft^{-1}. Compared to the relatively similar values of

compressibility coefficient in Table 3-2 calculated from field data at ten sites, the large spatial distribution of the values in Figure 3-12 and Figure 3-13 may be more of an artifact of the calibration process than a reflection of the actually aquifer properties. As a result, caution is recommended before accepting the specific results for each grid cell, which occupies one square mile, in Figure 3-11 and Figure 3-12 without additional investigation.

The HAGM was calibrated by an iterative trial-and-error adjustment of selected model input data in a series of transient simulations until the model output reasonably reproduced the water level and land surface subsidence. The documentation of the HAGM calibration process (Kasmarek, 2012) does not discuss the protocols used to constrain the aquifer properties to measured parameters. As a result, there may have been too much emphasis on achieving a good match between measured water levels and land subsidence during the model calibration and perhaps insufficient emphasis on constraining the spatial distribution of aquifer parameters to measured data. That said, there is nonetheless significant value in the information provided in Figure 3-10 through Figure 3-13 so long as one works with the range of aquifer parameters across large areas and not with a specific aquifer parameter assigned to a single grid cell.

3.2.3 Simulated Land Subsidence from the Lower Colorado River Basin Model

The LCRB model (Young and others, 2010) was developed as part of a project funded by the San Antonio Water System to support the design and operation of well field to pump an average of 20,000 AFY over a 30-year period. The project efforts did not include conducting field or laboratory testing to measure land subsidence or determine aquifer properties to predict land subsidence other than clay thickness. However, because the model included portions of Fort Bend, Harris, and Brazoria counties, the model used information gathered by the USGS and the HGSD to simulate land subsidence. The model is of interest because it includes portions of seven counties in GMA 15.

The LCRB is a MODFLOW-based groundwater model that uses the IBS package (Leake and Prudic, 1991) to predict land subsidence. The model consists of six layers. The LCRB model's top layer represents a shallow flow zone. The LCRB model's bottom two layers represent the upper and lower Goliad formations, which comprise the Evangeline Aquifer. The LCRB model's remaining three layers represent the Beaumont, the Lissie, and the Willis formations, which comprise the Chicot Aquifer.

Figure 3-14 shows the predicted subsidence for 1966, 1976, 1986, and 1996 based on model simulation that begins in 1900. The LCRB model predicts land subsidence of about one foot in Lavaca, Jackson, Wharton, and Matagorda counties. Among the concerns with these predictions is that a comprehensive and vetted calibration was not performed using measured land because of a lack of measured and estimated land subsidence in the main focus area of the model. The evaluation of the land subsidence predictions were based primarily on a visual comparison of contours produced from the analysis of field data.

Figure 3-15 and **Figure 3-16** show the inelastic specific coefficients for the most permeable formation in the Chicot Aquifer and the two formations that comprise the Evangeline Aquifer. The spatial distribution of the values were determined by algorithms used by the PEST software to adjust the specific unit compaction values to the thickness, depth, and distance from the coastline based on the attribute of each grid cell. The formations in the Chicot and the Evangeline aquifers have values that range between 3×10^{-6} ft^{-1} to 1×10^{-4} ft^{-1}. The average value for Lissie and the Willis formations is about 2×10^{-5} ft^{-1}. The average value for upper and lower Goliad formations is about 1×10^{-5} ft^{-1}.
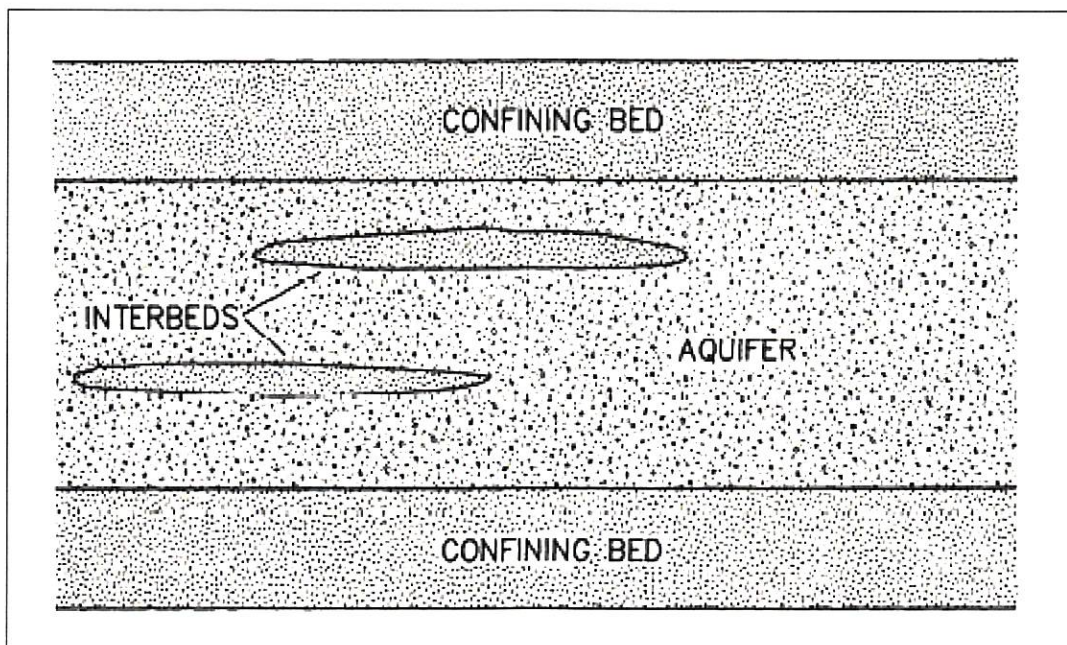
Figure 3-1   Schematic showing interbeds in a permeable aquifer. Beds may be discontinuous interbeds or continuous confining beds (from Leake and Prudic [1991])
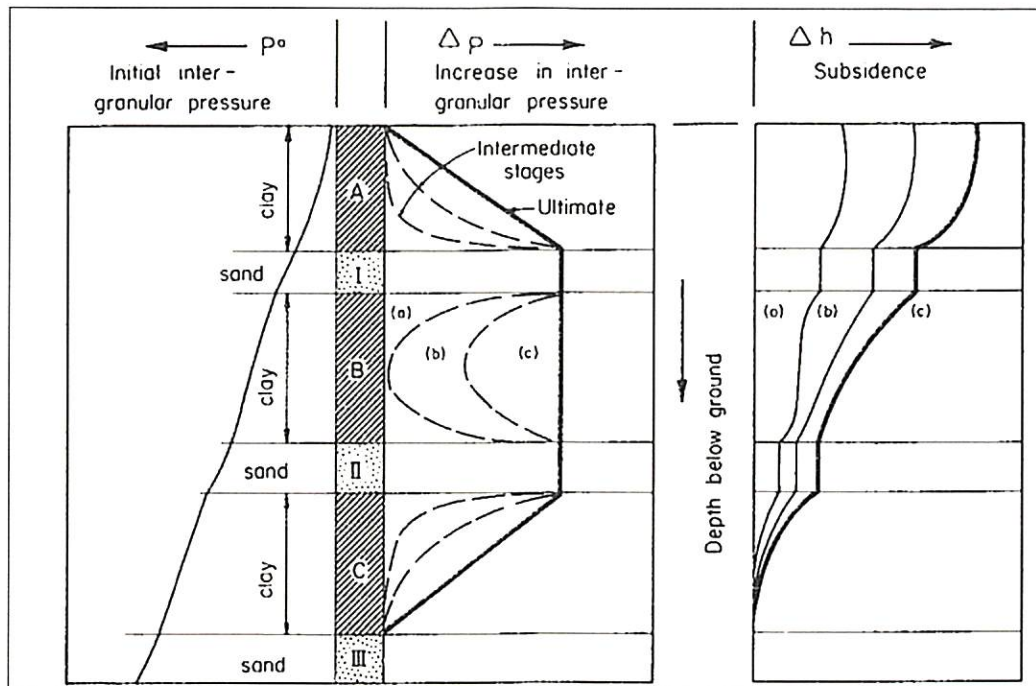
Figure 3-2   Schematic showing distribution of pressure over time in the permeable sands and in clay units over time. Initial depressurization occurs in sands and then the depressurization works outward from the sand bed inward toward the center of the clay beds. Full depressurization of clay units can lag significantly behind the full depressurization of the sands resulting in a time lag between the aquifer depressurization and land subsidence (from McGowen, [1976])
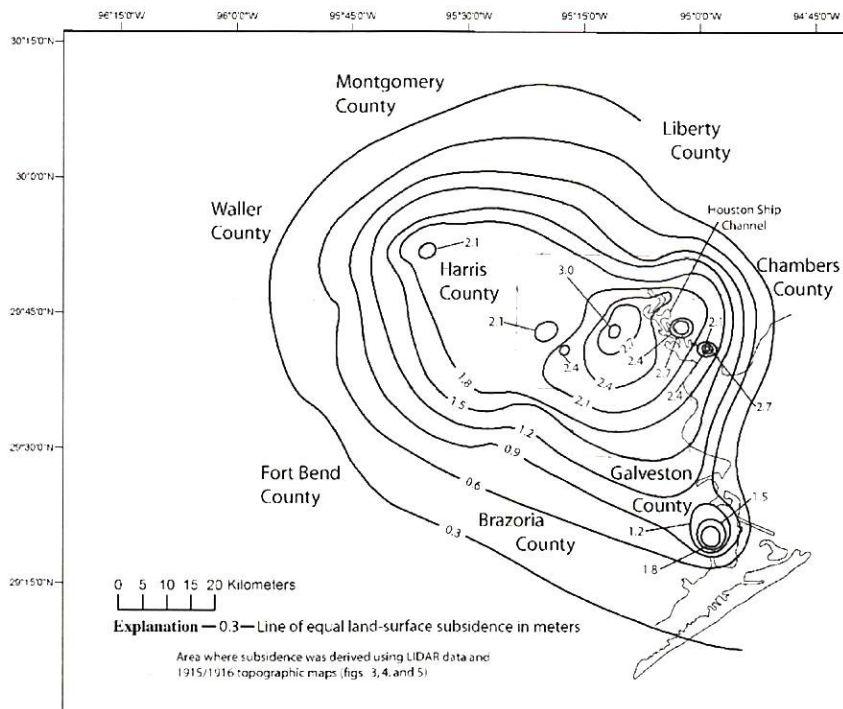
Figure 3-3   Approximate Land-Surface Subsidence, 1906-2000 as reported by Gabrysch and Neighbors (2005).
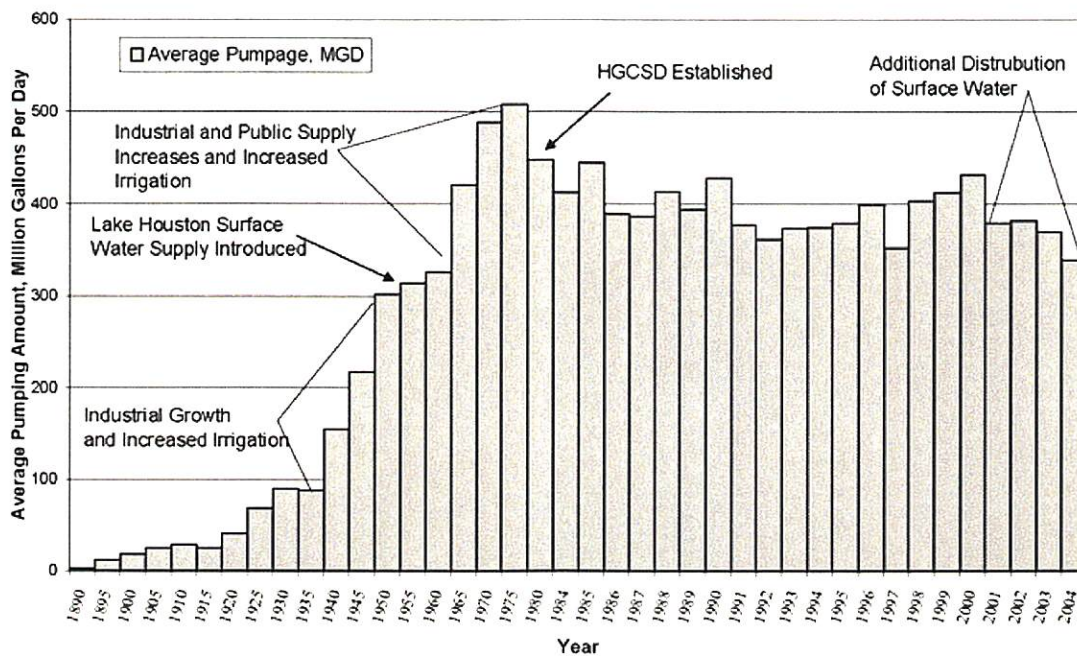
Figure 3-4   Historical Pumping of Groundwater in the Harris-Galveston Area (from Seifert and Drabek, [2006])

![INTERA]
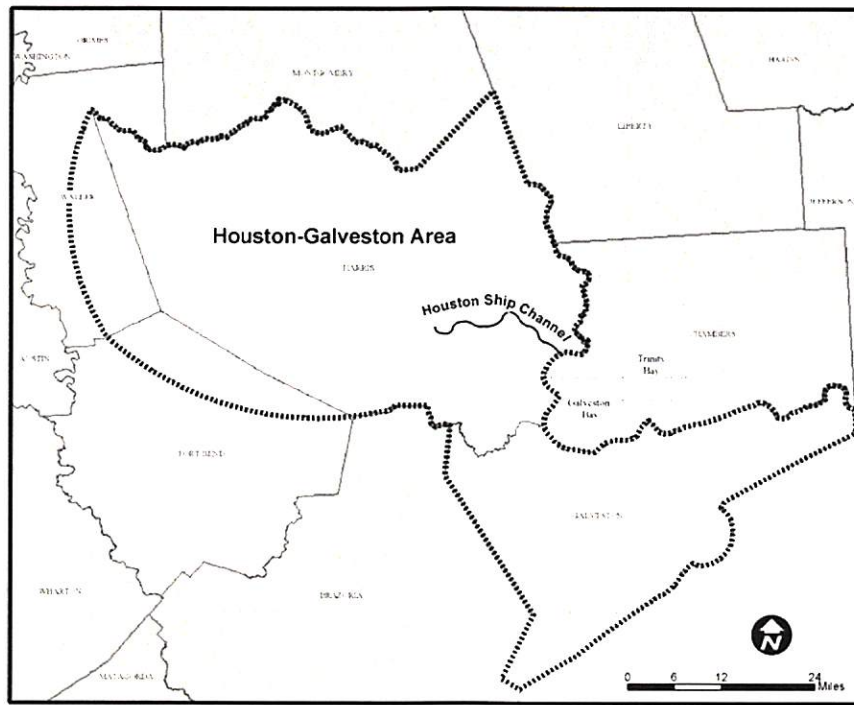
Figure 3-5   The Harris-Galveston Area (from Seifert and Drabek, [2006])
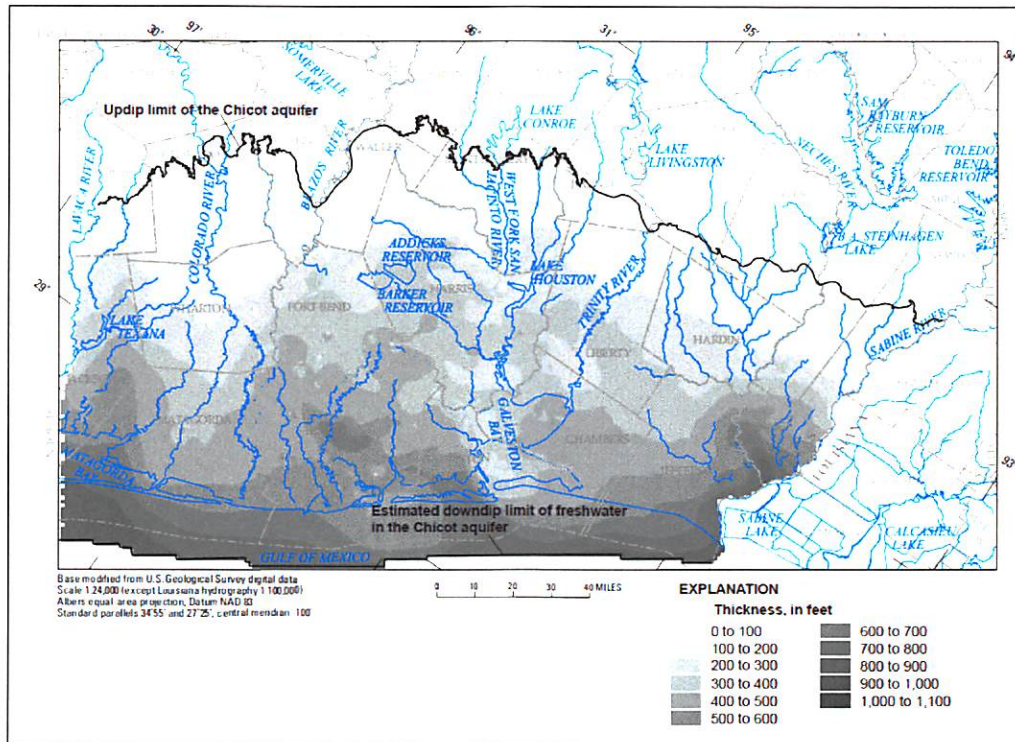
Figure 3-6   Cumulative clay thickness in the Chicot Aquifer (from Kasmarek and Robinson, [2004])
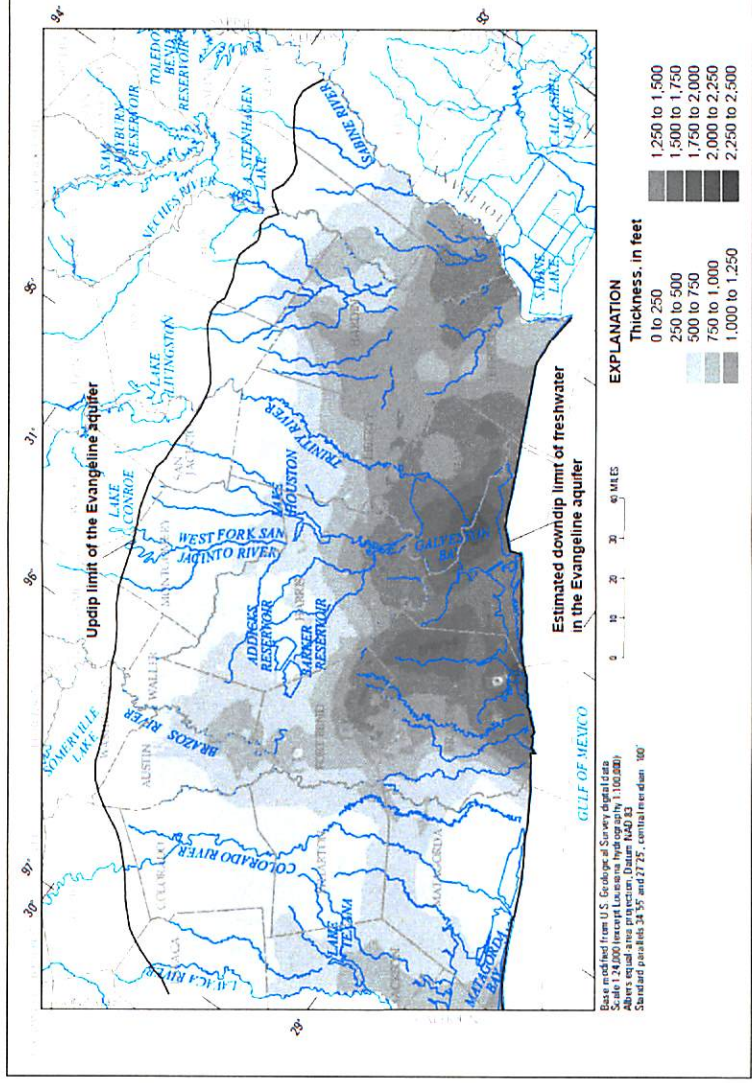
Figure 3-7   Cumulative clay thickness in the Evangeline Aquifer (from Kasmarek and Robinson, [2004])
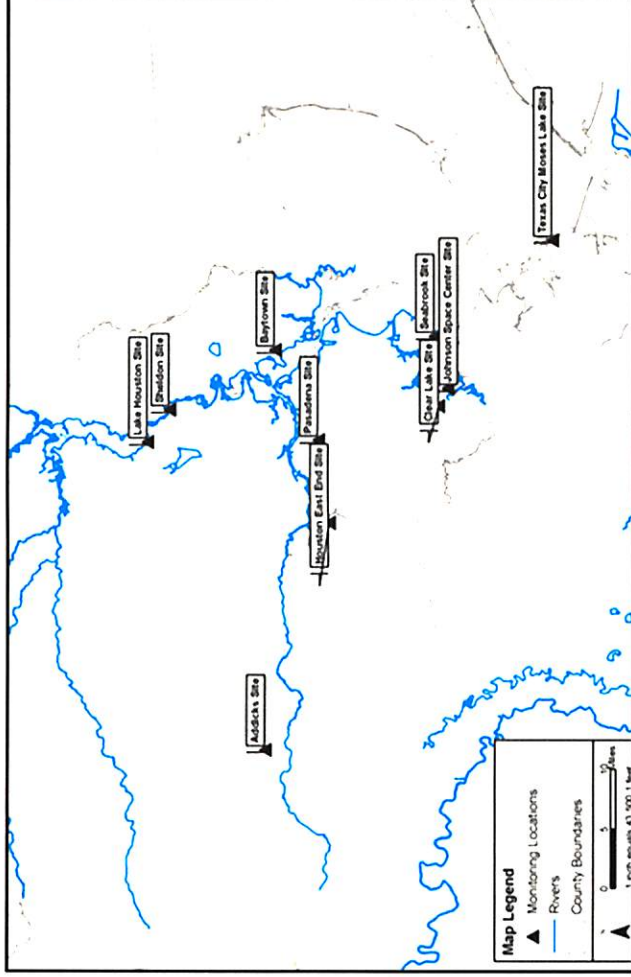
Figure 3-8   Location of ten areas where the USGS and the HGSD performed detailed site investigations in the late 1960s and 1970s.
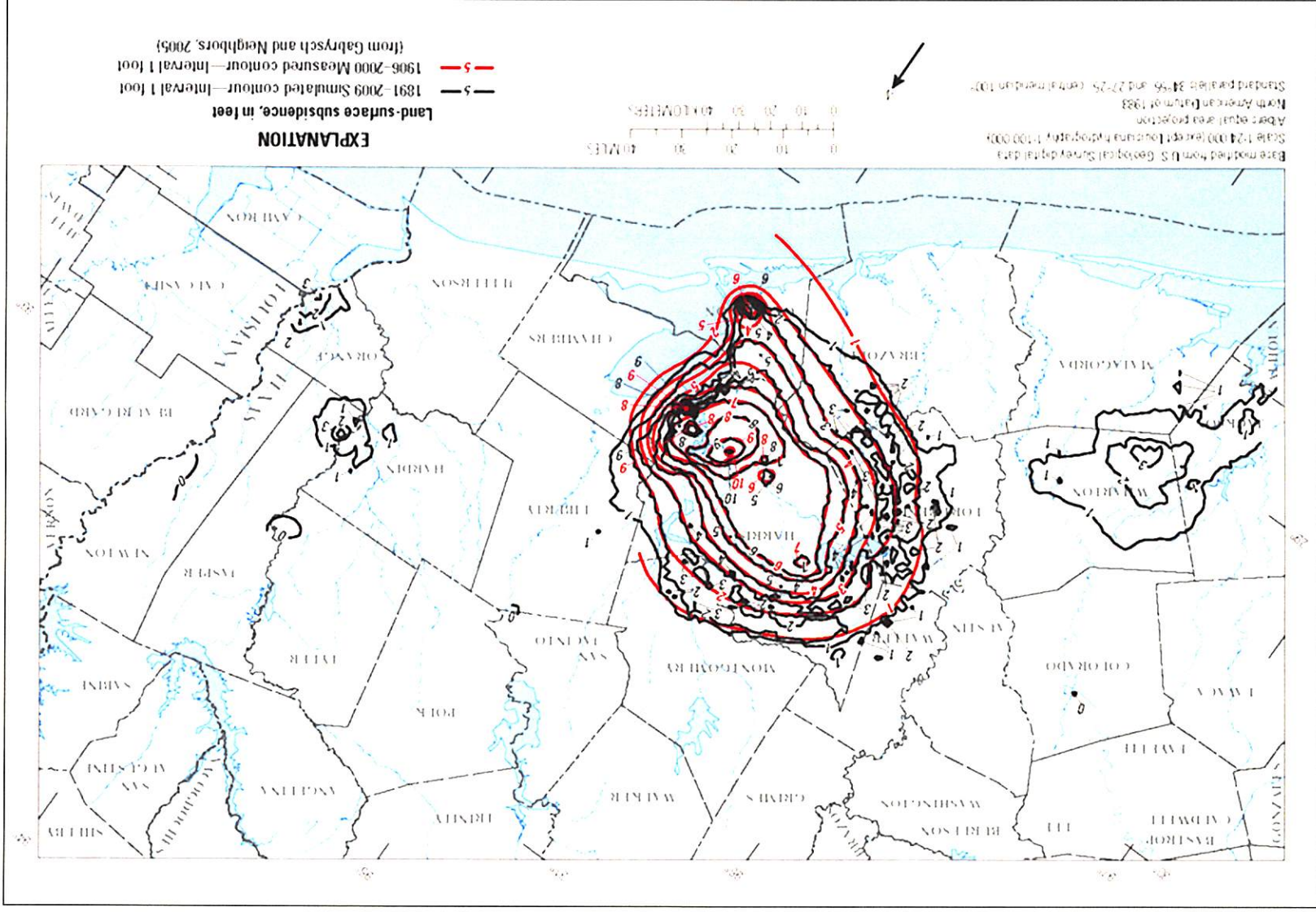
Figure 3-9   Simulated (1891-2009) and measured (1906-2000) land surface subsidence in the Houston Area (from Kasmerek, [2012])

EXPLANATION

Land-surface subsidence, in feet

— 5 — 1891-2009 Simulated contour—Interval 1 foot

— 5 — 1906-2000 Measured contour—Interval 1 foot
(from Gabrysch and Neighbors, 2005)

Base modified from U.S. Geological Survey digital data
Scale 1:24,000 (except Louisiana hydrography 1:100,000)
Albers equal area projection
North American Datum of 1983
Standard parallels 34°66' and 27°25' (central meridian 100°)

Figure 3-10   Spatial Distribution of the Preconsolidation Stress (represented as drawdown) for the Chicot Aquifer used by the HAGM (from Kasmarek, [2012])
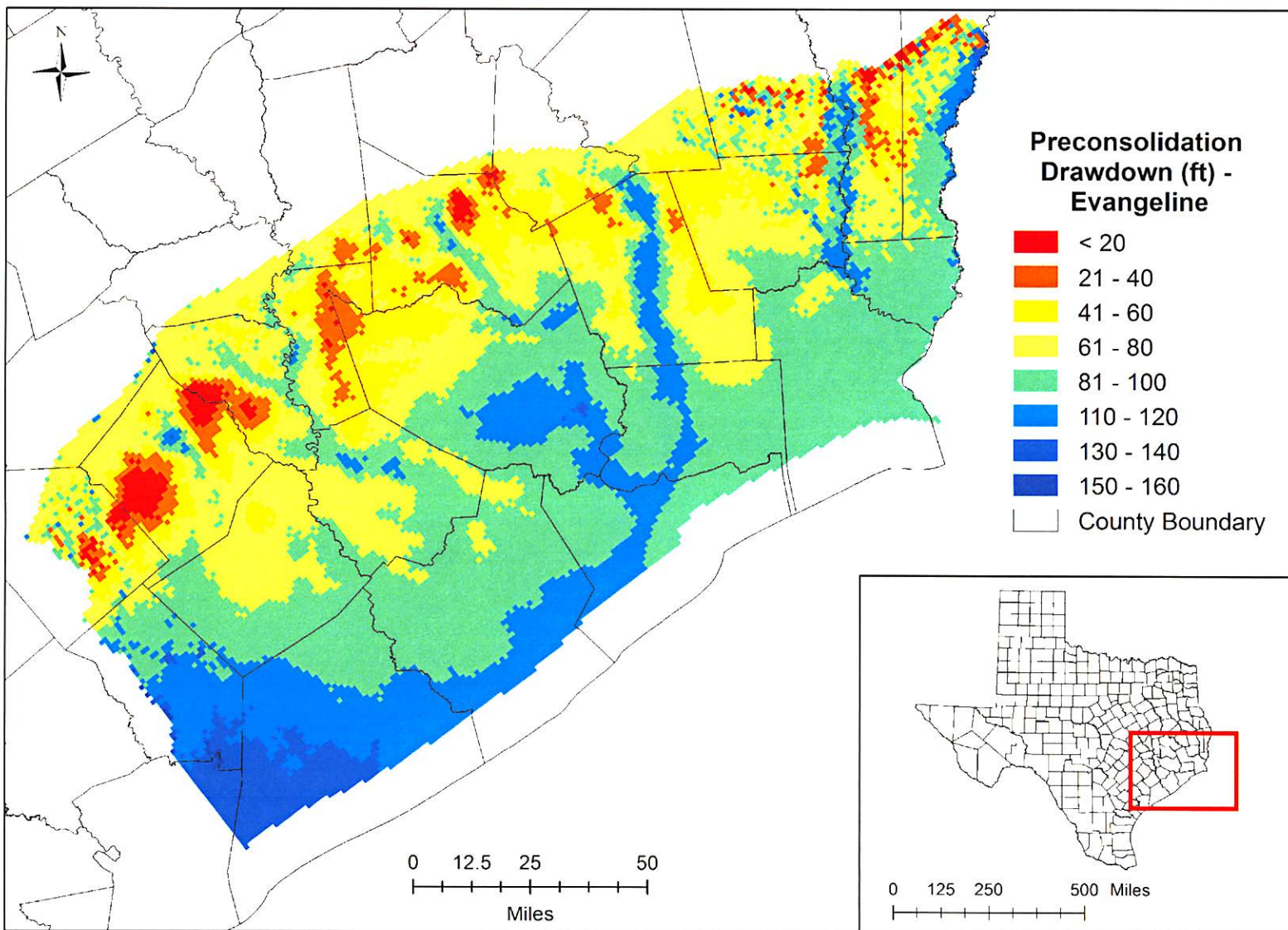
Figure 3-11　　Spatial Distribution of the Preconsolidation Stress (represented as drawdown) for the Evangeline Aquifer used by the HAGM (from Kasmarek, [2012])
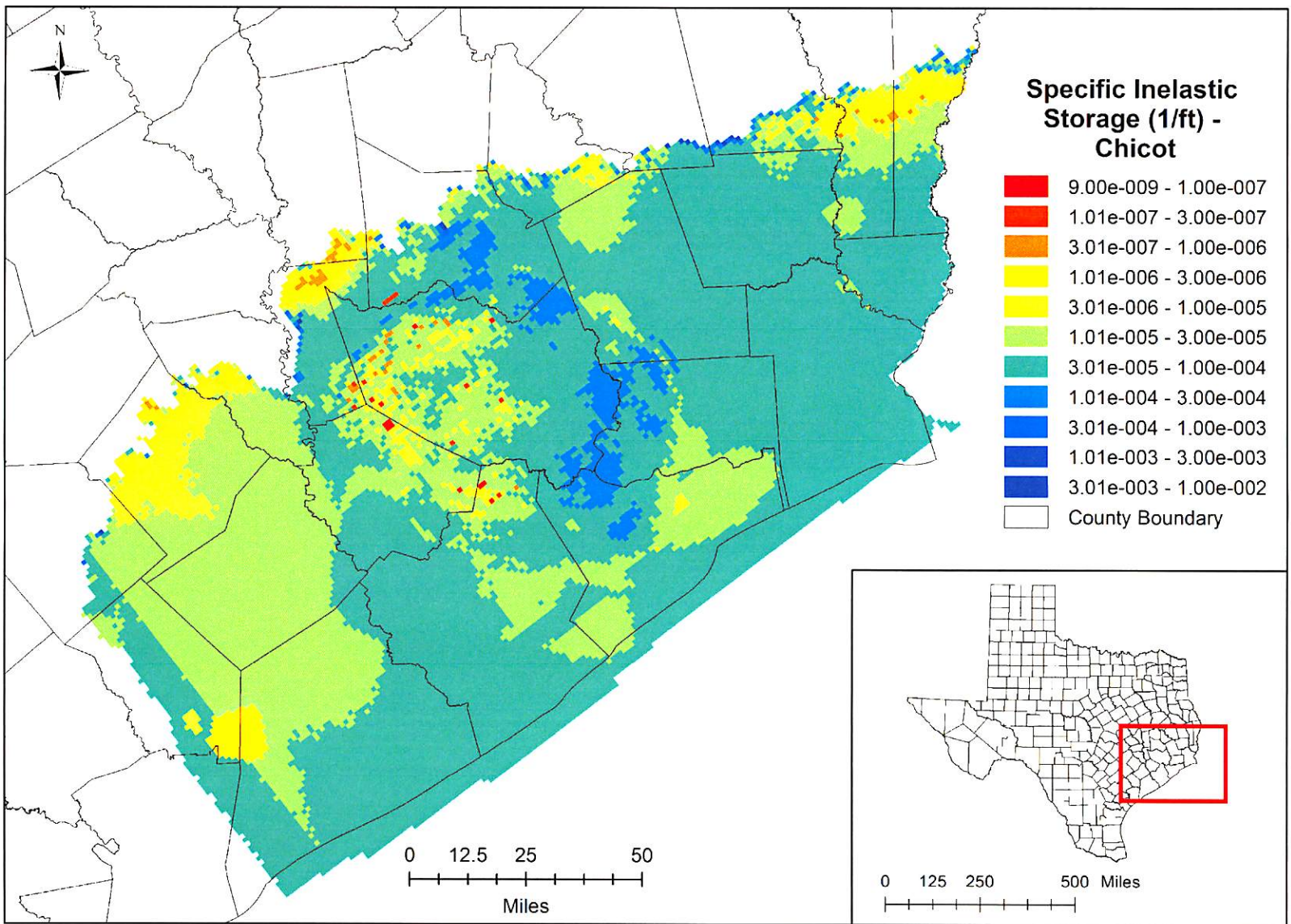
Figure 3-12   Spatial Distribution of the Inelastic Storage Coefficient for the Chicot Aquifer used by the HAGM (from Kasmarek, [2012])
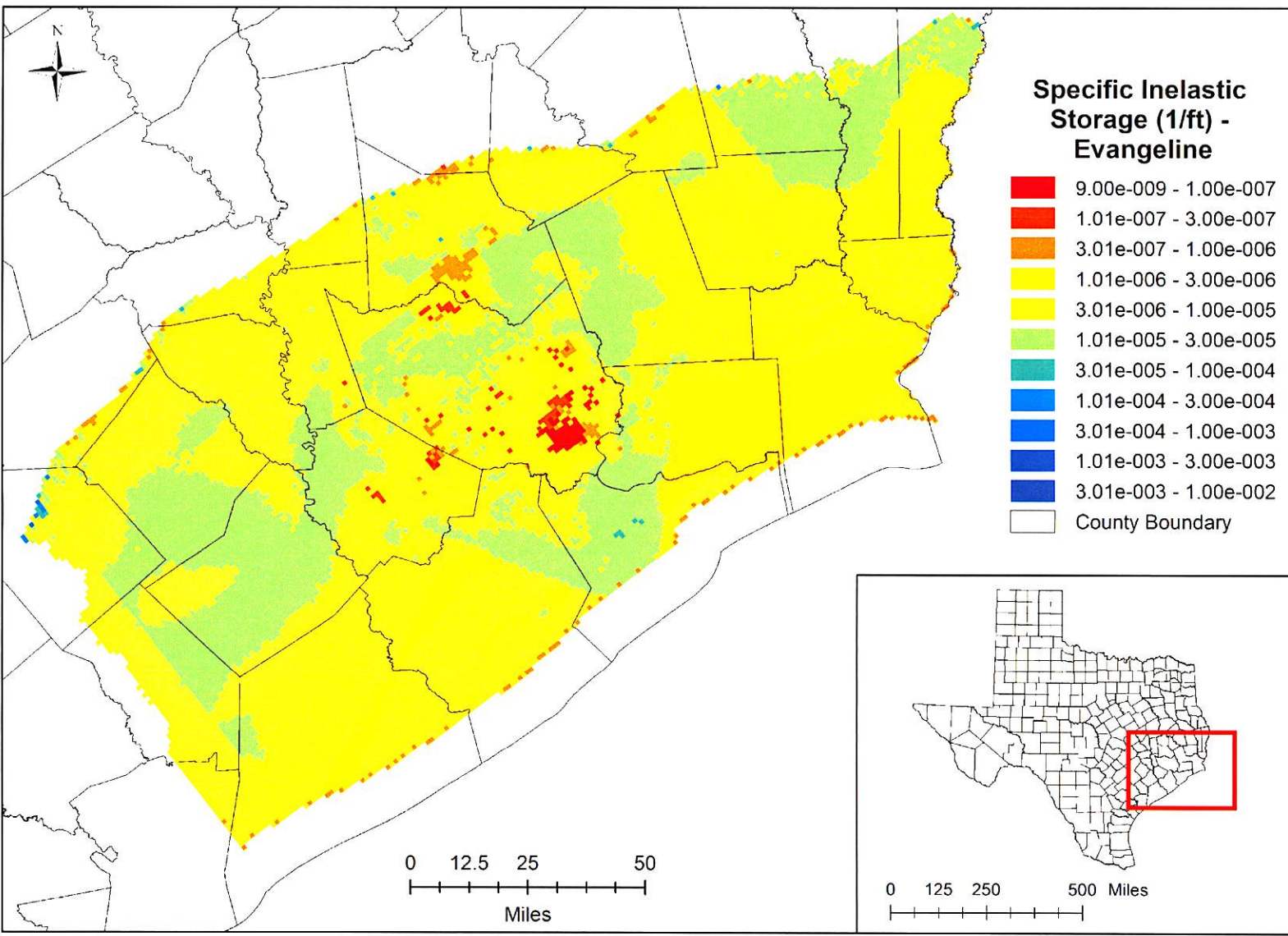
Figure 3-13   Spatial Distribution of the Inelastic Storage Coefficient for the Evangeline Aquifer used by the HAGM (from Kasmarek, [2012])
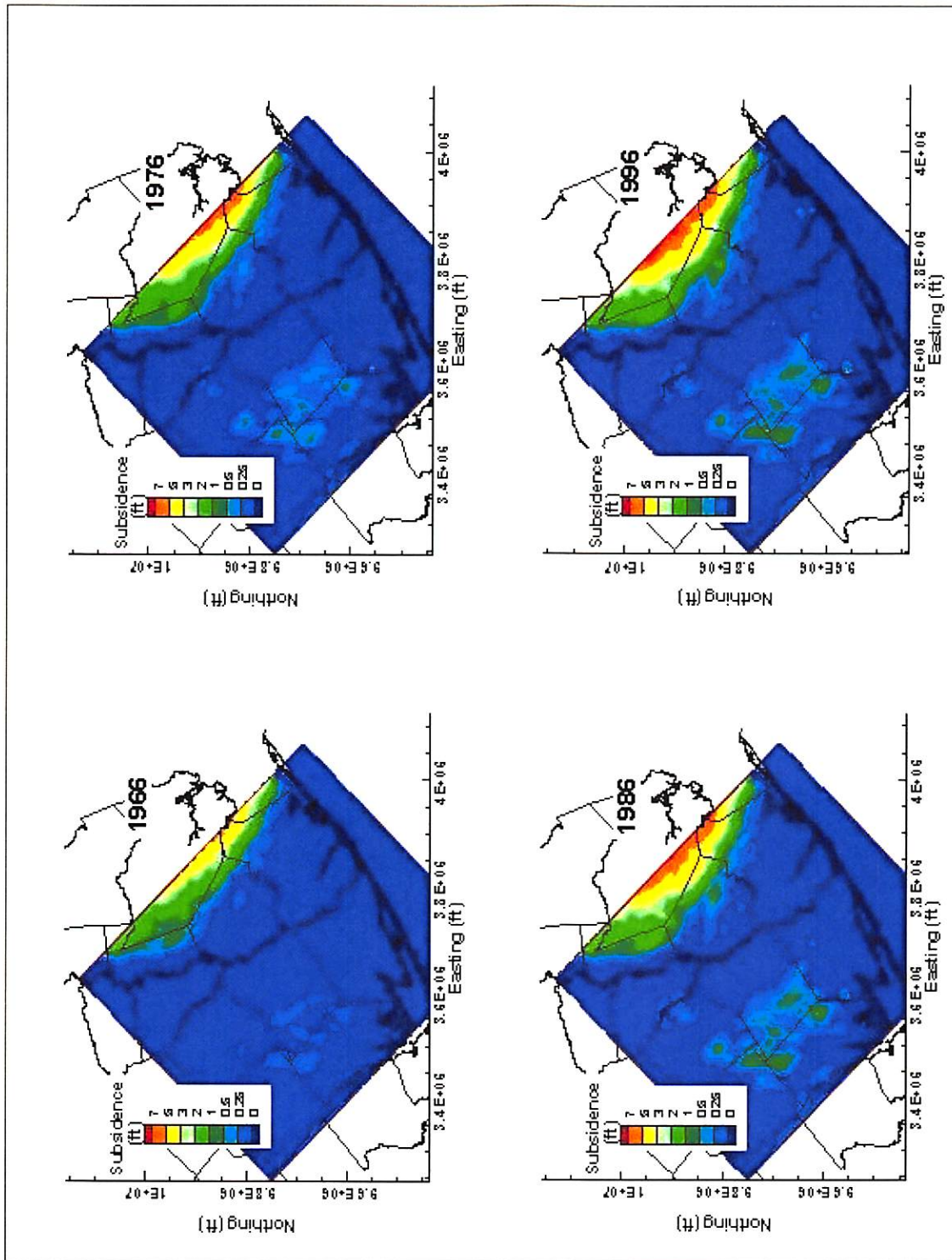
Figure 3-14   Spatial Distribution of the Preconsolidation Stress (represented as drawdown) for the Chicot Aquifer used by the HAGM (from Kasmarek, [2012])
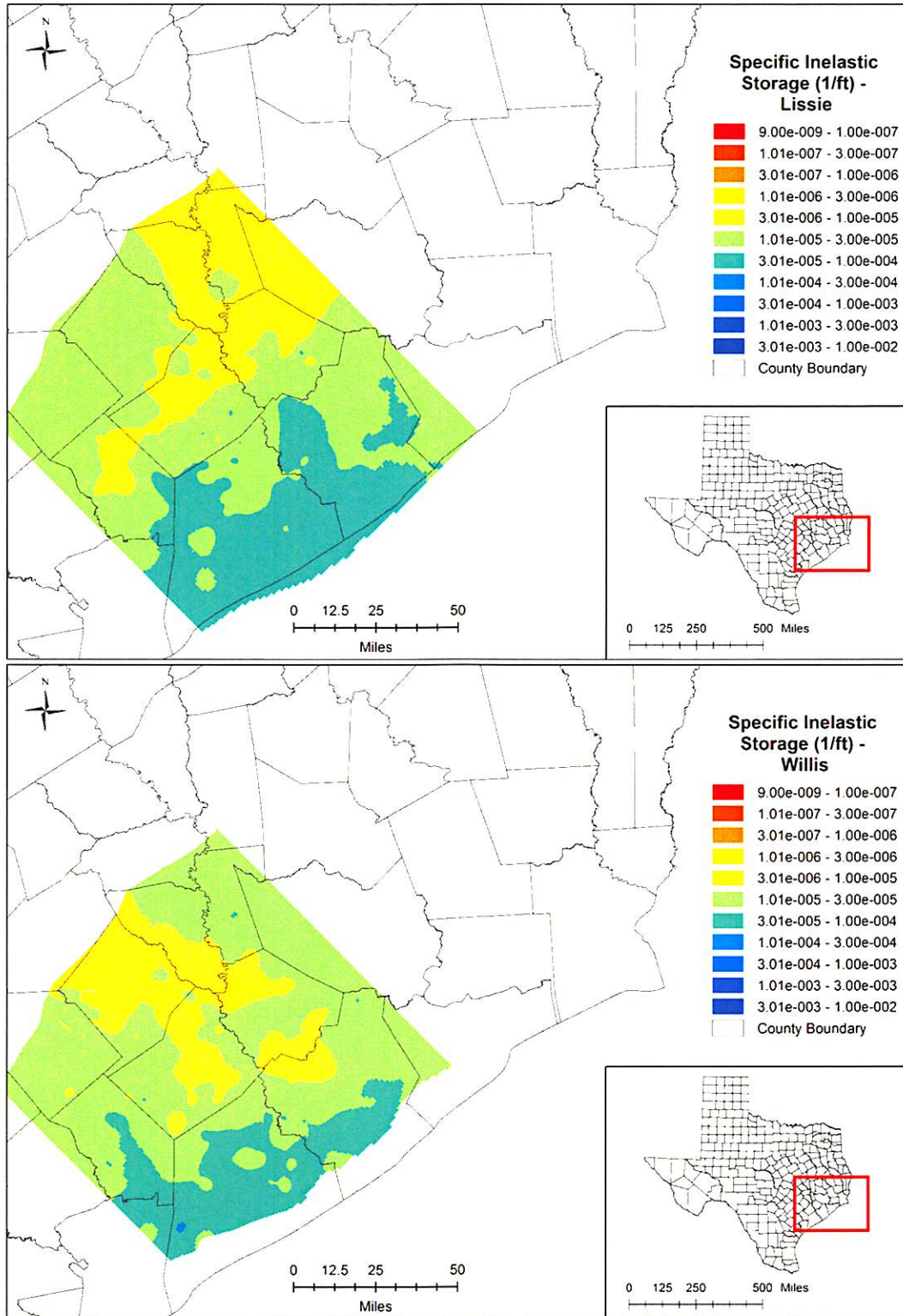
Figure 3-15 Spatial Distribution of the Inelastic Storage Coefficient for the Lissie and Willis Formation that comprise the Chicot Aquifer used by the LCRB Model (from Young and others, [2010])
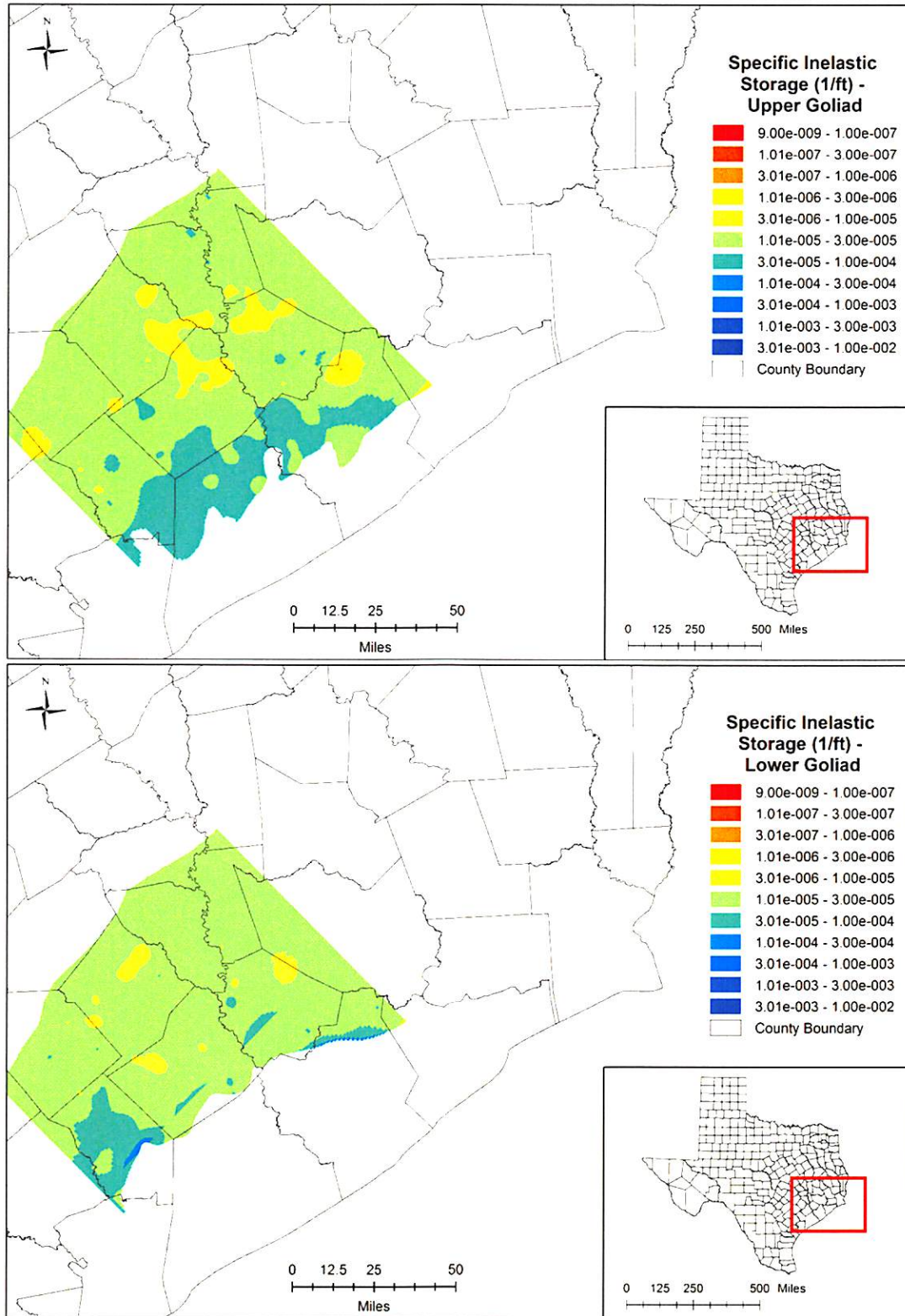
Figure 3-16 Spatial Distribution of the Inelastic Storage Coefficient for the Upper and Lower Goliad Formation that comprise the Evangeline Aquifer used by the LCRB Model (from Young and others, [2010])

4.0 POTENTIAL LAND SUBSIDENCE FROM OIL AND GAS PRODUCTION

The same principals and concepts involved with land subsidence caused by the depressurization of aquifers also apply to the land subsidence caused by the depressurization of oil and gas reservoirs. However, there are significant differences in the geotechnical properties and depressurizations associated with the pumping of aquifers and the pumping of hydrocarbon reservoirs. Compared to aquifers, oil and gas reservoirs are commonly older, deeper, more consolidated, and have less areal extent. In addition, the depressurization of fluid pressure caused by pumping in the oil and gas reservoirs is usually 10 to 100 times greater than pumping rates in major aquifers.

The section has two objectives. One objective is to present locations in Texas where oil and gas production has caused land subsidence. The second objective is to overview the potential impact of oil and gas production on land subsidence in the Harris-Galveston area.

4.1 Evidence of Subsidence from Oil and Gas Production in Texas

Sharp and Germait (1990) identify four criteria that must be met that in order for appreciable land-surface subsidence resulting from consolidation of the subsurface to occur as a result of pumping a hydrocarbon reservoir. These are: 1) large reduction in reservoir pressure, 2) production from a large vertical interval, 3) poorly consolidated reservoir rock, and 4) shallow reservoir depth of burial. In addition to consolidation, Ewing (1985), White and Tremblay (1995), and Morton and others (2001) have identified areas in Texas where pumping an oil and gas reservoir has caused land subsidence by reactivating near-surface faults by depressurizations. Chan and Zobeck (2007) also demonstrate that if the pressure drop in the producing formation is sufficiently large, then the subsurface state of stress is altered and faults that are near the threshold of failure may be reactivated and begin to move.

Kreitler and others (1990) reported large-magnitude, widespread depressurization beneath the Texas coastal plain in the 1.2 to 2.4 kilometer (km) depth range as a result of production of hydrocarbons and associated brines. Pressure gradients calculated by Kreitler and others (1990) from bottom-hole pressure measurements in thousands of wells were substantially below expected normal hydrostatic pressure gradients within the depths of fluid production. Analysis of the bottom hole pressures indicated that depressurization of over several thousand feet of hydraulic head occur at some oil and gas fields in the Catahoula Formation, which underlies the Jasper Aquifer. Such large depressurization are expected to cause some land subsidence if the other three conditions listed by Sharp and Germait (1990) exist.

Ratzlaff (1982) evaluated land subsidence in the Texas Coastal Region by comparing adjusted elevations of benchmarks for various periods of releveling and by comparing topographic maps of the same area for different years. His primary set of benchmark elevations was published by the NGS, with additional

elevations obtained from the Texas Department of Highways and Public Transportation and the Texas Department of Water Resources.

Ratzlaff (1982) concluded that land subsidence along the Texas coast was caused mostly by groundwater withdrawal; however, there are instances where hydrocarbon production contributed to land subsidence. Among the problems with isolating the impacts of pumping oil and gas on land subsidence is identifying areas where all three of the following has occurred: (1) land subsidence has been measured; (2) historical groundwater pumping is insufficient to have caused land subsidence; and (3) historical hydrocarbon production has been sufficiently large enough to cause land subsidence. Among the locations where all three of these conditions are met are:

- In Jefferson County, hydrocarbon production in the Spindletop Dome Area from 1925 to 1977 has caused approximately five feet of land subsidence

- In Jefferson County, hydrocarbon production from 1959 to 1977 at the Port Acres Gas Field has produced approximately three feet of land subsidence

- In southeastern Victoria County, hydrocarbon production has caused more than 0.5 ft of land subsidence

- In Neuces County, hydrocarbon production has caused about five feet of land subsidence at the Saxet Oil and Gas Field near Corpus Christi

In addition to the four cases above, Ratzlaff (1982) identifies several oil fields along the Texas Gulf Coast where the land subsidence of about 0.5 ft has occurred across the well field, which is significant is a significant magnitude of subsidence but only occurs over the area of a typical well fields of only a few square miles.

4.2 Evaluation of Subsidence Data from the Harris-Galveston Area

The areal extent of land subsidence in the Harris-Galveston area is one of the two largest areas of subsidence in the United States, the other area being in the San Joaquin Valley, California (Poland and others, 1975). Although subsidence in Houston unquestionably is caused principally by man-induced water-level declines, a contribution from oil and gas withdrawal has been suggested by many investigators (Gabrysch, 1969; Kreitler, 1977; Sharp and Hill, 1995); however, the relative contribution is uncertain.

To assess the potential role of hydrocarbon production on land subsidence in Harris-Galveston area, Holzer and Bluntzer (1984) developed and analyzed subsidence profiles across 29 oils and gas fields, which are shown in **Figure 4-1**. The oil and gas fields were selected using a comparison of maps of oil and gas fields with leveling lines depicted on the Geodetic Control Diagrams (NGS, 1969, 1970). Profiles from most of the fields extend at least 6 km (3.7 miles) in both directions from the perimeter of the field. Figure 4-1 shows the location and length of the profiles. For the majority of the fields the land subsidence was calculated over at least a 25-year period.

At each of the 29 sites, Holzer and Bluntzer (1984) calculated observed land subsidence and divided it by a regional component, which is attributed primarily to land subsidence cause by groundwater withdrawal, and a differential component, which is attributed primarily to land subsidence caused by the depressurization of the hydrocarbon reservoir. **Figure 4-2** provides a schematic of the calculation. The baseline used in Figure 4-2 to calculate the regional subsidence is based on measurements outside of the areal extent of the oil and gas field. Holzer and Bluntzer (1984) state that the differential land subsidence is positive at only six fields: Alco-Mag, Chocolate Bayou, Goose Creek, Hastings, Mykawa, and South Houston. With the exception of the three feet of land subsidence from 1917 to 1925 at Goose Creek, differential subsidence across oil and gas fields was smaller by a factor of two or more than regional subsidence. In addition, Holzer and Bluntzer (1984) show that negative differential subsidence (i.e., subsidence that was less than the surrounding area) was associated with four fields: Barbers Hill, Cedar Bayou, Pierce Junction, and Humble. In conclusion, Holzer and Bluntzer (1984) state that, with the exception of Goose Creek well field, the land subsidence associated with production at oil and gas fields appears to be small, with its contribution being less than one-third of the regional land subsidence.

Another study of the impact of hydrocarbon production in the Houston Galveston area was performed by Khorzad (1999, 2000). **Figure 4-3** shows the oil fields investigated by Khorzad (2000). To estimate the potential impact of petroleum extraction on land-surface subsidence, Khorzad (2000) collected field data and simulated the land-surface subsidence for 12 oil and gas fields in the Harris-Galveston area. The 12 fields were modeled based on the availability of borehole pressure data and adequate geophysical logs. Khorzad (2000) simulated the land subsidence using two analytical models. The Subsidence Reservoir Model accounts for subsidence in clays within the oil/gas reservoir. The Semi-Infinite Boundary Clay Model accounts for subsidence in clays that bound the oil/gas reservoir. The results of the two model simulations are presented in **Table 4-1**. The thickness, cumulative clay thickness, and largest clay thickness within the reservoir were determined from the geophysical logs, while reservoir depth and pressure declines were obtained from Texas Railroad Commission files.

![INTERA logo]

Table 4-1 Description and Estimated Subsidence for 12 Oil/Gas Reservoirs in Harris-Galveston Region (from Table 4-4 in Khorzad, 2000)

Field	Reservoir Depth (ft)	Time Span (yrs)	Reservoir Thickness (ft)	Total Clay Thickness (ft)	Largest Clay Thickness (ft)	Head Loss (ft)	Subsidence Reservoir Model (ft)	Subsidence SIBCM (ft)	Total Subsidence (in.)	Rate (in. yr¹)
Clear Lake	6037	14	60	22.01	6.99	309	0.098	0.0007	1.19	0.0850
Clinton	8858	26	80	29.99	12.01	1929	0.364	0.0328	4.72	0.1819
Durkee N.	7969	19	57	16.01	12.01	1645	0.197	0.0098	2.48	0.1307
Dyersdale	3540	22	17	4.00	2.00	358	0.033	0.0328	0.79	0.0358
Gillock	8451	20	18	6.00	2.99	513	0.006	0.0016	0.26	0.0130
Goose Creek	30	9	60	23.00	10.01	12283	0.951	0.0328	11.81	1.3122
Houston So.	5299	11	40	14.90	3.71	1857	0.361	0.0003	4.33	0.3937
Mykawa	3868	12	27	6.99	2.99	3652	0.558	0.3937	11.42	0.9512
New Mykawa	4865	20	55	12.01	4.04	3647	0.656	0.0066	7.95	0.3976
Satsuma	7605	19	36	6.99	2.99	2277	0.131	0.0066	1.65	0.0870
South Gillock	8740	20	52	19.00	10.01	4352	0.525	0.1969	8.66	0.4331
Taylor Lake E.	10161	10	26	12.01	4.99	7442	0.459	0.0098	5.63	0.5630

Notes:
The Subsidence Reservoir Model takes into account compaction of clay layers within the reservoir.
The Semi-Infinite Boundary Clay Model (SIBCM) takes into account compaction of clays bounding the reservoir.

Based on the results in Table 4-1 and other related information, Khorzad (2000) drew the following conclusions:

1. Pressure declines up to 3,073 pounds per square inch, or an equivalent head loss up to 7,096 ft (2,163 m) have been found at the South Gillock Field in Galveston County over a 20-year time span. This loss in pressure is a direct cause of compaction within petroleum reservoirs in the study area.

2. "Land Subsidence is occurring above a majority of the oil and gas fields in the Harris-Galveston region in measurable amounts from 1 to 33 mm yr-1 because of the under pressures indicated by bottom hole pressure data. Up to 30.00 cm (~1 ft) of subsidence has been calculated in the study area at the Goose Creek Field with a subsidence rate of 33.33 mm yr-1 (1.30 in. yr-1). The average amount of subsidence calculated above oil and gas fields was 12.89 cm (5.00 in.), with an average subsidence rate of 9.70 mm yr-1 (0.40 in yr-1)."

3. Groundwater use has decreased substantially since 1976, and the majority of the subsidence experienced from groundwater withdrawal from the years 1976 to the present occurred shortly after groundwater use decreased. The magnitude of subsidence caused by oil and gas production and the time since groundwater withdrawal has ceased suggest that oil and gas production is the principal cause of subsidence in the Harris-Galveston region.

Figure 4-1   Map of approximate regional subsidence, 1906 – 1978, showing oil fields investigated and subsidence-profile location in the Harris-Galveston Area (from Holzer and Blunter [1984])

Figure 4-2   Schematic of the calculation of differential subsidence (from Holzer and Bluntzer, 1984)
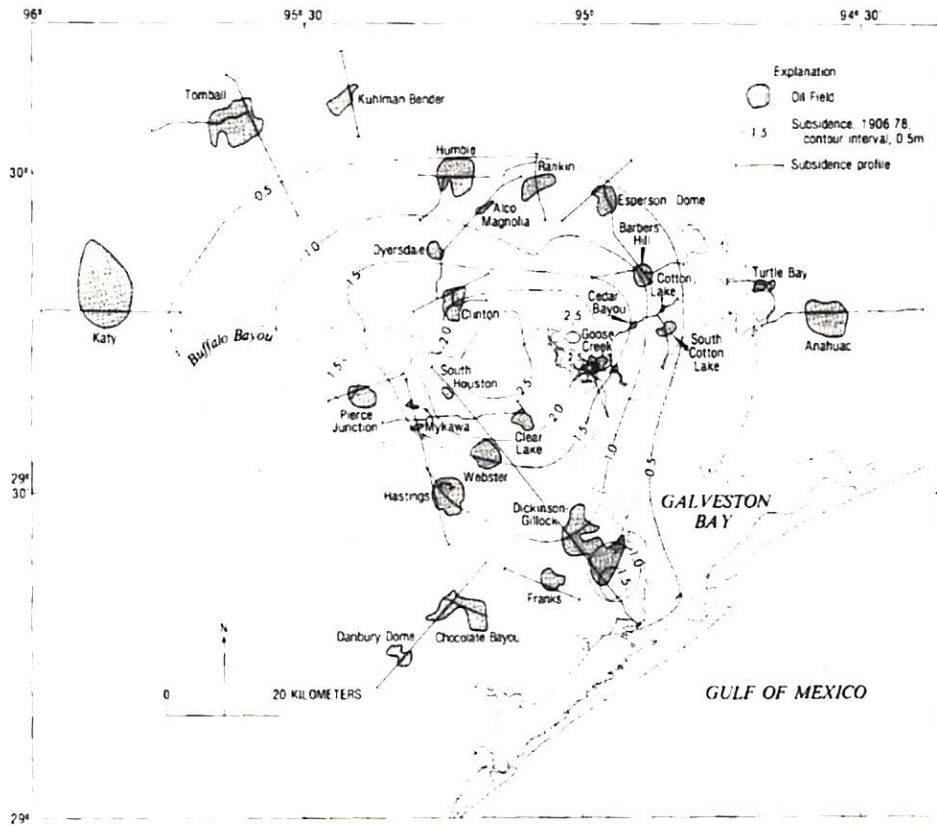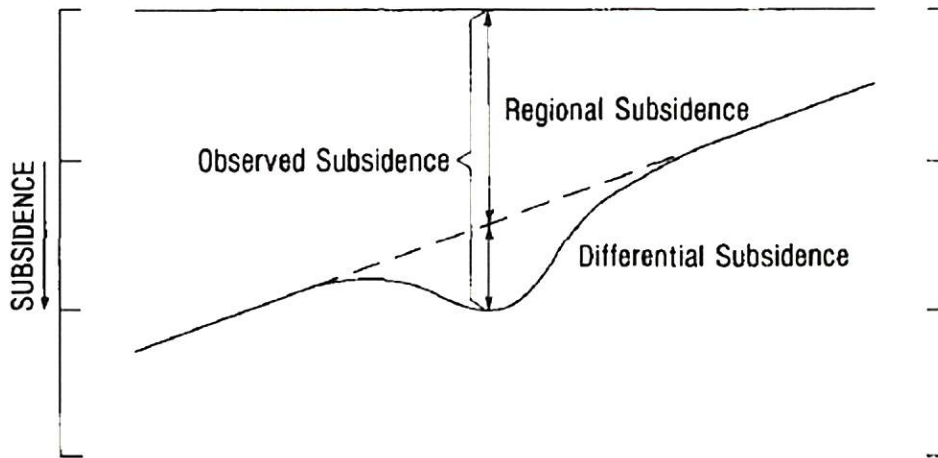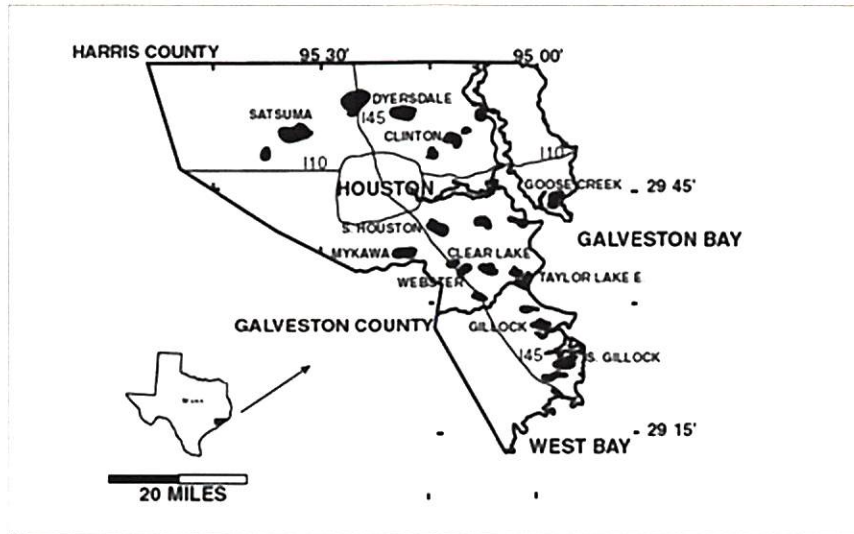
Figure 4-3   Map of approximate regional subsidence, 1906 – 1978, showing oil fields investigated and subsidence-profile location in the Harris-Galveston Area (from Khorzad [2000])

5.0 LAND SUBSIDENCE ESTIMATED FROM GROUND ELEVATION DATA

This section has two goals. One goal is to summarize previous estimates of measured land subsidence in the vicinity of GMA 15. The second goal is to assemble sources of measured ground surface elevations and calculate land subsidence for selected counties in GMA 15.

5.1 Previous Estimates of Land Subsidence in GMA 15

As discussed in Section 4.1, Ratzlaff (1982) evaluated land subsidence in the Texas Coastal Region by comparing adjusted elevations of benchmarks for various periods of releveling and by comparing topographic maps of the same area for different years. His primary set of benchmark elevations was published by the NGS, with additional elevations obtained from the Texas Department of Highways and Public Transportation and the Texas Department of Water Resources. He divided the Texas Coast into five subregions. Ratzlaff (1982) assigned counties in GMA 15 to subregion 3 and subregion 4.

Ratzlaff (1982) includes Wharton, Matagorda, Jackson, Calhoun, and Victoria Counties in subregion 3. Ratzlaff's discussion of land subsidence in subregion 3 includes the following statements:

"Land-surface subsidence during 1918-73 in subregion 3 (see [**Figure 5-1**]) is generally less than 0.5 foot (0.15 m). An area of subsidence of at least 0.5 foot (0.15 m) extends into Matagorda and Victoria Counties from Jackson County, with the greatest amount of subsidence, more than 1.5 feet (0.46 m), in southeastern Jackson County and northwestern Matagorda County. The principal cause for the subsidence in subregion 3 is ground-water withdrawals.

Withdrawals of oil, gas, and associated ground water have probably caused the subsidence in the areas adjacent to the oil and gas fields. The subsidence at Bay City probably is the result of withdrawal of both fresh ground water and oil, gas, and associated ground water. The subsidence in eastern Matagorda County is probably caused by withdrawals of ground water for irrigation.

The large area of subsidence in the eastern one-half of Jackson County and the northwestern part of Matagorda County, most of which occurred between 1950 and 1973, is the result of declines in water levels resulting from an increase in ground-water withdrawals for irrigation in the early 1950's (Loskot and others, 1982). The area of subsidence extending westward from Jackson County into Victoria County is also the result of an increase in ground-water withdrawals for irrigation.

Land-surface subsidence in southeastern Victoria County is probably related to oil and gas production. There are very few water wells and only a small amount of ground-water withdrawls in the subsided area. Water levels in observation wells within the subsided area declined more

than 1 foot (0.3 m) from 1958 to 1973 (Texas Department of Water Resources, unpublished data); but these declines were not sufficient to cause the subsidence shown for the area."

Ratzlaff (1982) includes Refugio, Aransas, San Patricio, Nueces, Kleberg and Jim Wells Counties in subregion 4. Ratzlaff's discussion of land subsidence in subregion 4 includes the following statements:

"Land-surface subsidence in subregion 4 (see [**Figure 5-2**]) is generally less than 0.5 foot (0.15 m). The maximum periods of record are 1918-51 in Refugio and San Patricio Counties and 1942-75 in Nueces County. The subsidence for these two periods is shown on Figure 5-2.

The maximum measured subsidence in Refugio is 0.74 foot (0.23 m), which occurred between 1918 and 1951. Approximately 90 percent of the subsidence occurred between 1918 and 1943. It is not possible to determine the cause of subsidence from the data available. The few records of water levels that are available indicate that the deep wells, 800-900 feet (245-275 m), were flowing wells. Mason (1963, p. 27) states that, "In most of the county, the water levels have declined in recent years due to increased pumping, and as a result, many wells have stopped flowing or their flows have decreased.

The water level in a deep well within the subsided area declined from 60 feet (18 m) above land-surface datum in 1937 to 19.7 feet (6 m) below land-surface datum in 1961. This may have been enough reduction of head to cause the subsidence. The Refugio Old and Refugio New Oil and Gas Fields were discovered in 1920 and 1931, and the subsequent withdrawal of oil, gas, and associated ground water may have contributed to the subsidence."

Loskot and others (1982) evaluated elevation benchmarks established by the NGS to determine land subsidence in Colorado, Jackson, Wharton, and Lavaca counties. Their evaluation was incomplete because most of the benchmarks had not been resurveyed since the early 1940s. The area without resurvey included over half of Wharton County.

In their analysis, Loskot and others (1982) were limited to estimating land subsidence to the areas in which the benchmark altitudes were resurveyed in 1973. At Hallettsville, 0.256 foot (0.078 m) of subsidence occurred between 1933 and 1973, while only 0.043 foot (0.013 m) of subsidence occurred before 1943. In Jackson County, near the Wharton County line, the land surface subsided 0.571 foot (0.174 m) between 1943 and 1973. Loskot and others (1982) also estimate 0.702 foot (0.214 m) of subsidence occurred between 1935 and 1973 in southeastern Lavaca County and about two feet of land subsidence at the town of Francitos in Jackson County, with 1.7 feet occurring between 1952 and 1973.

Based on his analysis of land subsidence and drawdown at the town of Francitos, Baker (1965) reports that the ratio of land subsidence to water level decline agrees closely with the ratio of about one foot of subsidence to every 100 ft of decline determined by Winslow and Doyle (1954) in the northern part of the Harris-Galveston area.

Estimates of Land Subsidence in GMA 15
Based on Ground Surface Elevation Data
and Models   47   February 3, 2016

To estimate land subsidence data in Matagorda County, Hammond (1969) uses elevation data collected between 1918 to 1951. Hammond calculates land subsidence along a transect from Francitos in Jackson County through Bay City in Matagorda County to Sweeny in Brazoria County. Hammond (1969) estimates 0.2 foot of land subsidence at Francitos and between 0.1 and 0.14 ft for the cities of Blessings and Bay City.

The TWDB groundwater investigations for Victoria (Marvin and others, 1962), Calhoun (Marvin and others, 1962), Karnes (Anders, 1960), DeWitt (Follett and Gabrysch, 1970), Goliad (Dale and others, 1957), and Refugio (Mason, 1963) counties do not discuss land subsidence.

5.2   Data Sources for Measured Ground Elevations

In this section, we will introduce data sources that will be used to estimate land subsidence. The three types of ground elevation data used to calculate land subsidence are: (1) NGS benchmark data, (2) old topographic maps, and (3) LIDAR data.

In general, the NGS benchmark data was used to estimate the precise elevations at given point locations in the past. The old topographic maps were used to reflect the elevation contours in the study area before the 1960s. The LIDAR data contains high-resolution elevation data after 2006 for most of the study area.

5.2.1   National Geodectic Survey PIDs

The NGS was established by President Thomas Jefferson in 1807 as the Survey of the Coast. Its mission was, and still is, to survey the U.S. coastline and create nautical charts of the coast to help increase maritime safety. As the nation grew westward, surveys of the U.S. interior began. In 1878, the agency was given a new name, the U.S. Coast and Geodetic Survey (USCGS), which it maintained until 1970. In 1970, a governmental reorganization created the National Oceanic and Atmospheric Administration (NOAA), and the National Ocean Service (NOS) was created as a line office of NOAA. To acknowledge the geodetic portion of the NOAA mission, the part of NOS responsible for geodetic functions was named the National Geodetic Survey.

In the U.S., survey marks that meet certain standards for accuracy are part of a national database that is maintained by the NGS. All NGS benchmark control points have PIDs associated with them. A PID for a control point does not change and consists of six alphanumeric characters, with any alpha characters being upper case, such as TX1098. Often, benchmark control points are represented in the field by a metal disk permanently affixed to a solid and stable surface, or less frequently by an existing structure such as a church spire or communication tower.

A PID is a geographically referenced benchmark point upon which a land surface elevation is measured. A PID in the subsidence study has the following properties: spatial coordinates, the measured elevation value, year in which the measurement was taken, notes on measurement method and other properties.

The measurement year and the elevation measured are the most important properties needed to conduct the subsidence analysis.

An NGS PID data set was downloaded from NGS's website (http://geodesy.noaa.gov/) as a series of point shapefiles, with each shapefile representing a county. INTERA combined the shapefiles in the area of interest into one single file to facilitate further analysis. In the report, the terms "NGS benchmark data" and "PIDs data" are used interchangeably. We will also refer to a benchmark point as a PID. **Figure 5-3** shows the location of more than 2,200 PID locations. **Table 5-1** lists the number of PID locations surveyed by survey year for eight selected counties.

Table 5-1   Temporal and Spatial Distribution of NGS PIDs in the Study Area

County	Number of PID locations			
	Total	Before 1950	1950 to 1980	After 1980
Calhoun	183	132	40	11
Colorado	173	134	36	3
De Witt	51	46	3	2
Jackson	304	126	168	10
Matagorda	394	257	121	16
Refugio	197	118	71	8
Victoria	259	166	90	3
Wharton	295	221	47	27

5.2.2   Topographic Maps

Thirty-three USGS 7.5 minute quadrangle maps were used for the study. All of the maps were downloaded from the USGS website (http://www.usgs.gov/). On a quadrangle map, the north and south limits of the quadrangle are not straight lines, but are actually curved to match Earth's lines of latitude on the standard projection. The east and west limits are usually not parallel, as they match Earth's lines of longitude. In the United States, a 7.5 minute quadrangle map covers an area of about 65 square miles in Texas.

The quadrangle maps were downloaded as scanned images of elevation contour maps, which were hand-drawn by the geologists in the 1950s and 1960s. **Figure 5-4** shows the location of the 33 quadrangle maps. **Appendix B** provides images of the 33 quadrangle maps. The 33 maps cover about 2,150 square miles. All of the quadrangle maps have topographic contour intervals of five or 10 feet. In order to use the scanned images in the analysis, INTERA hired a team to digitize the individual contours and create shapefiles of polylines. After the digitizing process, there are approximately 40 shapefiles storing the contour lines.

5.2.3   LIDAR Surveys

LIDAR is a remote sensing method that uses light in the form of a pulsed laser to measure ranges (variable distances) to the Earth. These light pulses—combined with other data recorded by the airborne system—generate precise, three-dimensional information about the shape of the Earth and its surface

characteristics. A LIDAR instrument principally consists of a laser, a scanner, and a specialized global positioning system (GPS) receiver. Airplanes and helicopters are the most commonly used platforms for acquiring LIDAR data over broad areas.

The LIDAR data in this research is used to represent the current digital elevation model (DEM). The LIDAR data was obtained from two data sources: TNRIS and HALFF Associates. **Figure 5-5** shows the LIDAR coverage provided by TNRIS. The TNRIS LIDAR includes the vast majority of Matagorda, Jackson, Victoria, Calhoun, and Refugio counties. There was only partial coverage for DeWitt County and no coverage for Wharton County. For all counties except for Calhoun County, the TNRIS LIDAR data was produced in 2006 as part of a Federal Emergency Management Agency project. The LIDAR data for Calhoun County was produced in 2011 as part of a USGS project. INTERA investigated alternative sources for LIDAR coverage and was able to obtain LIDAR coverage for Wharton County from HALFF Associates in Austin, Texas. HALFF provided LIDAR data flown in 2006 across most of Wharton County that was augmented by 2-ft contours generated from photogrammetric methods along the Colorado River corridor. For convenience, the data from HALFF will be referenced collectively as LIDAR throughout the rest of the report. Figure 5-5 shows the coverage provided by the HALFF data. The LIDAR data from TNRIS and from HALFF have a spatial resolution of about five feet and one foot, respectively. To use the LIDAR data in the land subsidence analysis, the information was converted in a DEM raster format. A DEM raster format is a standard geospatial format developed by the USGS to store digital elevation data.

5.3   Calculation of Land Subsidence

Two sets of land subsidence calculations were performed using the LIDAR data. One set of calculations uses ground elevation data from the PIDs and LIDAR. The other set uses ground elevation data from the quadrangle maps and LIDAR. When calculating subsidence from ground surface elevation data, two potentially important considerations are the spatial and temporal pumping distributions across the area of interest. For accurate estimation of historical land subsidence, the early measurements of ground elevation should have been measured before the onset of large increases in pumping. **Figure 5-6** shows a compilation of historical pumping estimates from 1900 to 2000 for Lavaca, Jackson, Matagorda, and Wharton counties in GMA 15. The pumping data show that significant increases in pumping began in 1945. Thus, in order to develop estimates of total land subsidence in these counties, and presumably in the other counties in GMA 15, the first measurement of ground surface elevation should be before 1945, if possible. If not possible, the earliest set of reliable groundwater elevation data should be used.

5.3.1   Ground Surface Elevations from PID and LIDAR Data

For each PID location, a ground surface elevation was extracted from the LIDAR data. Because of the LIDAR's high spatial resolution, the location of the PID was matched to a measurement location in the LIDAR data within a horizontal distance of five feet. The cutoff date for the first set of NGS ground surface elevation was set to 1949.

The study did not have the resources to vet each of the land surface calculations involving a PID and the LIDAR data that was either very high or low. As part of our study, however, we did spot-check land subsidence values that seemed unreasonably high or low. At these locations, we investigated whether the elevation changes were a poor location for measuring land subsidence by reviewing satellite images, by identifying possible land use changes and by examining the PID data sheets and LIDAR data for possible problems. Our limited investigations confirmed that reasons other than land subsidence are responsible for the outliers .

Because of a concern regarding unrepresentative land subsidence values calculated at some PID locations, 1,750 PIDs locations in Table 5-1 were divided into groups so that statistical analysis could be performed to help eliminate the influence of improper or unrepresentative estimates of land subsidence. With considerations for similar values and for county borders, the PID locations were grouped into 54 polygons. All of the polygons except for one have an area greater than 40 square miles. For each set of values in a polygon, the average and the median land subsidence were calculated. In **Figure 5-7,** both of these values are shown in the 54 polygons. Because of the occurrence of outliers in most of the polygons, the averages were calculated using only values falling above the 25th percentile and below the 75th percentile. **Table 5-2** lists the maximum land subsidence calculated for a polygon that has appreciable area in a county. The information in Table 5-2 suggests that all of the eight counties have already experienced at least 0.8 foot of land subsidence since 1950.

Table 5-2   Maximum Land Subsidence, calculated across a large region in a county based on comparison of PID elevations prior to 1950 and on LIDAR elevations after 2006

| County | Estimate of Demonstrated Land Subsurface(ft) for an area of about 40 square miles | |
	Value (ft)	Description of Area
Calhoun	1.2	Northwest quadrant along border with Victoria County
DeWitt	1.8	Within the city limits of Cuero
Jackson	2.2	Southeast region near boundary with Matagorda
Matagorda	2.3	Northwest region near boundary with Wharton and Jackson County
Refugio	0.8	Along eastern border with Aransas County
Victoria	0.8	Southwest and southern Region
Wharton	2.7	Southwest region near border with Jackson and Matagorda County

The purpose and value of Figure 5-7 is to convey a general message of the magnitude and range of land subsidence occurred across an eight-county area since 1950. A more spatially specific approach to land subsidence is provided **Figure 5-8**. Figure 5-8 shows where at least 1.5 ft of subsidence has been calculated at two PIDs locations that are closer than two miles apart. **Figure 5-9** shows where at least 1.5 ft of subsidence has been calculated at two PIDs locations that are closer than two miles apart. In Figure 5-8 and Figure 5-9, the paired locations are where there is a high level of confidence that land subsidence greater than 1.5 ft and 2 ft has occurred, respectively. Such locations have potential value for aiding our understanding and modeling the land subsidence process. **Table 5-3** provides the number of instances where the calculated land subsidence is greater than 1.5 ft and 2 ft at PID locations closer than within two

miles of each other. As indicated in Tables 5-2 and 5-3, land subsidence greater than 1.5 ft has occurred in six of the seven counties of interest, with greatest evidence of land subsidence occurring in the region near where the borders of Wharton, Matagorda, and Jackson counties merge.

Table 5-3 Number of Paired PID locations where land subsidence is greater than 1.5 feet and 2.0 ft by county from before 1950 to after 2006

County	Number of Instances where the calculated land subsidence is greater than 1.5 ft (or 2.0 ft) at PID Locations within 2 miles of each other	
	1.5 ft	2 ft
Calhoun	3	0
DeWitt	14	8
Jackson	23	16
Matagorda	63	29
Refugio	16	6
Victoria	11	9
Wharton	64	38

5.3.2 Quadrangle Maps and LIDAR

Across the 2,150 square miles covered by thirty-three quadrangle maps shown in Figure 5-4, land subsidence values were displayed with 500-ft spacing. At each of these locations, land subsidence was calculated from the surface elevation extracted from the rasters generated from the LIDAR data and from the digitized contours from the quadrangle maps. The 500-ft spaced land subsidence values were averaged across one square mile blocks and are displayed in **Figure 5-10**. Two features readily evident in Figure 5-10 are the square blocks of red and blue. The red blocks indicate where the ground elevation has not subsided but has rebounded by more than six feet. The blue blocks indicate where ground elevations have subsided more than one foot.

The red blocks in Figure 5-10 occur in Jackson and Matagorda counties, where the ground elevation has increased between six and 28 ft since the 1952. The red blocks in Jackson County are attributed to the creation of Lake Texana, which was formed as a result of Palmetto Bend Dam, which was created in 1968. The red blocks in Matagorda County are attributed to a small lake built in the later 1980s for the South Texas Nuclear Generating Station.

In Figure 5-10, the land subsidence value for each square represents the average of about 100 point measurements. To aid in understanding the meaning of the average value, the standard deviation of the 100 measurements are shown in Figure 5-10. For many of the one square mile areas, the standard deviation, which is a measure of the spread in the data, far exceeds the average value. A standard metric for comparing the standard deviation to the mean of the data is the coefficient of variation (CV). The definition of CV is the standard deviation divided by the mean value. The higher the CV, the greater the spread of the data and the less reflective the average is of most of the sampled population. Based on the

land subsidence in the Harris-Galveston area, land subsidence caused by consolidation of clays deposits should not be characterized by high spatial variability at the scale of less than 1-mile unless the land.

Figure 5-11 shows the distribution of standard deviations calculated for the approximately 100 individual land subsidence values used to calculate the average land subsidence value for the one-mile square areas. The majority of the one-mile square areas. with standard deviations greater than three feet contain a stream or river. The one-mile square areas. with the highest standard deviations occur along the Colorado River in Wharton and Matagorda counties, along the Guadalupe River in Victoria and Calhoun counties, and along the Lavaca and Navidad rivers in Jackson County. The occurrence of one-mile square areas. with high standard deviation near rivers is likely caused by two conditions. The first condition is that the hand-drawdown topographic maps are not accurate near the rivers because of the lack of benchmarked measurements to represent the steeper topographic gradients near riverbanks and tributary streams properly. The second condition is the areas near rivers are more susceptible to land-changing processes such as erosion and flooding than other areas of the county.

Figure 5-12 was derived from Figure 5-8 by removing the one-mile square areas with a CV greater than 0.75. Figure 5-8 contains approximately 2,024 one-mile square areas, while Figure 5-12 contains 208 one-mile square areas. Most of the one-mile square areas with low CVs are associated either with blue squares in the vicinity of Wharton, Jackson, and Matagorda counties that are associated with land subsidence, or else with the red squares associated with the creation of a lake after 1960. Outside of Wharton County, there are nine one-mile square areas that indicate a rise in ground surface elevation. Eight of the nine one-mile square areas. are in near Bloomington in Victoria County. The reason for this apparent rise in ground surface elevation was not investigated. In the central portion of Wharton County, there are approximately 20 one-mile square areas that indicate a rise in ground elevation, which is contrary to information shown in Figure 5-8. One possible explanation for the different results is that the extensive land use changes from 1950 to 2006 associated with rice farming at the location of the 20 one-mile square areas is somehow responsible.

Table 5-3 provides a summary of the land subsidence in Figure 5-12. To clarify the terms in Table 5-3, the information for Wharton County will be explained. For Wharton County, the data analysis indicates that there are 47 square miles where land subsidence is between one and three feet, and 11 square miles where land subsidence is greater than three feet. For these 57 square miles, the average land subsidence is 2.39 ft. For the seven counties listed in **Table 5-4**, there are 159 one-mile square areas with measured land subsidence greater than 1 foot. The average amount of land subsidence calculated for the 159 square miles is 2.3 feet.

![INTERA logo]

Table 5-4   Number of one-mile square mile areas where land subsidence is greater than 1 foot for the time period before 1965 and after 2006

County	Number of 1 square mile areas with a CV < 0.75 for the approximately 100 land subsidence measurements		
	Greater than 3 ft	Between 1 and 3 ft	Average Land Subsidence (ft) Area with >1 feet of subsidence
Calhoun	0	1	2.06
De Witt	0	0	--
Jackson	5	50	2.17
Matagorda	3	35	2.33
Refugio	0	0	--
Victoria	1	6	2.21
Wharton	11	47	2.39

5.3.3 Summary

This section investigates land subsidence across GMA 15 by conducting a literature review of hydrogeology reports and by analyzing historical ground surface elevation data assembled from NGS benchmarks, old topographic maps, and LIDAR.

The literature review discovered that many of the state water reports for counties in GMA 15 were completed in the 1950s and 1960s, with little or no discussion regarding land subsidence. Ratzlaff (1982) is the most comprehensive report for many of the counties in GMA 15, and his analysis includes sparse elevation data after 1973. A limitation of Ratzlaff (1982) and other studies is a lack of locations where ground surface elevation has been measured repeatedly over time. Also, Ratzlaff (1982) does not present sufficient information to investigate how the spatial pattern of land subsidence is related to the spatial and temporal distribution of pumping or drawdown measurements across a county. In fact, none of the reports reviewed discuss how the spatial and temporal distribution of groundwater and oil and gas production across GMA 15 could affect the spatial variation of land subsidence. Despite these limitations, the existing reports nonetheless provide ample evidence that land subsidence has occurred across most of the counties in GMA 15 and should be an important concern regarding the management of groundwater.

The literature review provides considerable data that tie oil and gas production to land subsidence. Where such land subsidence has occurred, the areal extent of the land subsidence appears to be limited to the footprint of the oil field and therefore typically impacts only a few square miles. Most of the depressurization of the oils field responsible for land subsidence has occurred in the Catahoula Formation, which underlies the Jasper Aquifer. Despite consisting of old and relatively consolidated sediments, the land subsidence occurs as a result of pumping oil and gas fields in the Catahoula because of the large amount of depressurization. As discussed in Section 4.2 (see Table 4-1), depressurization of an oil and gas

reservoir in the Harris-Galveston Region by over 2,000 ft are not uncommon. In southern Victoria and in Jackson counties, Kreitler and others (1988) show that over 2,000 ft of depressurization has occurred.

As a general rule, land subsidence is more likely to be caused by pumping shallow aquifers than by pumping deep oil and gas reservoirs for two reasons. One reason is that, in the Gulf Coast aquifers, the clays are a part of the youngest geologic formation in Texas and are often under consolidated. Another reason is that the Gulf Coast aquifers, such as the Chicot and Evangeline aquifers, are laterally extensive and relatively permeable. These hydrogeological conditions promote the overlap of drawdown impacts from large well field overlap so that large areas of land subsidence can develop.

Based on the limited spatial measured land subsidence discovered during the literature review, land subsidence is most prevalent in an area near the confluence of the borders of Wharton, Matagorda, and Jackson counties, where extensive pumping has occurred to support agriculture and oil and gas activities. In this area, the maximum land subsidence reported from 1918 to 1973 is about 1.5 ft near the town of Francitos in Jackson County

Concerns that land subsidence continued after 1973 are warranted for two reasons. One reason is that total annual pumping in GMA 15 has been at higher rates for the last 40 years than in 1973. This trend is substantiated by the historical pumping curves for Wharton, Matagorda, Jackson and Lavaca counties in Figure 5-6. Another reason for land subsidence to continue beyond 1973 is that land subsidence does not respond instantaneously to drawdown. As discussed in Section 3, the consolidation is time-dependent and is affected by the thicknesses of the clay beds. Based on the distribution of clay beds in the Chicot and Evangeline aquifers provided by Young and others (2009), up to a decade may be required for the thicker clay beds to drain and become consolidated.

To calculate land subsidence, the study assembled ground surface elevation data from NGS PIDs, old topographic maps, and LIDAR from seven counties. The LIDAR data covers approximately 2,500 square miles and was shot after 2006. The topographic maps cover about 2,150 square miles and were constructed between 1950 and 1960. The NGC PID data provide ground surface elevations at 1,700 point locations prior to 1950. These three data sets were used to create three types of land subsidence maps. One map type is comprised of 54 polygons. The 54 polygons cover the seven counties, and each polygon is assigned an average land subsidence value based on the LIDAR and PID data. Another map type identifies locations where two NGS locations are within two miles of each other and mark land subsidence of at 1.5 or 2 ft based on the LIDAR and PID data. A third map type shows 208 one-mile square areas, with a measurable average land subsidence based on the topographic map and LIDAR data. Analysis of these three map types supports the following statements:

1.)   The literature review indicates that land subsidence in GMA 15 has occurred from pumping from oil and gas reservoirs and from groundwater from aquifers.

2.) The LIDAR and PID data indicate that DeWitt, Jackson, Matagorda, Refugio, Victoria, and Wharton counties have experienced at least two feet of land subsidence and that Calhoun County has experienced at least two feet of land subsidence.

3.) The LIDAR and topography map data indicate that Calhoun, DeWitt, Jackson, Matagorda, Refugio, Victoria, and Wharton counties have experienced at least two feet of land subsidence since 1950.

4.) The LIDAR and topography map data indicate that Calhoun, DeWitt, Jackson, Matagorda, Refugio, Victoria, and Wharton counties have experienced at least two feet of land subsidence since 1950.

5.) A joint analysis of the PID, topographic map, and LIDAR data indicates that more than two feet of average subsidence has occurred across about 100 square miles covering southwest Wharton, southeast Jackson, and northwest Matagorda counties.
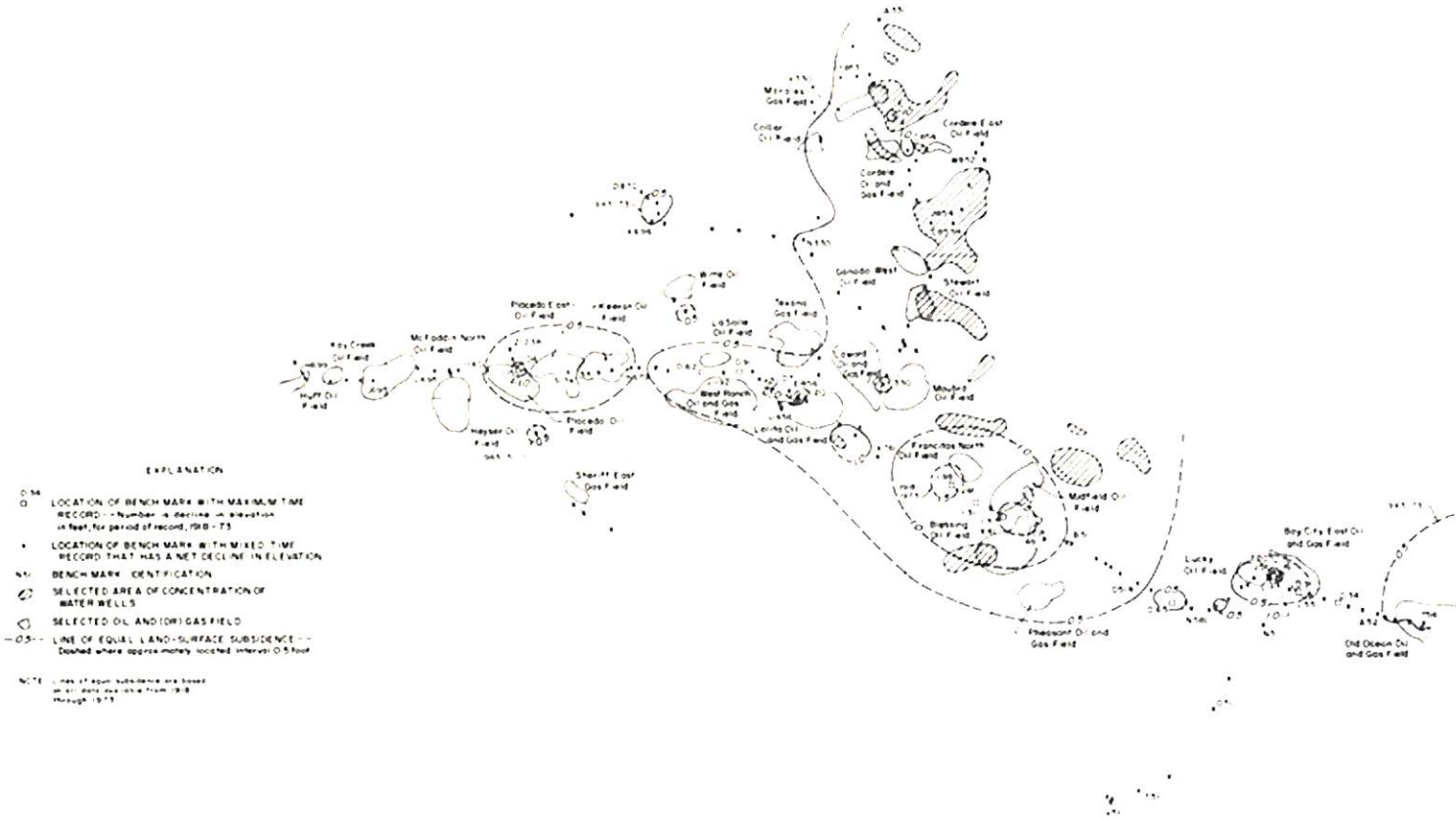
Figure 5-1   Land subsidence from 1918 to 1973 for Subregion 3 including Victoria, Calhoun, Wharton, and Matagorda counties

Figure 5-2   Land subsidence from 1918 to 1951 and from 1942 to 1975 for Subregion 4 including Refugio, San Patricio and Neuces counties (from Ratzlaff, 1982)

Elevation Year

- ■ 0 - 1949
- ● 1950 - 1980
- ◆ 1981 - 2012

Zone

☐ County Boundary

0 5 10 20
Miles
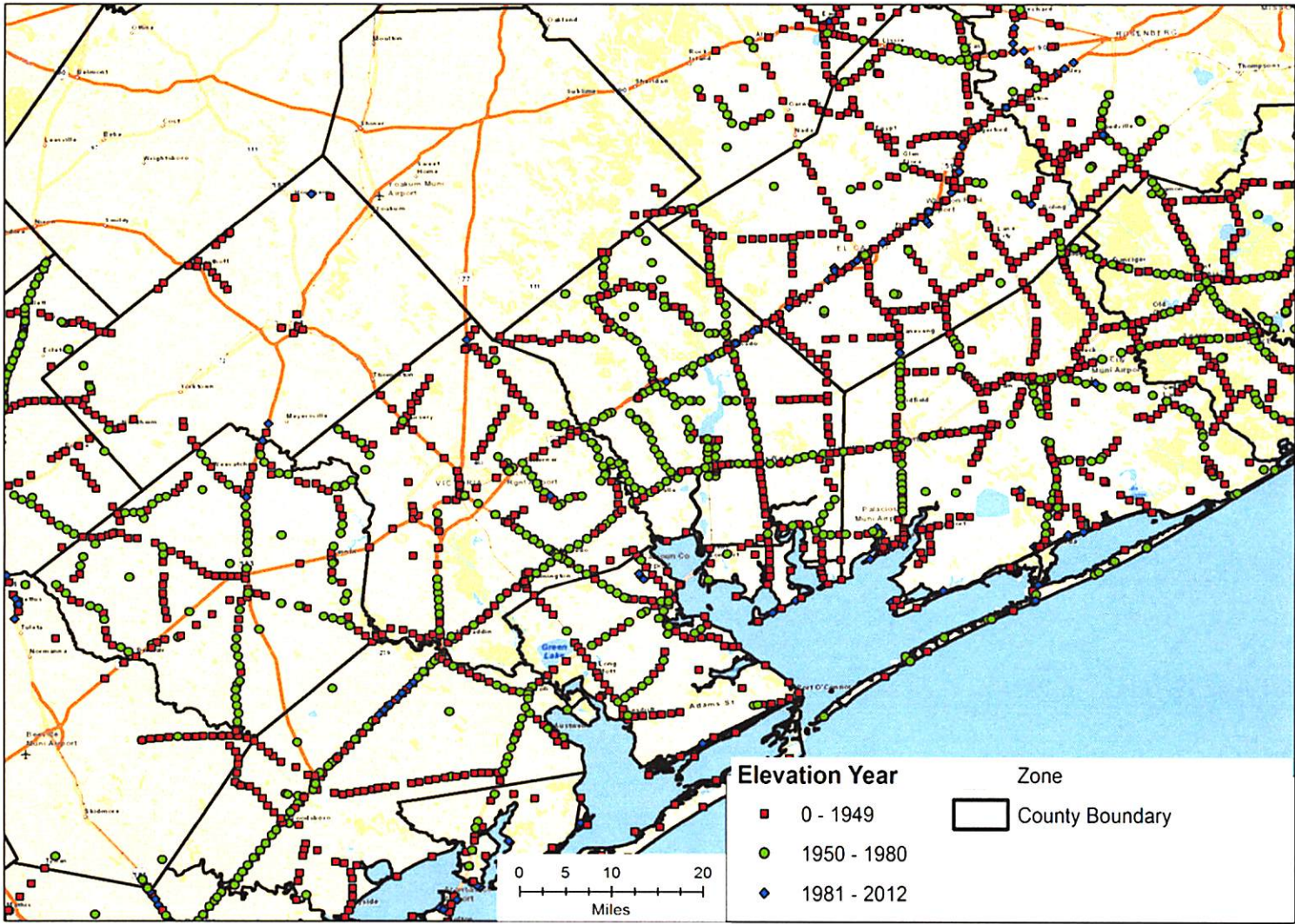
Figure 5-3   The dataset of NGS benchmark PIDS downloaded from http://geodesy.noaa.gov/ and used for the study.
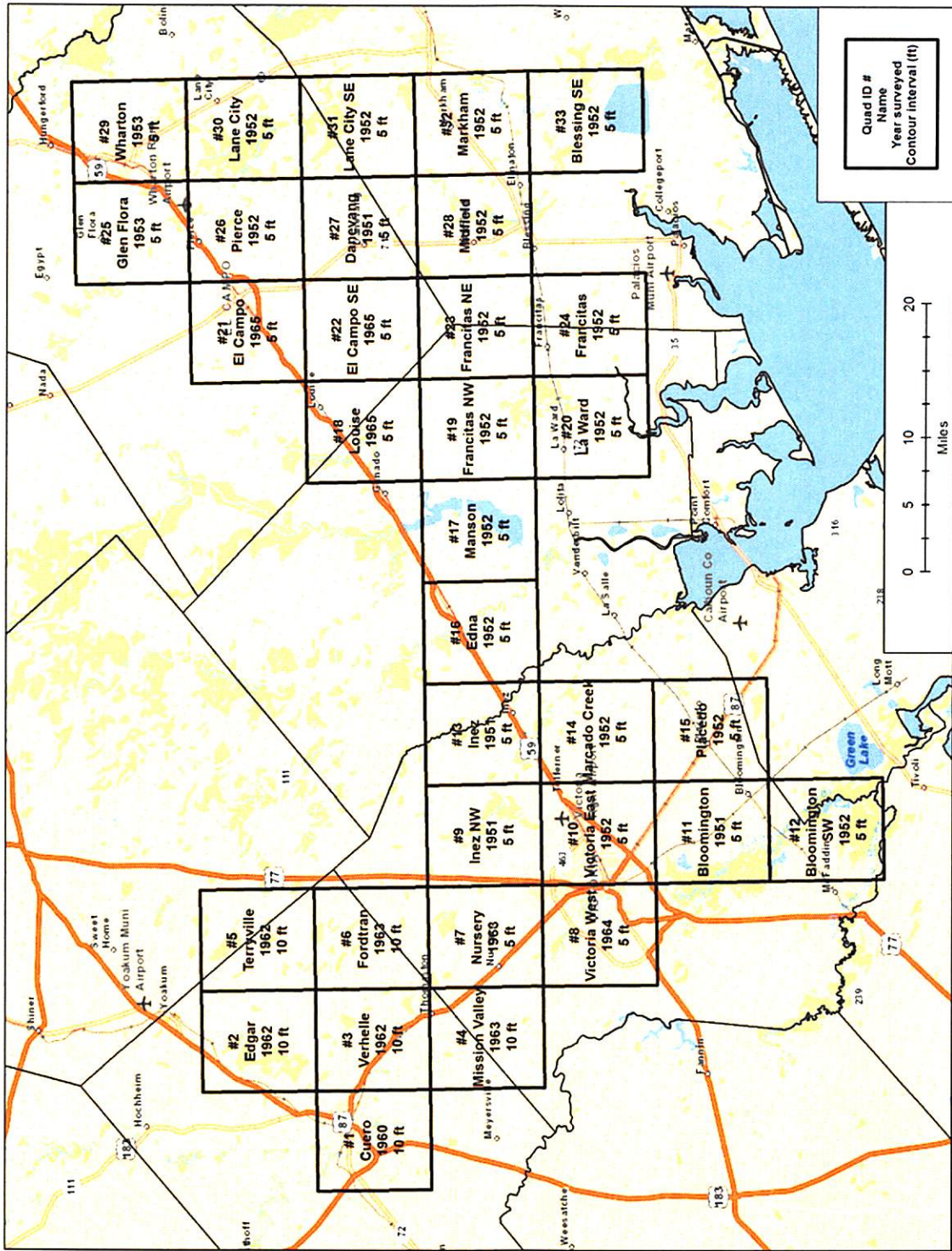
Figure 5-4 The location of 33 USGS Quadrangle Maps from the http://www.usqs.gov/ used for the study

Figure 5-5   The location of the LIDAR data obtained from TNRIS and HALFF & Associates and used for the study
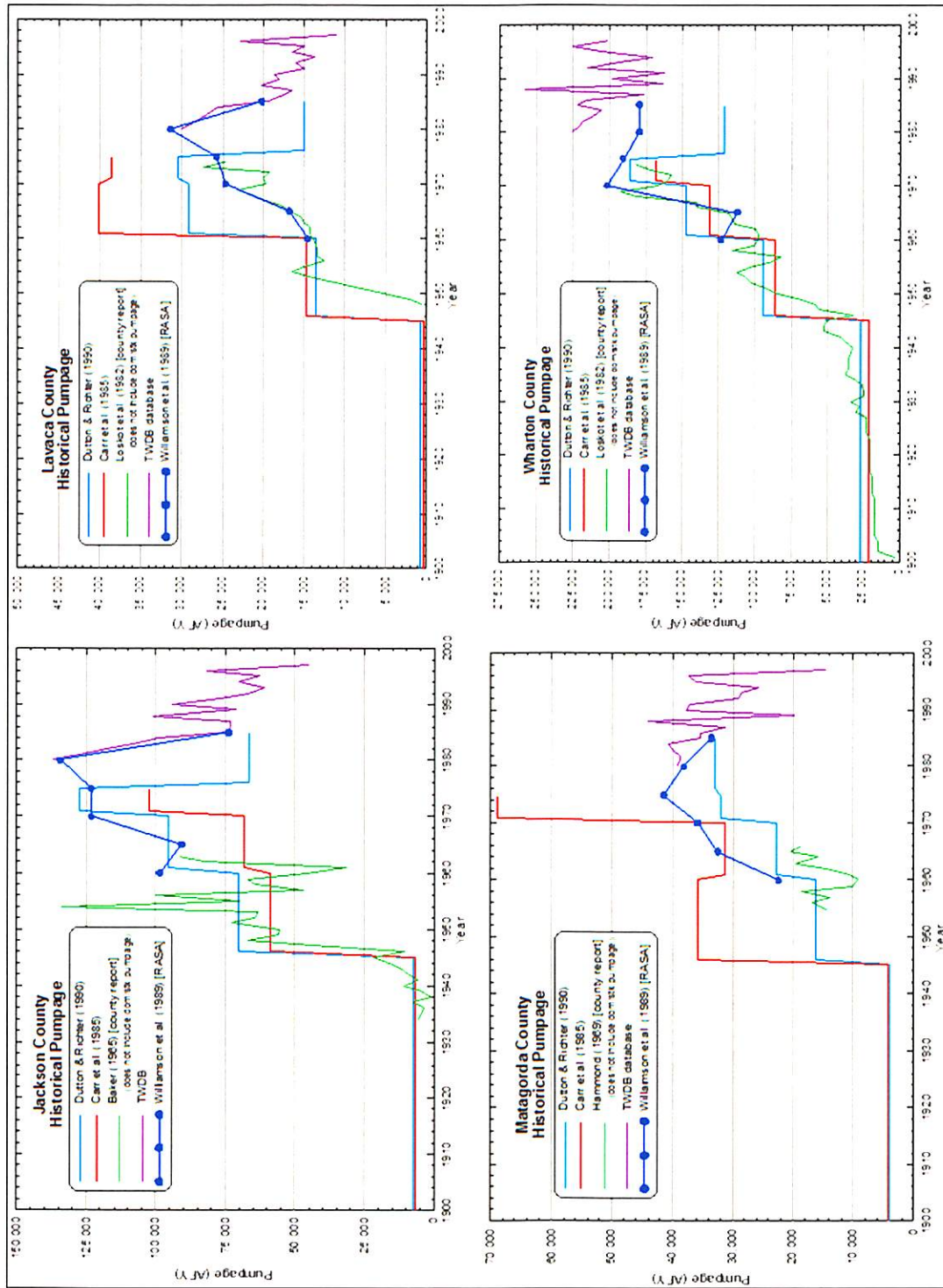
Figure 5-6 Historical pumping totals from 1900 to 2000 for Jackson, Matagorda, Wharton, and Lavaca counties used by Young an others (2006) as part of the development of the site conceptual model for the LCRB model (figures from Young and others, 2006).
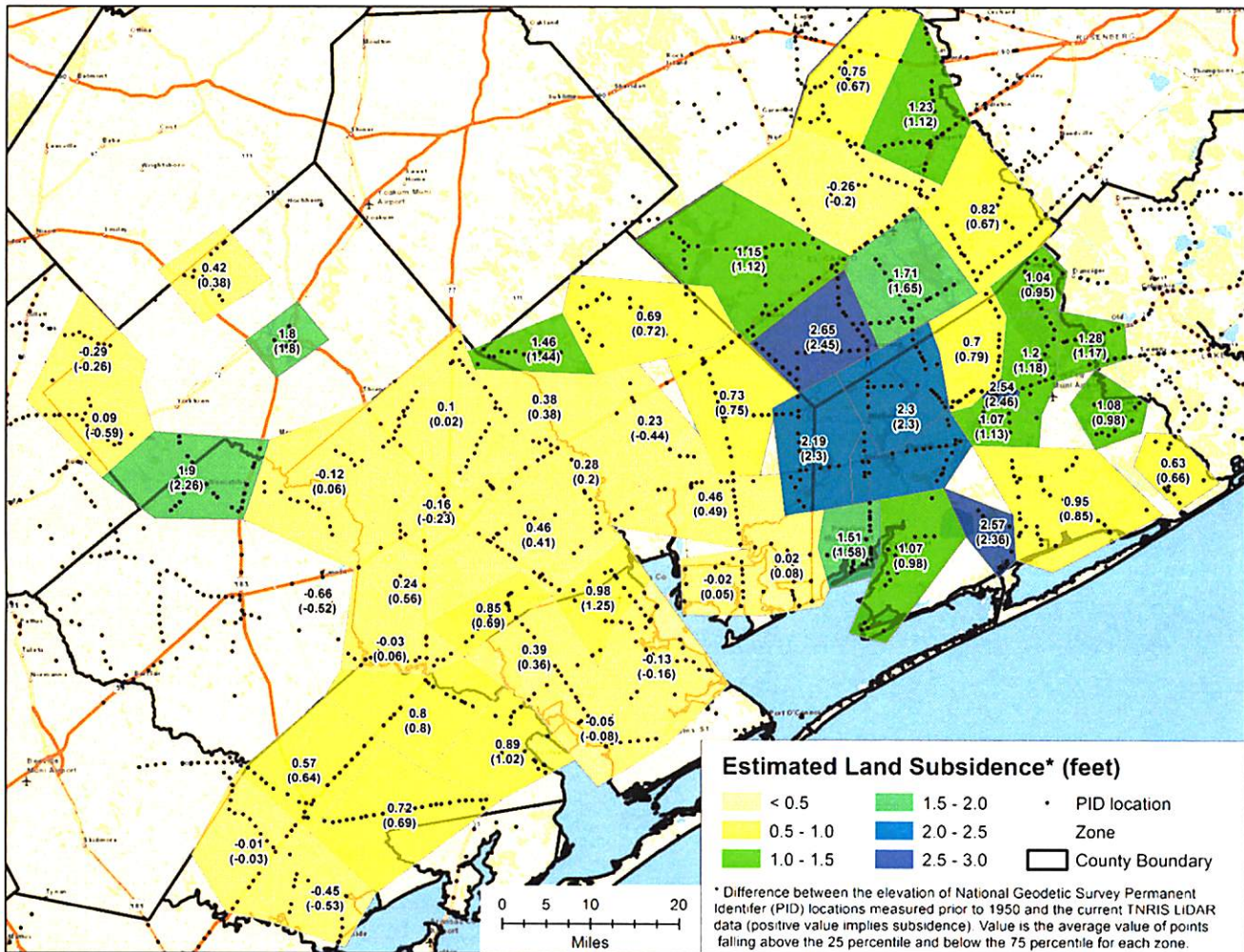
Figure 5-7   Estimated average land subsidence from before 1950 to after 2003 for specific polygons as determined by the difference between ground surface elevation from PIDs surveyed prior to 1950 and from LIDAR surveys after 2006 at the locations of the PIDs. Land Subsidence values are expressed as averages and medians (in parenthesis) of the differences calculated at PIDS located inside the polygons. Positive values indicate lower ground surface elevation at later time. Negative values indicate higher ground surface elevation at later time.
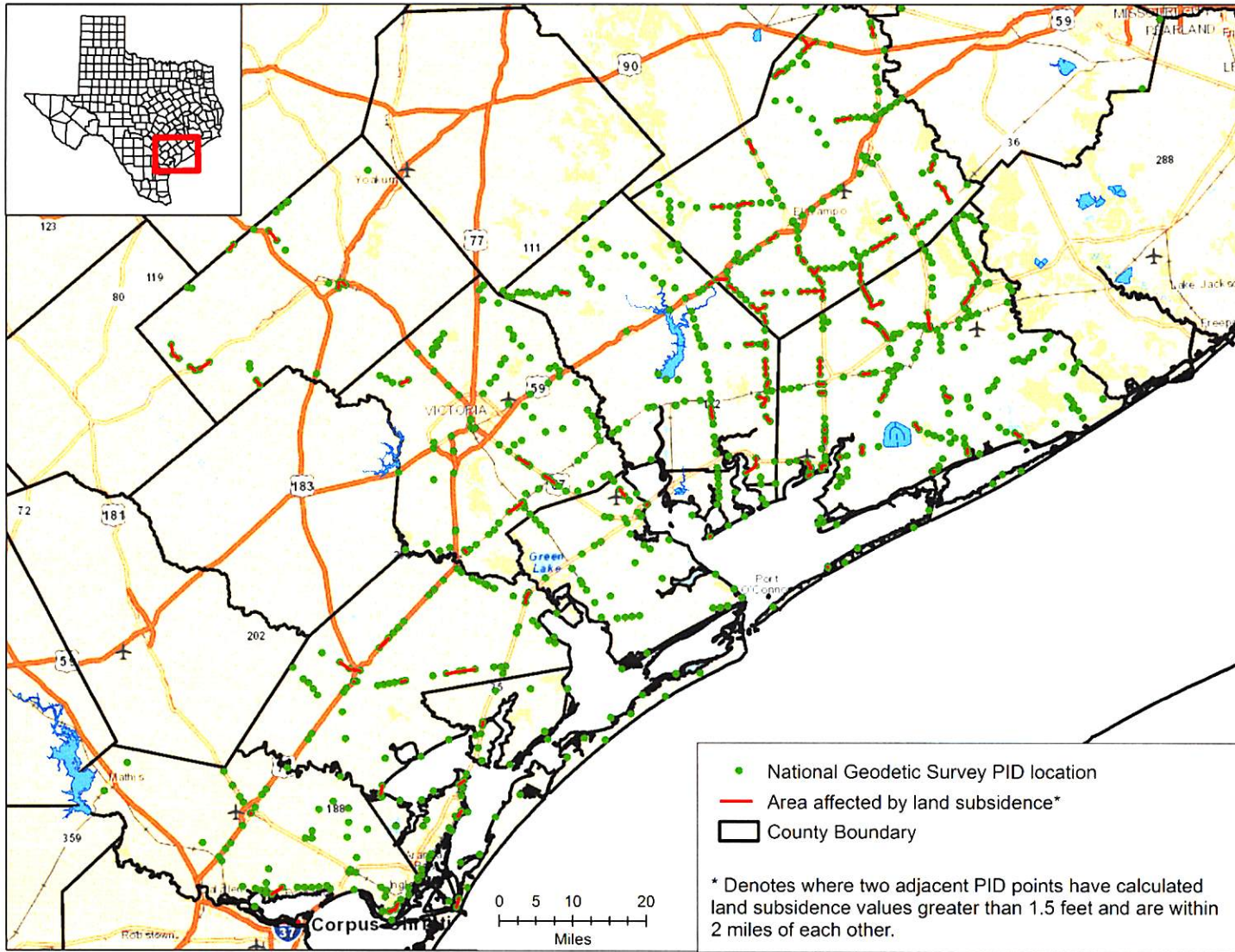
Figure 5-8   Locations of NGS PIDs where calculated land subsidence is greater than 0.5 ft and where nearby PIDs have calculated subsidence values greater than 1.5 ft
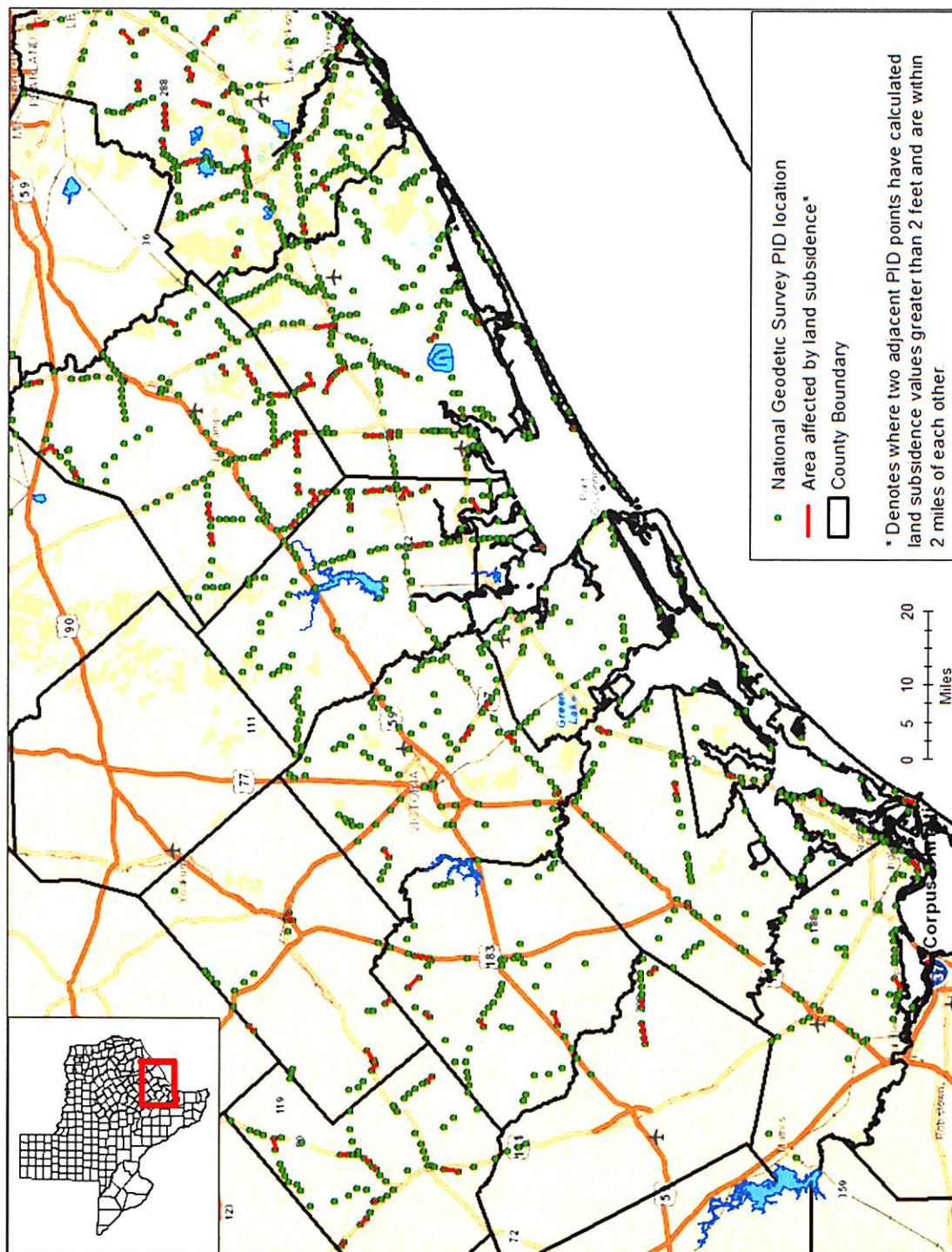
Figure 5-9 Locations of NGS PIDs where calculated land subsidence is greater than 0.5 ft and where calculated subsidence values greater than 2.0 ft

Legend:
- National Geodetic Survey PID location
- Area affected by land subsidence*
- County Boundary

*Denotes where two adjacent PID points have calculated land subsidence values greater than 2 feet and are within 2 miles of each other
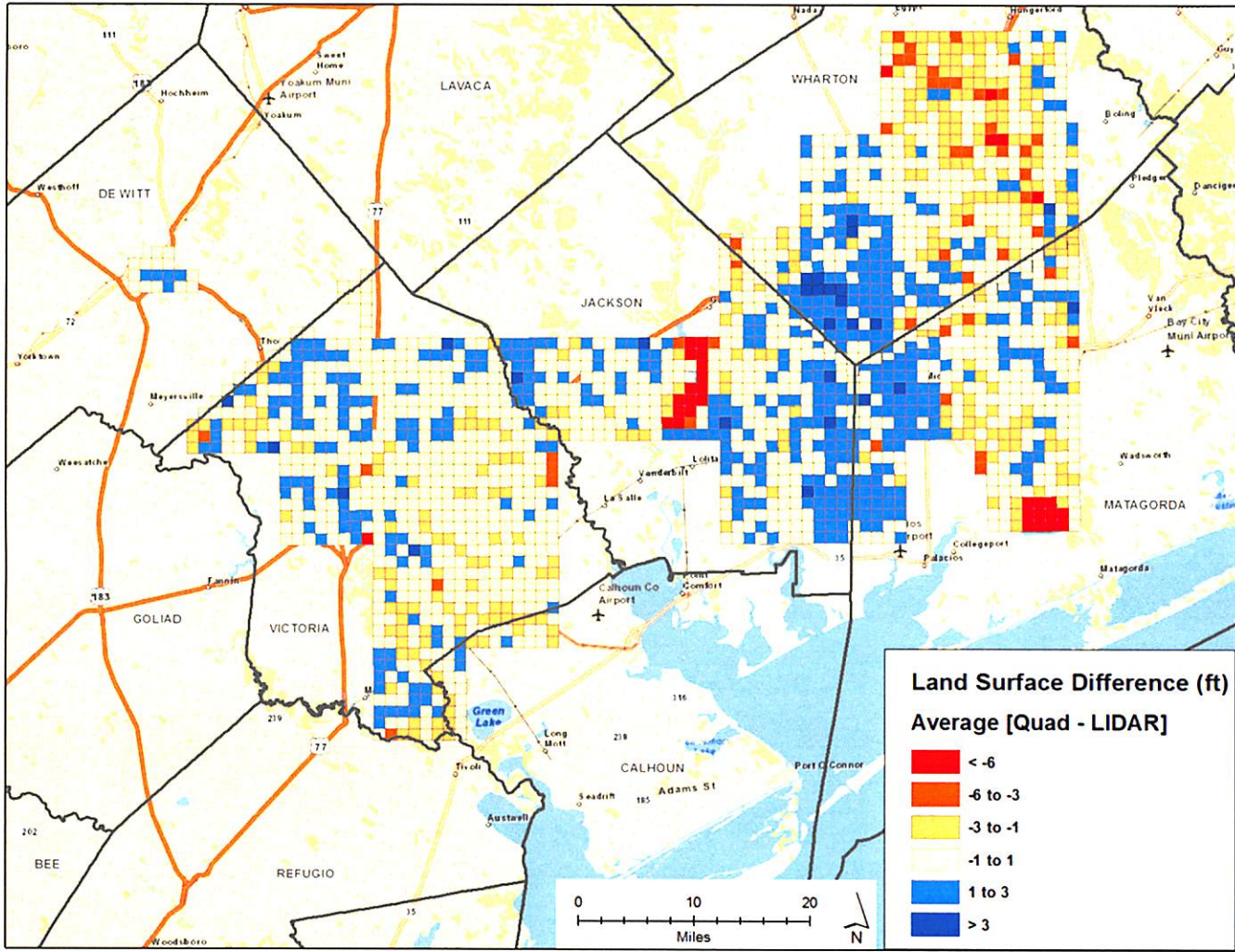
Figure 5-10 Estimated average land subsidence for 1 square mile areas as determined by the difference between ground surface elevation from USGS quadrangle maps constructed between 1950 and 1965 and from TNRIS LIDA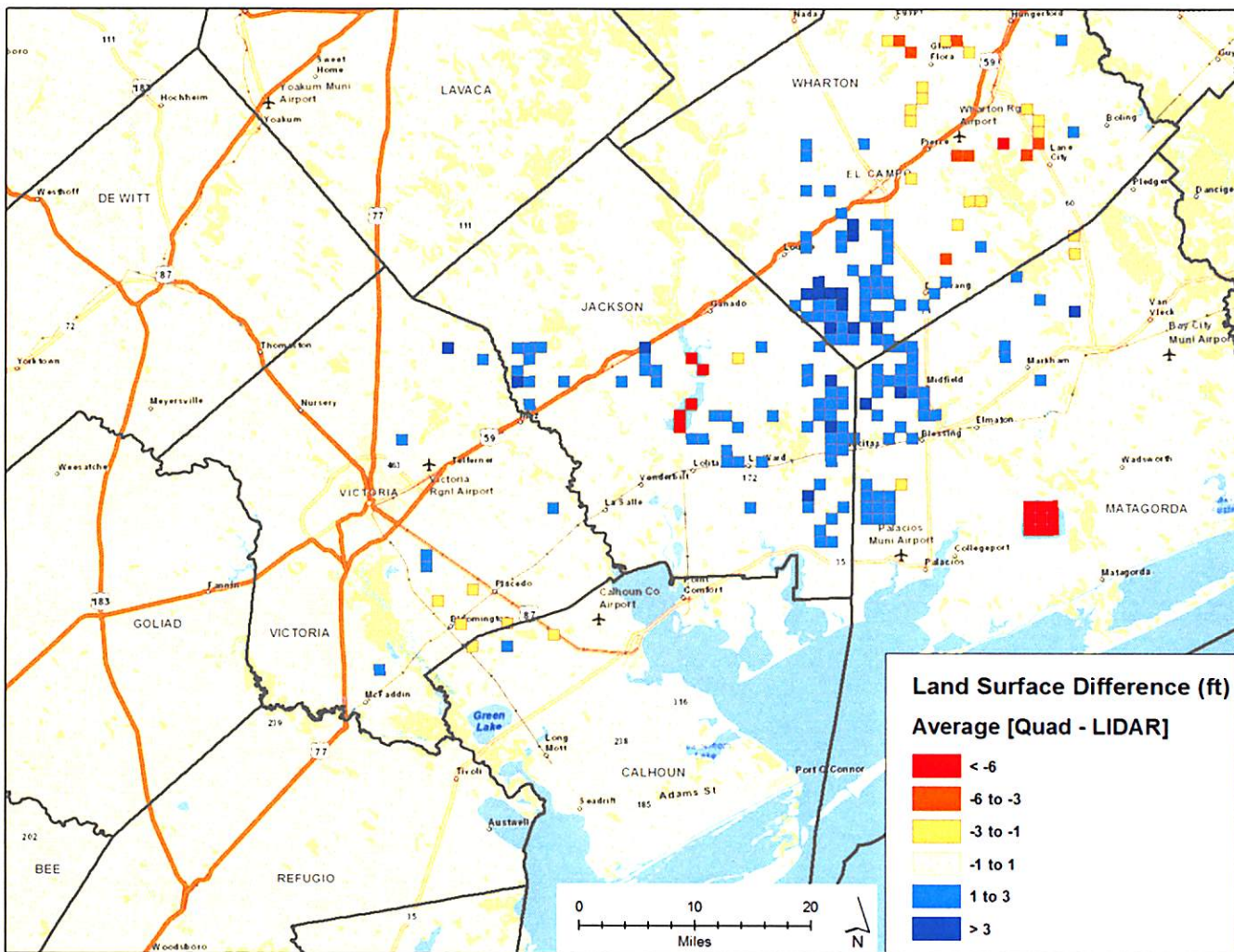R surveys conducted after 2006. Land Subsidence values are averages of approximately 100 point locations distribution on a 500 ft grid. Positive values indicate lower ground surface elevation at later time. Negative values indicate higher ground surface elevation at later time. .
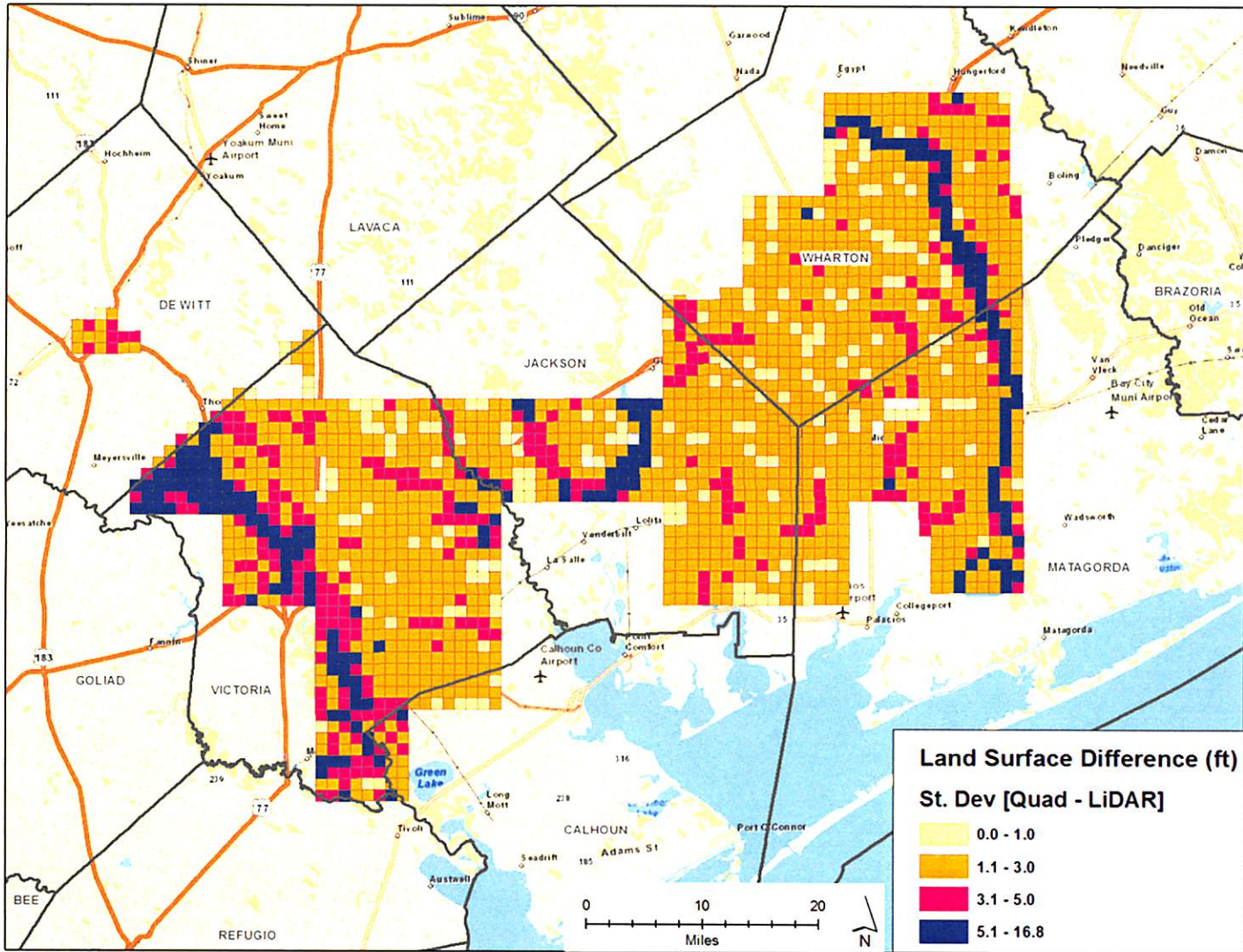
Figure 5-11   Estimated standard deviation of approximately 100 values of land subsidence per square mile. Land subsidence determined by the difference between ground surface elevation from USGS quadrangle maps constructed between 1950 and 1965 and from TNRIS LIDAR surveys conducted after 2006. Land Subsidence values calculated on a 500 ft grid.

Figure 5-12 Estimated average land subsidence based on approximately 100 points as determined for 1 square mile squares where the coefficient of variation is less than 0.75. Land subsidence calculated on a 500 ft grid by the difference between ground surface elevation from USGS quadrangle maps constructed between 1950 and 1965 and from TNRIS LIDAR surveys conducted after 2006. Positive values indicate lower ground surface elevation at later time. Negative values indicate higher ground surface elevation at later time

6.0 SCOPING CALCULATIONS FOR PREDICTING SUBSIDENCE

This section provides an approach for performing scoping calculations to estimate how much land subsidence will occur as a result of future pumping. The approach is based on a one-dimensional solution of clay consolidation developed by Terzaghi (1925). Application of the approach requires an estimate of future drawdown in the aquifer, the total thickness of clay in the aquifer, and a value for the compressibility coefficient for clays in the aquifer The section provides used the approach to predict land subsidence at fourteen sites in GMA 15 based on results from GAM runs, on the aquifer clay thicknesses from Young and others (2010; 2012), and clay compressibility coefficients developed by Gabrysch (1982).

6.1 Objective

The objective of the scoping calculation is to provide GCDs a means to evaluate the likelihood of land subsidence occurring based on projected pumping. The scoping calculations are not intended to provide anything more than a first-order approximation. The requirements imposed on the scoping calculations are the following:

- The inputs for the calculations represent measurable quantities that can be estimated from a hydrogeological description of the aquifer system.

- The calculations are based on the principles of consolidation of clays as explained by Terzaghi (1925).

- The calculations are easily performed without specialized software or computers.

- The calculations produce land subsidence values that are consistent and in general agreement with the findings of this report.

- The calculations are based on assumptions that are not overly restrictive as to prevent the widespread application in GMA 15.

6.2 Approach

The approach is based on the equations that MODFLOW IBS Package (Leake and Prudic, 1991) and MODFLOW SUB Package (Hoffman and others, 2003) use to calculate land subsidence. The approach requires that **Equation 6-1** be applied piecemeal though different aquifers to the base of the Gulf Coast Aquifer System. An application to the entire Gulf Coast Aquifer System would require solving Equation 6-1 for the Chicot Aquifer, the Evangeline Aquifer, the Burkeville Confining Unit, and the Jasper Aquifer.

$$\Delta b = \Delta d * \alpha_{eff} * C_t \qquad \text{(Eq. 6-1)}$$

Where:

Δb = Amount that the aquifer thickness has compacted

Δd = Amount of drawdown in the aquifer since predevelopment

α_{eff} = Effective compressibility coefficient for clays in the aquifer

C_t = Total thickness of the clay units in the aquifer

The solution to Equation 6-1 requires values for drawdown, clay thickness, and compressibility coefficient. Discussed below are data options for these input variables.

6.2.1 Drawdown Data

The change in drawdown in Equation 6-1 can be determined from measured or simulated drawdowns. **Figures 6-1** to **Figure 6-4** show contours of simulated drawdown by the Central Gulf Coast GAM (Chowdhury and others, 2004). The figures display the drawdown in GMA 15 for the four model layers for years 2000 and 2070. The four model layers represent the Chicot Aquifer, the Evangeline Aquifer, the Burkeville Confining Unit, and the Jasper Aquifer. In the figures, the drawdown is measured from 1940, which is the starting year in the GAM simulation that represents predeveloping conditions, when no pumping is simulated by the model. The drawdowns for 2000 are based on the GAM Run performed by Chowdhury and others (2004). The drawdowns for 2070 are based on a GAM Run performed by INTERA and submitted to the TWDB as a basis for provisional Desired Future Conditions (DFC) on October 21, 2015 (Young, 2015). For each of the four model layers, the figures provide a continuous set of drawdown values across GMA 15. Estimates of drawdown can be visually estimated from the figures or can be extracted at a specific location using software that reads MODFLOW output files.

6.2.2 Clay Thickness Data

The TWDB conducted two projects (Young and others, 2010; 2012) to update the stratigraphic and lithologic characterization of the Gulf Coast Aquifer System. Based on the analysis of over 1,000 geophysical logs, the projects redefined the upper and lower boundaries and constructed sand thickness maps for the hydrostratigraphic units that comprise the Gulf Coast Aquifer System.

Figures 6-5 through **Figure 6-8** provide clay thickness maps based on the sand and clay profiles produced by Young and others, (2010; 2012) for the Chicot Aquifer, Evangeline Aquifer, the Burkeville Confining Unit, and the Jasper Aquifer, respectively. For each of the geological units, the clay thicknesses increase to the coast. This trend primarily occurs because the nits thicken in the down-dip direction. Along the coast, the maximum clay thicknesses for the Chicot Aquifer, Evangeline Aquifer, the Burkeville Confining Unit, and the Jasper Aquifer are approximately 750 ft, 2,000 ft, 500 ft, and 3,000 ft, respectively.

For each of the four model layers in the GAM, the figures provide a continuous set of clay thickness values that can be used to estimate the drawdown occurring at any location in GMA 15. Estimates of drawdown can be visually estimated from the figures or can be extracted for a specific location using software that reads geographic information system (GIS) files submitted to the TWDB by Young and others (2010; 2012).

6.2.3 Clay Compressibility Values

Several sources of values for compressibility coefficients are available for use in Equation 6-1. They include values from the field tests performed by Gabrysch (1982), from the calibration of the HAGM (Kasmarek,

2012), and from laboratory tests (McClelland Engineering, 1979). For the purpose of this report, we will use values provided by Gabrysch (1982), which are provided in Table 3-2. Table 3-2 provides compaction coefficient values calculated from ten sites in the Harris-Galveston based on measured clay thickness, drawdown, and land subsidence. The values range between $7.2 \times 10^{-6} \text{ft}^{-1}$ and $4.0 \times 10^{-5} \text{ft}^{-1}$. The arithmetic average and geometric average of the values are $2.1 \times 10^{-5} \text{ft}^{-1}$ and $1.8 \times 10^{-5} \text{ft}^{-1}$, respectively.

6.3 Predicted Land Subsidence

To demonstrate scoping calculation for predicted land subsidence, fourteen sites were selected. These sites are mapped in **Figure 6-9**. **Table 6-1** presents the drawdown and clay thicknesses associated to each location. The drawdown information was extracted at the location of each site from the MODFLOW output files used to generate Figures 6-1 to 6-4. The drawdown information was extracted at the location of each site from the GIS files used to generate Figures 6-5 to 6-8. The calculated subsidence for 1940 to 2000 ranges from 0.1 foot to 3.2 ft. The calculated land subsidence values at the fourteen locations were compared to the calculated land subsidence based on data provided in Section 5.0. The calculated values are consistent and in general agreement with the field measured values. The land subsidence predicted in 2070 is provided as a scoping calculation for the additional land subsidence that future pumping will cause. It should be note that the land subsidence values for 2070 are based solely on drawdown in 2070. No checks were performed to identify whether or not a greater drawdown than the 2070 drawdown occurred between 2000 and 2070.

Table 6-1 Use of Equation 6.1 to predict land subsidence at fourteen sites in GMA 15 for the years 2000 and 2070 based on a α_{eff} of $2.0 \times 10^{-5} \text{ft}^{-1}$ using drawdown simulated by the Central Gulf Coast GAM (Chowdhury and others, 1999) and clay thickness data from Young and others (2010; 2012)

| ID | County | Drawdown (ft) | | | | | | | | Clay Thickness (ft) | | | | Land Subsidence (ft) | |
		Chicot		Evangeline		Burkeville		Jasper		Chicot	Evangeline	Burkeville	Jasper	1940-2000	1940-2070
		1940-2000	1940-2070	1940-2000	1940-2070	1940-2000	1940-2070	1940-2000	1940-2070						
1	Calhoun	7.4	3.4	12.4	18.9	-	-	-	-	226	1299	418	925	0.4	0.5
2	Calhoun	-0.8	2.2	22.9	40.6	-	-	-	-	369	1442	407	1377	0.7	1.2
3	Dewitt	-	-	0.8	1.0	3.4	9.8	7.9	24.1	-	349	318	516	0.1	0.3
4	Dewitt	-	-	9.5	15.6	51.7	73.0	142.3	185.2	-	116	331	537	1.9	2.5
5	Jackson	18.7	55.7	64.7	88.1	39.2	56.3	22.0	45.4	139	683	224	618	1.4	2.2
6	Jackson	12.1	32.4	55.9	78.4	33.0	52.6	-	-	360	1096	339	966	1.5	2.3
7	Matagorda	-1.7	1.2	39.4	57.4	-	-	-	-	482	1569	652	1220	1.2	1.8
8	Matagorda	2.1	0.8	37.9	49.0	13.1	27.0	-	-	203	1264	415	1400	1.1	1.5
9	Refugio	5.2	1.8	3.4	10.1	-0.1	3.9	-	-	128	835	270	722	0.1	0.2
10	Refugio	0.3	1.2	4.1	15.5	-	-	-	-	264	1141	264	726	0.1	0.4
11	Victoria	5.0	8.0	13.2	40.1	1.7	6.4	-	-	207	757	225	550	0.2	0.7
12	Victoria	27.0	34.9	45.3	52.5	38.0	43.9	26.2	33.0	108	605	190	785	1.2	1.4
13	Wharton	75.4	94.1	156.7	149.8	61.9	90.2	27.9	59.9	84	780	266	610	3.2	3.7
14	Wharton	8.7	27.5	57.4	91.0	44.5	80.9	38.2	72.2	78	599	287	842	1.6	2.8
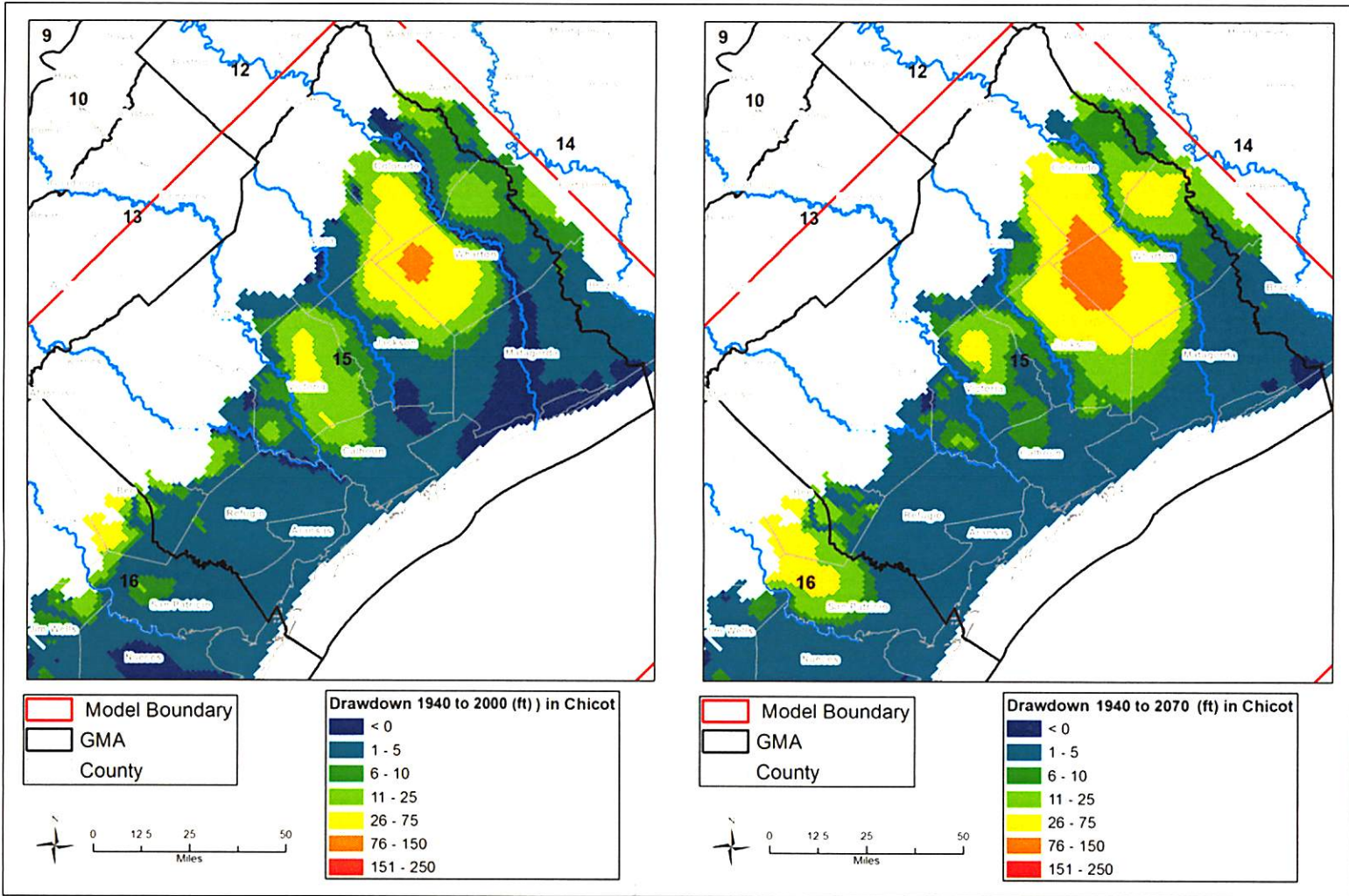
Figure 6-1   Drawdown in the Chicot Aquifer simulated by the Central Gulf Coast GAM based on the GMA 15 DFC Baseline Run #1 well file for the period 1940 to 2000 and for the period 1940 to 2070
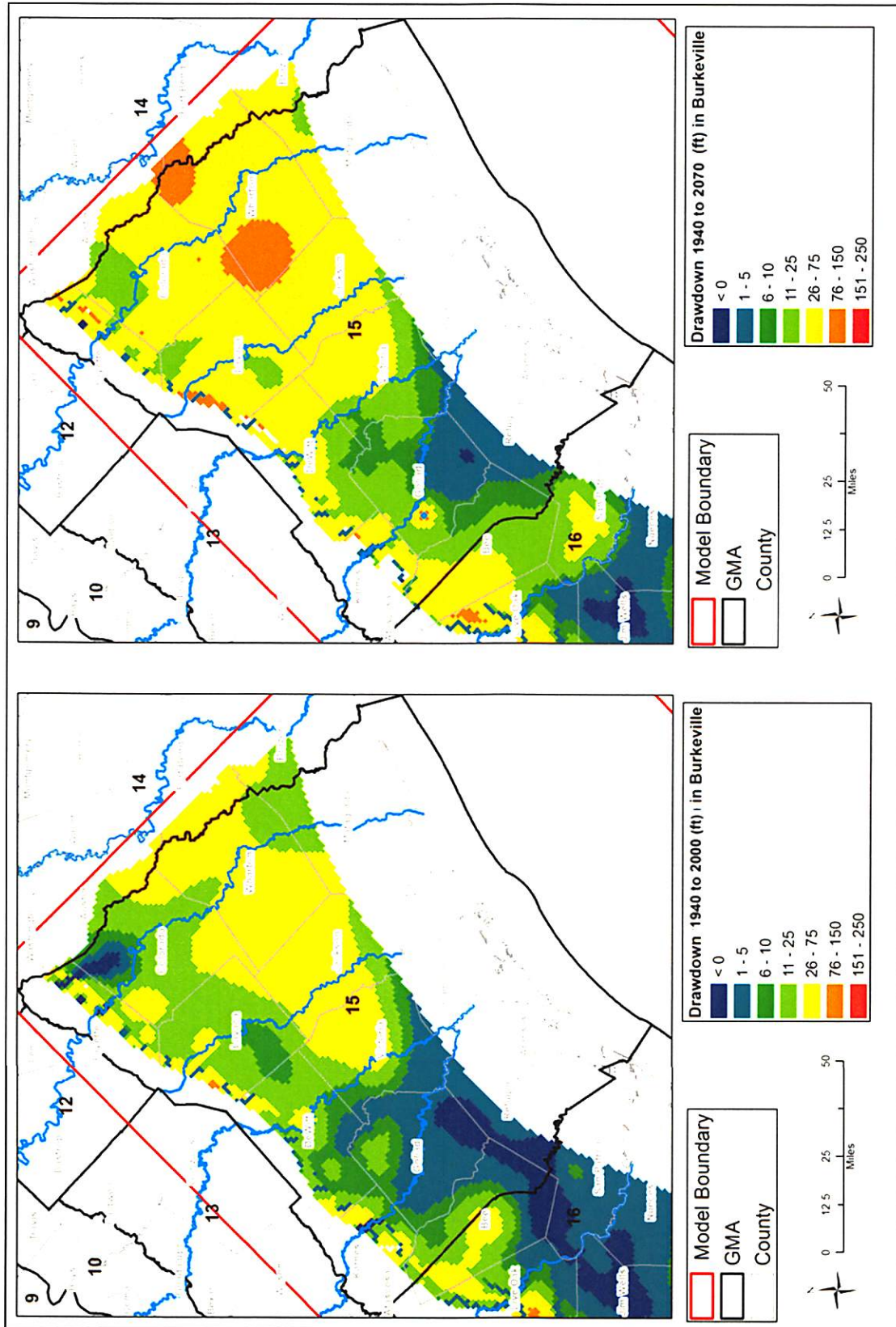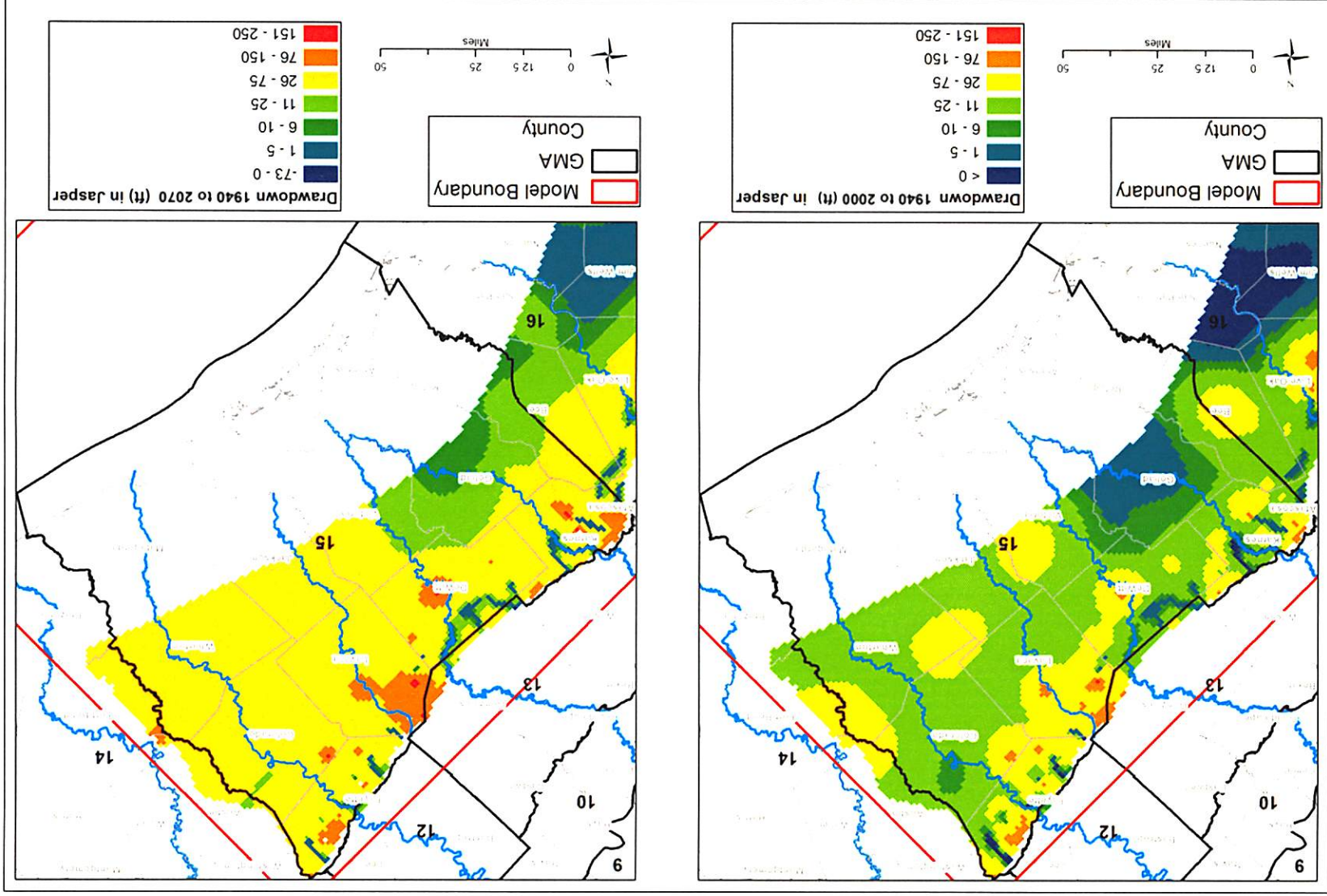
Figure 6-3   Drawdown in the Burkeville Confining Layer simulated by the Central Gulf Coast GAM based on the GMA 15 DFC Baseline Run #1 well file for the period 1940 to 1999 and for the period 1940 to 2070

Figure 6-4 Drawdown in the Jasper Aquifer simulated by the Central Gulf Coast GAM based on the GMA 15 DFC Baseline Run #1 well file for the period 1940 to 2000 and for the period 1940 to 2070

Estimates of Land Subsidence in GMA 15
Based on Ground Surface Elevation Data
and Models
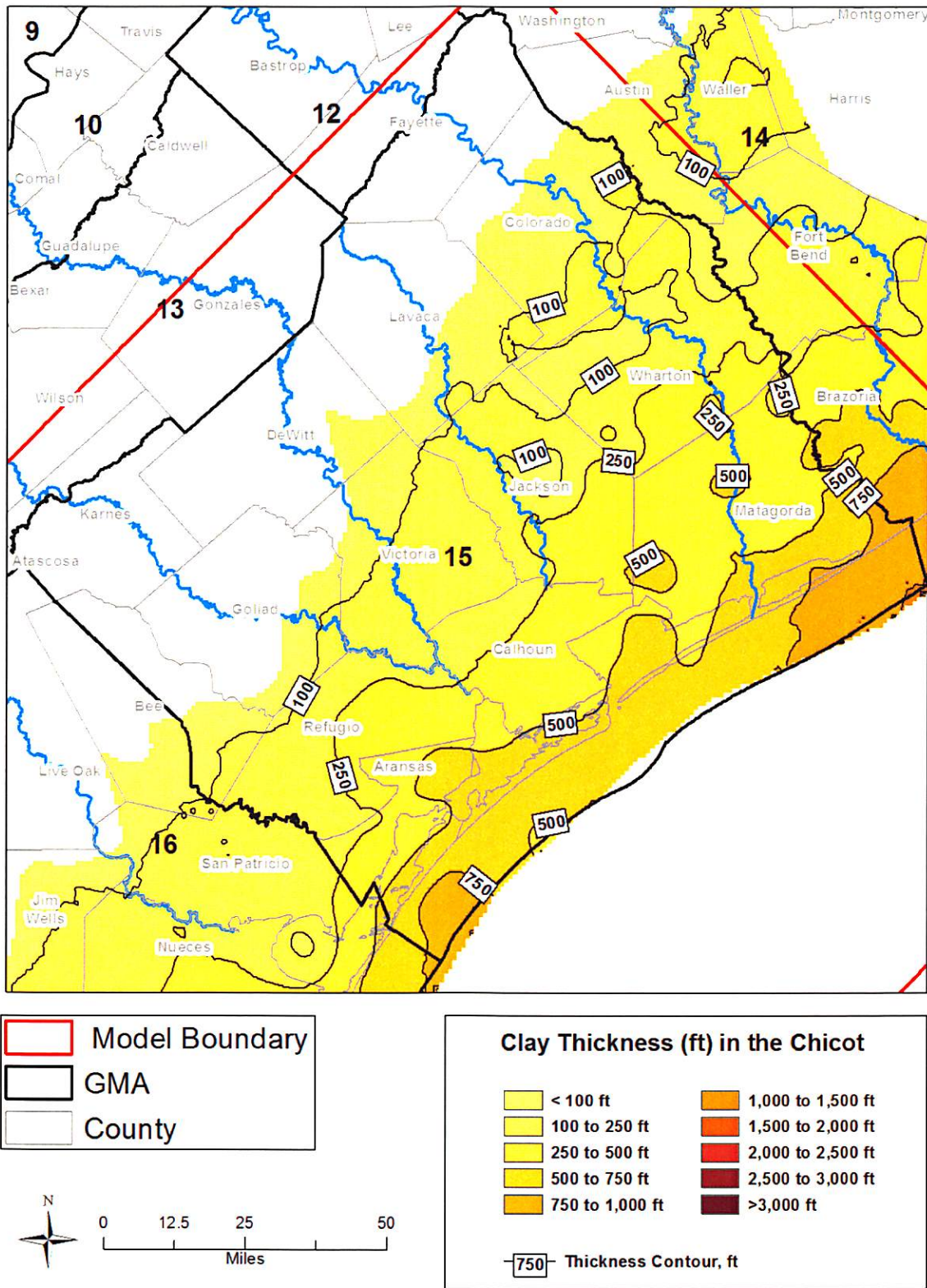
Figure 6-5 Clay thickness in the Chicot Aquifer based on lithology data from Young and others (2010)

Figure 6-6 Clay thickness in the Evangeline Aquifer based on lithology data from Young and others (2010)

Figure 6-7   Clay thickness in the Burkeville Confining Unit based on lithology data from Young and others (2010)

Estimates of Land Subsidence in GMA 15
Based on Ground Surface Elevation Data
and Models   77   February 3, 2016
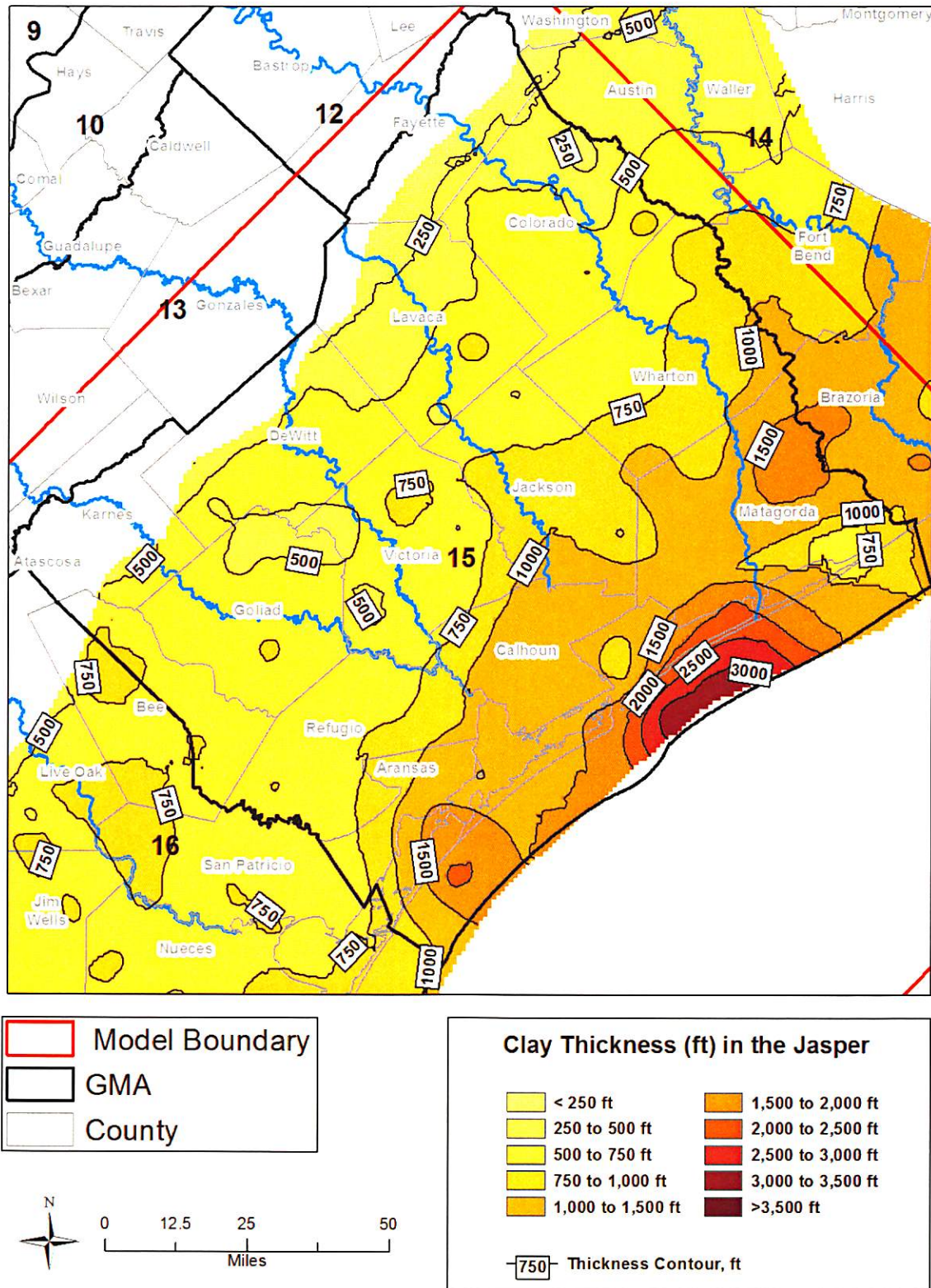
Figure 6-8   Clay thickness in the Jasper Aquifer based on lithology data from Young and others (2010)
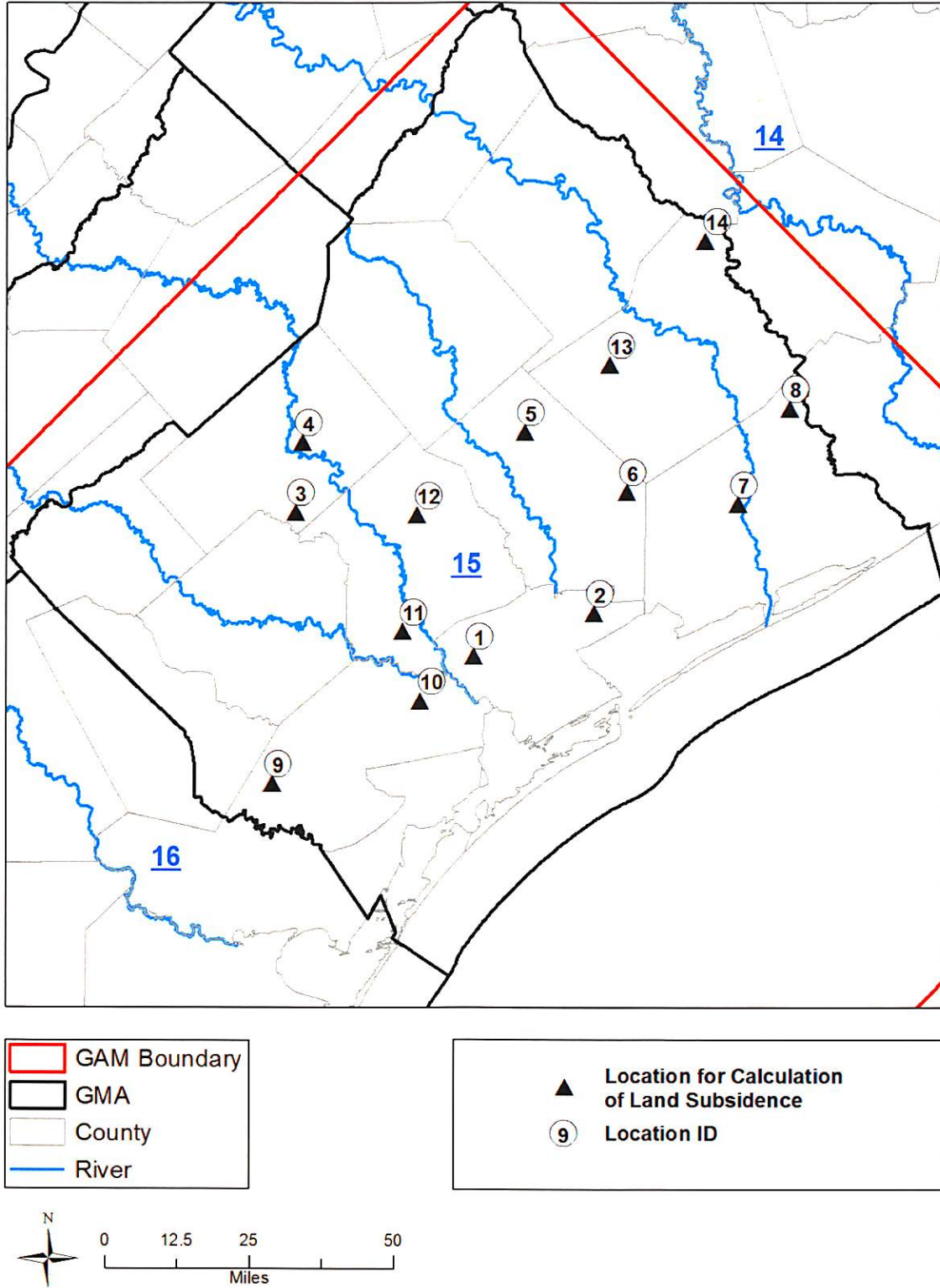
Figure 6-9 Locations in GMA 15 where land subsidence is calculated in Table 6-1.

7.0 MONITORING METHODS FOR LAND SUBSIDENCE

The monitoring of land subsidence in the Harris-Galveston has been ongoing for almost a century, beginning with Pratt and Johnson (1926) documenting subsidence in the vicinity of the Goose Creek oil fields. Listed below is a summary of monitoring methods and their evolution through time.

7.1 Releveling Surveys

Prior to the advent of Global Positioning System (GPS) technology, the standard practice for measuring land surface subsidence was to perform periodic releveling of surveyed benchmarks. The primary agency responsible for performing the releveling historically has been the USCGS and its successor agency, the NGS. The NGS releveling consisted of conventional differential leveling at the highest accuracy level rating. Simple algebraic subtraction along level lines yielded the subsidence that occurred between any two releveling epochs. A releveling epoch performed by the HGSD before the late 1980s involved about 2,500 locations and cost about $1,170,000 (2001 dollars) (Zilkoski and others, 2003.) The high cost of a releveling epoch partly accounts for the lack of releveling epochs across much of the Gulf Coast since the 1950s.

7.2 Extensometers

Extensometers can be considered as deeply anchored benchmarks. **Figure 7-1** shows a schematic of a borehole extensometer. The construction of an extensometer begins with drilling a borehole to a depth at which the strata are considered stable, such traditionally has been assumed to be the base of the Evangeline Aquifer in the Harris-Galveston area. The borehole is then lined with a steel casing with slip-joints to prevent it from crumpling as subsidence occurs. An inner pipe rests on a concrete plug at the bottom of the borehole and extends to the top. This inner pipe then transfers the stable elevation below to the surface. A measurement of the distance from the inner pipe to the surrounding land surface provides the amount of compaction that has occurred. A chart recorder provides a continuous record of subsidence over time. The USGS began installing extensometers in the Harris-Galveston region in the early 1960s. Borehole extensometers provide excellent subsidence data, but their high cost prohibits their use in sufficient numbers to provide adequate information for an entire study area. Zilkoski and others (2003) estimate the average cost of an extensometer at approximately $800,000 in 2001 dollars.

7.3 GPS–based Methods

In 1993, the HGSD and the NGS signed a cooperative agreement to jointly pursue improved, less expensive methods of monitoring land-surface subsidence in the Houston area. This agreement supported an experimental study using a GPS to measure subsidence. The study involves a network of fixed location and mobile GPS measuring set-ups. The fixed location set ups are called Continuously Operating Reference Stations (CORS). The first CORS were established at the extensometers. Currently, there are more than 40 CORS in the Houston area (Wang and Soler, 2014).

The mobile units are referred to as Port-A-Measure (PAM) units. The GPS measurements at the extensometer locations are used as reference benchmarks for the measurements at the mobile GPS locations. The first PAM units began collecting data in January 1994. The PAM network has been continuously expanded, and the number of total stations was 80 as of 2014 (Wang and others, 2015). Each PAM unit includes a trailer, its own power supply, and a cellular phone. The PAM sites use dual-frequency, full-wavelength GPS instruments (with geodetic antennas), to collect data at 30-second intervals, which is then averaged over 24 hours. That means that specific stations being monitored can be assessed on a daily basis. The vertical accuracy is "plus or minus" one centimeter.

One of the monitoring issues that can affect the measurement of ground surface elevation in the Houston area is the clay-rich soils with a high shrink-swell potential (vertisols). The soil-moisture active zone, the depth at which large variations in soil moisture cause shrink-swell behavior, can extend 4 to 6 m (15 to 20 ft) below the surface. Measurements show that as much as 6 to 9 cm (0.2 to 0.3 ft) of vertical movement can occur in a few days, as expansive clay soils respond to seasonal variations in rainfall and temperature (Zilkoski and others, 2003). The reference mark devised for the PAM sites (see **Figure 7-2**) minimizes this movement.
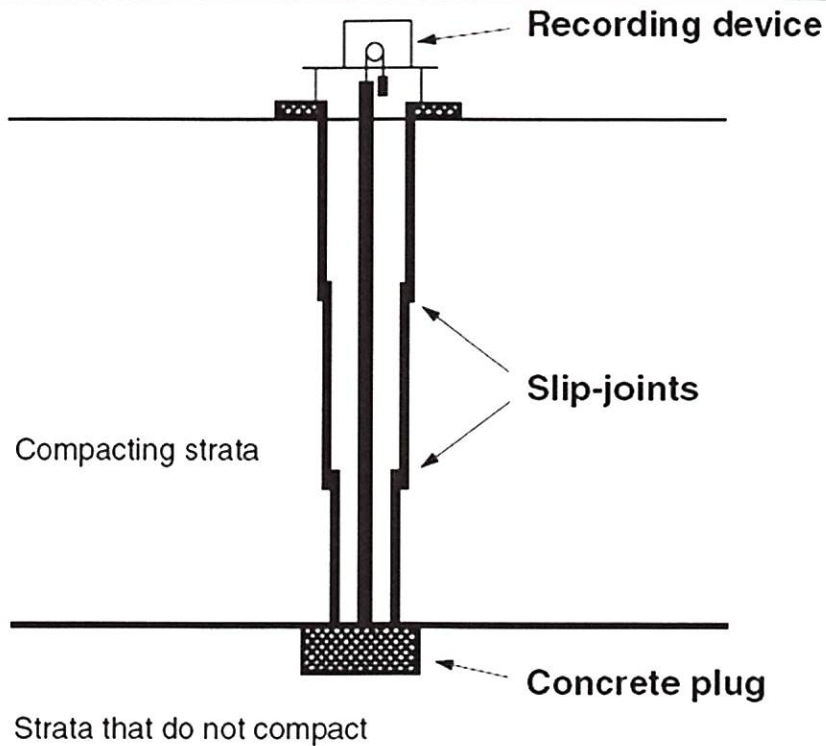
Figure 7-1 Schematic of a Borehole Extensometer Used by the Harris-Galveston Coastal Subsidence District (modified from Zilkoski and others, 2003).
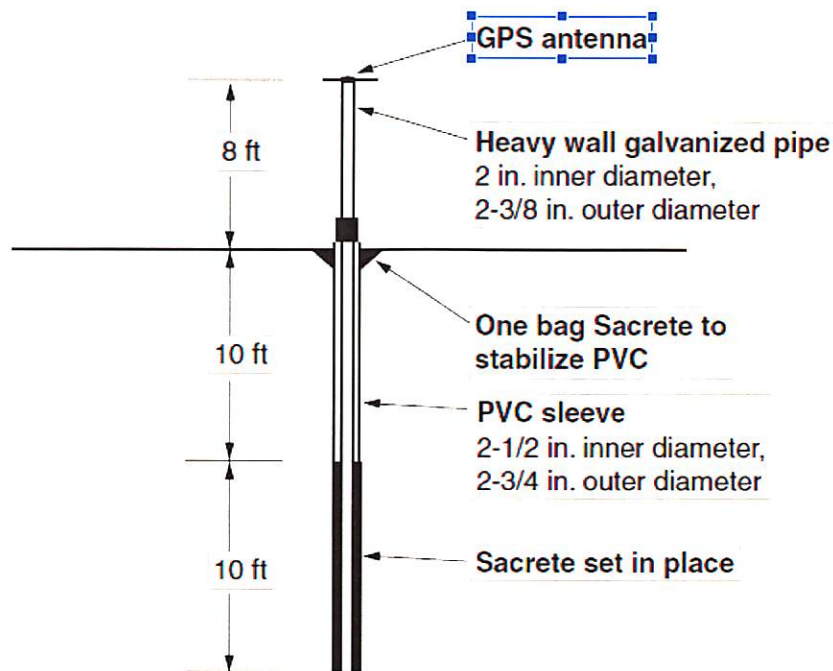
Figure 7-2 Schematic of a Port-A-Measure (PAM) monument (modified from Zilkoski and others, 2003).

8.0 REFERENCES

Anders, R. B. 1960. Ground-water geology of Karnes County, Texas: Texas Board Water Engineers Bulletin 6007, 107 pgs.

Baker, E. T. 1965. Groundwater Resources of Jackson County, Texas: Texas Water Development Board Report 1, 229 p.

Casagrande, A. 1936. The Determination of the Pre-Consolidation Load and Its Practical Significant, Discussion D-34, Proceedings of the First International Conference on Soil mechanics and Foundations Engineering, Cambridge, Vol III, p. 60-64.

Chan, A. and M.D. Zoback. 2007. The Role of Hydrocarbon Production on Land Subsidence and Fault Reactivation in the Louisiana Coastal Zone, *Journal of Coastal Research*, Vol 23, (3). Pg 771-786

Chowdhury, A., S. Wade, R.E. Mace, and C. Ridgeway. 2004. Groundwater Availability of the Central Gulf Coast Aquifer System: Numerical Simulations through 1999: Texas Water Development Board, unpublished report.

Dale, O.C., E. Moulder, and T. Arnow. 1957. Ground-Water Resources of Goliad County, Texas, Bulletin 5711. Texas Board of Water Engineers, Austin. TX

Domenico, P.A. and F.W. Schwartz. 1990. Physical and chemical hydrogeology: New York, NY, John Wiley & Sons, Inc., 824 p.

Ewing, T.E. 1985. Subsidence and Surface Faulting in the Houston-Galveston Area, Texas Related to Deep Fluid Withdrawal. Dorfman MH, Morton RA (eds.) *Geopressured Geothermal Energy*, Proceedings of the Sixth U. S. Gulf Coast Geopressured Geothermal Energy Conference. Pergamon Press, New York pp 289-298

Follett, C.R. and R.K. Gabrysch. 1965. Ground-Water Resources of De Witt County, Texas: Water Commission, Bulletin 6518.

Freeze, R.A. and J.A. Cherry, J.A. 1979. Groundwater: Englewood Cliffs, N.J. Prentice Hall, 604 pp.

Gabrysch, R.K, 1969. Land-Surface Subsidence in the Houston-Galveston Region Texas: Tokyo, Japan, 1969, Proceedings, International Symposium on Land-Surface Subsidence Publication No. 88, AIHS, p. 43-54.

Gabrysch, R. 1975. Land-surface subsidence in the Houston-Galveston region, Texas: Texas Water Development Board Report, 188. 19 p.

Gabrysch, R.K. 1982. Ground-Water Withdrawals and Land-Surface Subsidence in the Houston-Galveston Region, Texas, 1906—1980. United States Geological Survey Open-File Report 82-571, 68 p.

Gabrysch, R.K. and C.W. Bonnet. 1975. Land-Surface Subsidence in the Area of Moses Lake near Texas City, Texas.

Gabrysch, R.K. and C.W. Bonnet. 1976a. Land-Surface Subsidence at Seabrook, Texas: U.S. Geological Survey Water Resources Investigation 76-31, 53 p.

Gabrysch, R.K. and C.W. Bonnet. 1976b. Land-Surface Subsidence in the Area of Moses Lake near Texas City, Texas: U.S. Geological Survey Water-Resources Investigation 76-32, 42 p.

Gabrysch, R.K. and L.S. Coplin. 1990. Land-Surface Subsidence Resulting from Ground-Water Withdrawals in the Houston-Galveston Region, Texas, Through 1987. Report of Investigations No. 90-01, U.S. Geological Survey in cooperation with the Harris-Galveston Coastal Subsidence District.

Gabrysch, R.K. and R. J. Neighbors. 2000. Land-Surface Subsidence and its Control in the Houston-Galveston Region, Texas, 1906-1995: Proceedings of the Sixth International Symposium on Land-Surface Subsidence, Ravenna, Italy, September 24-29, p81-92.

Gabrysch, R. K. and R. J. Neighbors. 2005. Measuring a Century of Subsidence in Houston-Galveston Region, Texas: U.S., in Seventh International Symposium on Land Subsidence, Shanghai, China, October 23-28, 2005, Proceedings 379-387.

Helm, D. C. 1975. One-Dimensional Simulation of Aquifer-System Compaction near Pixley, California: 1. Constant parameters, Water Resources Research, v. 11, no. 3, pg 155-182.

Hammond, W.W. Jr. 1969. Ground-Water Resources of Matagorda County, Texas: Texas Water Development Board Report 91, 163 p.

Hanson, R.T. 1989. Aquifer-System Compaction, Tucson Basin and Avra Valley, Arizona: U.S. Geological Survey Water-Resources Investigations Report 88-4172, 69 p.

Hanson, R.T. and J.F. Benedict. 1994. Simulation of ground-water flow and potential land subsidence, upper Santa Cruz Basin, Arizona: U.S. Geological Survey Water-Resources Investigations Report 93-4196, 47

Holzer, T. L. 1981. Preconsolidation Stress of Aquifer Systems in Area of Induced Land Subsidence, Water Resources Research, Vol 17, No. 3 p. 693-704.

Holzer, T.L. and R.L. Bluntzer. 1984. Land-Surface Subsidence Near Oil and Gas Fields, Houston, Texas. Ground Water, V. 22 (No. 4): 450-459.

Hoffman, J., S. A. Leake, D. L. Galloway, and A. M. Wilson. 2003. MODFLOW-2000 Ground-water Model – User Guide to the Subsidence and Aquifer-System Compaction (SUB) Package. USGS Open-File Report 03-233, United States Geological Survey

Kasmarek, M. C. 2012. Hydrogeology and Simulation of Groundwater Flow and Land-Surface Subsidence in the Northern Part of the Gulf Coast Aquifer System, Texas, 1891-2009. United States Department of the Interior, United States Geological Survey Scientific Investigations Report 2012-5154, 55 p

Kasmarek, M.C. and E. W. Strom. 2002. Hydrogeology and Simulation of Ground-Water Flow and Land-Surface Subsidence in the Chicot and Evangeline Aquifers, Houston Area, Texas. U.S. Geological Survey Water Resources Investigations Report 02-4022, 61 p.

Kasmarek, M.C. and J.L. Robinson. 2004. Hydrogeology and Simulation of Ground-Water Flow and Land-Surface Subsidence in the Northern Part of the Gulf Coast Aquifer System, Texas, United States Department of the Interior, United States Geological Survey Scientific Investigations Report 2004-5102, 111 p.

Khorzad, K. 1999. Land-Surface Subsidence along the Texas Gulf Coast due to Oil and Gas Withdrawal: *Environmental Geosciences*, Vol 6, (3 . p 157.

Khorzad, K. 2000. Land-Surface Subsidence along the Texas Gulf Coast due to oil and gas withdrawal: (Unpublished Master's thesis). The University of Texas at Austin, 84 p.

Kreitler, C. W. 1977. Faulting and Land Subsidence from Ground-Water and Hydrocarbon Production: Houston-Galveston, Texas. in *2nd International Land Subsidence Symposium Proceedings, Anaheim , California, 1976*. International Association of Hydrological Sciences Publication 121. pp. 435-446.

Kreitler, C.W., M.S. Akhter, A.C. Donnelly, and W.T. Wood. 1988. Hydrogeology of Formations Used for Deep-Well Injection, Texas Gulf Coast: Prepared for the USEPA by the Bureau of Economic Geology, University of Texas, Austin.

Kreitler, C.W., M.S. Akhter, and A.C.A. Donnely.1990. Hydrogeologic Hydrochemical Characterization of Texas Frio Formation Used for Deep-Well Injection of Chemical Wastes. Environ Geol Water Sci 16:107-12.

Leake, S.A. and D.E. Prudic. 1991. Documentation of a Computer Program to Simulate Aquifer-System Compaction Using the Modular Finite-Difference Groundwater Flow Model. U.S. Geological Survey, *Techniques of Water-Resources Investigations*, Book 6, Chap A2, p. 68.

Loskot, C. L., W.M. Sandeen, and C.R. Follett. 1982. Ground-Water Resources of Colorado, Lavaca, and Wharton Counties, Texas: Texas Department of Water Resources Report 270, 252 p.

Marvin, R.F., G.H. Shafer, and O.C. Dale. 1962. Ground-Water Resources of Victoria and Calhoun Counties, Texas: Texas Board of Water Engineers Bulletin 6202. 147 p.

Mason, C. C. 1963. Ground-Water Resources of Refugio County, Texas: Texas Water Commission Bulletin 6312, 122 p.

McDonald, M. G. and A.W. Harbaugh. 1988. A modular three-dimensional finite-difference ground-water flow model: U.S. Geological Survey, Techniques of Water-Resources Investigations of the United States Geological Survey, Book 6: Model Techniques, Chapter A1.

McGowen, J.H., L.F. Brown, Jr., T.J. Evans, W.L. Fisher, and C.G. Groat. 1976. Environmental Geologic Atlas of Texas, Bay City- Freeport Area: The University of Texas at Austin, *Bureau of Economic Geology Environmental Atlas 1*, 98 p., 29 figs., 13 tables, 9 maps.

McClelland Engineering, Inc. 1979. Subsidence Cause and Effect Harris-Galveston Coastal Subsidence District Phase 1-A Study, Report to Espey, Huston & Associates, Inc., Houston, Texas

Meinzer, O.E. 1928. Compressibility and elasticity of artesian aquifers: Economic Geology, v. 23, no. 3, p. 263-291.

Meinzer, O.E. and H.A. Hard. 1925. The artesian-water supply of the Dakota sandstone in North Dakota with special reference to the Edgeley Quadrangle: U.S. Geological Survey Water-Supply Paper 520-E, p. 73–95.

Morton, R.A., N.A. Purcell, and R.L. Peterson. 2001. Field evidence of subsidence and faulting induced by hydrocarbon production in coastal southeast Texas. Trans Gulf Coast Assoc Geol Soc 51:239–248.

Poland, J. F., B. E. Lofgren, R. L. Ireland, and R. G. Pugh. 1975. Land Subsidence in the San Joaquin Valley, California, as of 1972. U.S. Geological Survey Professional Paper 437-H. 78 pp.

Ratzlaff, K.W., 1982. Land-Surface Subsidence in the Texas Coastal Region: Texas Department of Water Resources Report 272, 26 p.

Revil, A., D. Grauls, and O. and Brevart. 2002. Mechanical Compaction of sand/clay mixtures. Journal of Geophysical Research, Vol 107, No. B11. P. 11-1 to 11-15.

Ridgeway, C. and R. Goswami. 2014. Groundwater Availability Modeling Gulf Coast Aquifer, Public Presentation: Stakeholder Advisory Forum (SAF), Corpus Christi, Texas. June 17th 2014.

Riley, F. S. 1969. Analysis of Borehole Extensometer Data from Central California: International Association of Scientific Hydrology Publications 89, p. 423- 431.

Seifert, J. and C. Drabek. 2006. Chapter 13: History of Production and Potential Future Production of the Gulf Coast Aquifer, in Aquifers of the Gulf Coast, Texas Water Development Board Report 365, Austin, Texas

Sharp J.M. and S.J. Germait. 1990. Risk assessment and causes of subsidence along the Texas Gulf Coast. In: (Fairbridge, R.W., and Paepe., eds.) Proceedings of NATO Conference on the Greenhouse Effect, Sea Level and Drought. Kluwer Academic Publishers, Dordrecht.

Sharp, J.M., Jr. and D.W. Hill. 1995. Land-Surface Subsidence along the Northeastern Texas Gulf Coast: Effects of Deep Hydrocarbon Production. *Environmental Geology*, V. 25: 181-191.

Strom E.W., N.A. Houston, N.A., C.A. and Garcia. 2003a. Selected Hydrogeologic Datasets for the Chicot Aquifer, Texas: USGS Open-File Report 03-97, 1 CD-ROM.

Strom E.W., N.A. Houston, and C.A. Garcia. 2003b. Selected Hydrogeologic Datasets for the Evangeline Aquifer, Texas: USGS Open-File Report 03-298, 1 CD-ROM.

Strom E.W., N.A. Houston, and C.A. Garcia. 2003c. Selected Hydrogeologic Datasets for the Jasper Aquifer, Texas: USGS Open-File Report 03-299, 1 CD-ROM.

Terzaghi, K. 1925. Principles of soil mechanics: IV, Settlement and consolidation of clay, Eng. News-Rec., p. 874-878.

Terzaghi, K. and R.B. Peck.. 1967. Soil mechanics in engineering practice. New York, John Wiley and Sons, Inc. 2d ed., 729 p.

Wang, G. and T. Soler. 2014. Measuring Land Subsidence Using GPS: Ellipsoid Height vs. Orthometric Height, J. Surv. Eng., 141, 1– 12, 2014.

Wang, G., J. Welch, T.J. Kearns, J. Yang, and J. Serna. 2015. Introduction to GPS geodectic infrastructure for land subsidence monitoring in Houston Texas, USA. Proceedings, IAHS, 372. P. 297-303.

White, W.A. and T.A. Tremblay. 1995. Submergence of Wetlands as a Result of Human-Induced Subsidence and Faulting along the Upper Texas Gulf Coast. J Coastal Res 11:788-80.

Winslow, A. G., and W.W. Doyle. 1954. Land-Subsidence and its Relationship to the Withdrawal of Groundwater in the Houston-Galveston region, Texas: *Econ. Geology*, v. 49 (4), pg 412-422.

Young, S.C., V. Kelley, eds., N. Deeds, P. Knox, T. Budge, and E. Baker. 2006. A Site Conceptual Model to Support the Development of a Detailed Groundwater Model for Colorado, Wharton, and Matagorda Counties: Lower Colorado River Authority, Austin, Texas.

Young, S.C., V. Kelley, T. Budge, and N. Deeds. 2009. Development of the LSWP Groundwater Flow Model for the Chicot and Evangeline Aquifers in Colorado, Wharton, and Matagorda Counties: Lower Colorado River Authority, Austin, Texas.

Young, S.C., P.R. Knox, E. Baker, T. Budge, S. Hamlin, B. Galloway, R. Kalbouss, and N. Deeds. 2010. Hydrostratigraphic of the Gulf Coast Aquifer from the Brazos River to the Rio Grande: Texas Water Development Board Report, 203 p.

Young, S.C., T. Ewing, S. Hamlin, E. Baker, and D. Lupton. 2012. Updating the Hydrogeologic Framework for the Northern Portion of the Gulf Coast Aquifer, Unnumbered Report: Texas Water Development Board.

Young, S. C. 2015. Letter to Cindy Ridgeway dated October 21, 2015 with Reference, Evaluation of Provisional Desired Future Conditions for GMA 15 based on GAM Simulations, Sent to the Texas Water Development Board, Austin, TX.

Zilkoski, D. B., L. Hall, G. Mitchell, V. Kammula, A. Singh, W. Chrismer, and R. Neighbors. 2003. The Harris-Galveston coastal subsidence district/national geodetic survey automated global positioning system subsidence monitoring project, Proc., US Geological Survey Subsidence Interest Group Conf., Galveston, Texas, 27–29 November 2001, USGS OpenFile Report, 03–308, 13–28, 2003.

INTERA

APPENDIX A: PRESENTATION TO THE TWDB ON APRIL 28, 2015, TITLED "ESTIMATES OF LAND SUBSIDENCE BASED ON ANALYSIS OF TOPOGRAPHIC DATA"

Estimates of Land Subsidence Based on Analysis of Topographic Data

Estimated Land Subsidence* (feet)

< 0.5	1.5 - 2.0	· PID location
0.5 - 1.0	2.0 - 2.5	Zone
1.0 - 1.5	2.5 - 3.0	County Boundary

0   5   10   20
Miles

* Difference between the elevation of National Geodetic Survey Permanent Identifier (PID) locations measured prior to 1950 and the current TNRIS LiDAR data (positive value implies subsidence). Value is the average value of points falling above the 25 percentile and below the 75 percentile for each zone

**Presentation to
Texas Water Development Board
Austin, Texas**

By Steven Young, Ph.D., PE. PG.

INTERA
GEOSCIENCE & ENGINEERING SOLUTIONS

April 28, 2015
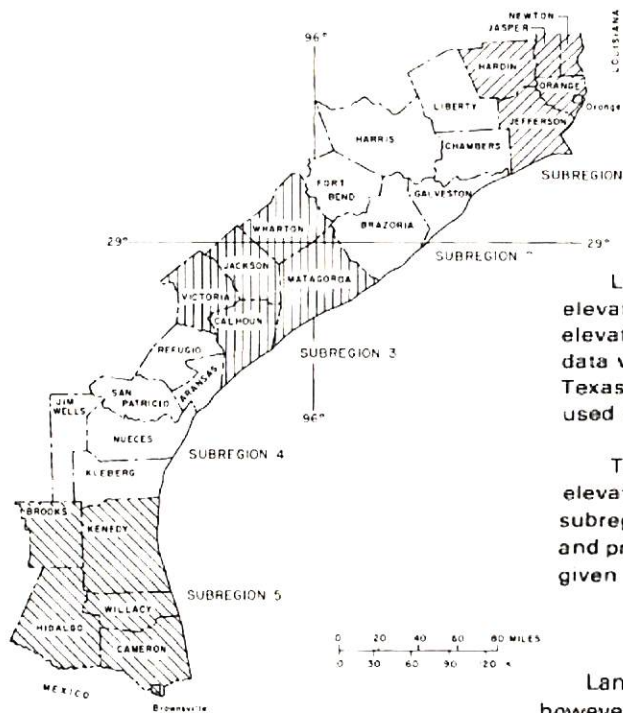
Land-surface subsidence in the study area was determined by comparing bench-mark elevations for different periods of leveling The data were obtained from lists of adjusted elevations published by the National Geodetic Survey for the various periods. Additional elevation data were obtained from the Texas Department of Highways and Public Transportation and the Texas Department of Water Resources. In subregion 1 (Figure 1), topographic maps were also used to delineate land-surface subsidence.

The bench marks shown on the illustrations in this report are those that had a net loss in elevation. The time period for the corresponding losses is not necessarily the same throughout a subregion; consequently, the subsidence contours shown for each subregion are based on known and projected values for the most prevalent time period Special symbols on the illustrations are given to those bench marks that represent the maximum time period between level runs.

Land-surface subsidence in the Texas coastal region is generally less than 0 5 foot (0.15 m); however, two large areas where land-surface subsidence exceeds 0.5 foot (0.15 m) are the Houston-Galveston area in subregion 2 and a rice irrigation area in subregion 3. Elsewhere in the coastal region, subsidence exceeding 0.5 foot (0.15 m) is more localized.

A-4

3

Estimated Land Subsidence from 1918 to 1973 in SubRegion 3 (Ratzlaff, 1982)
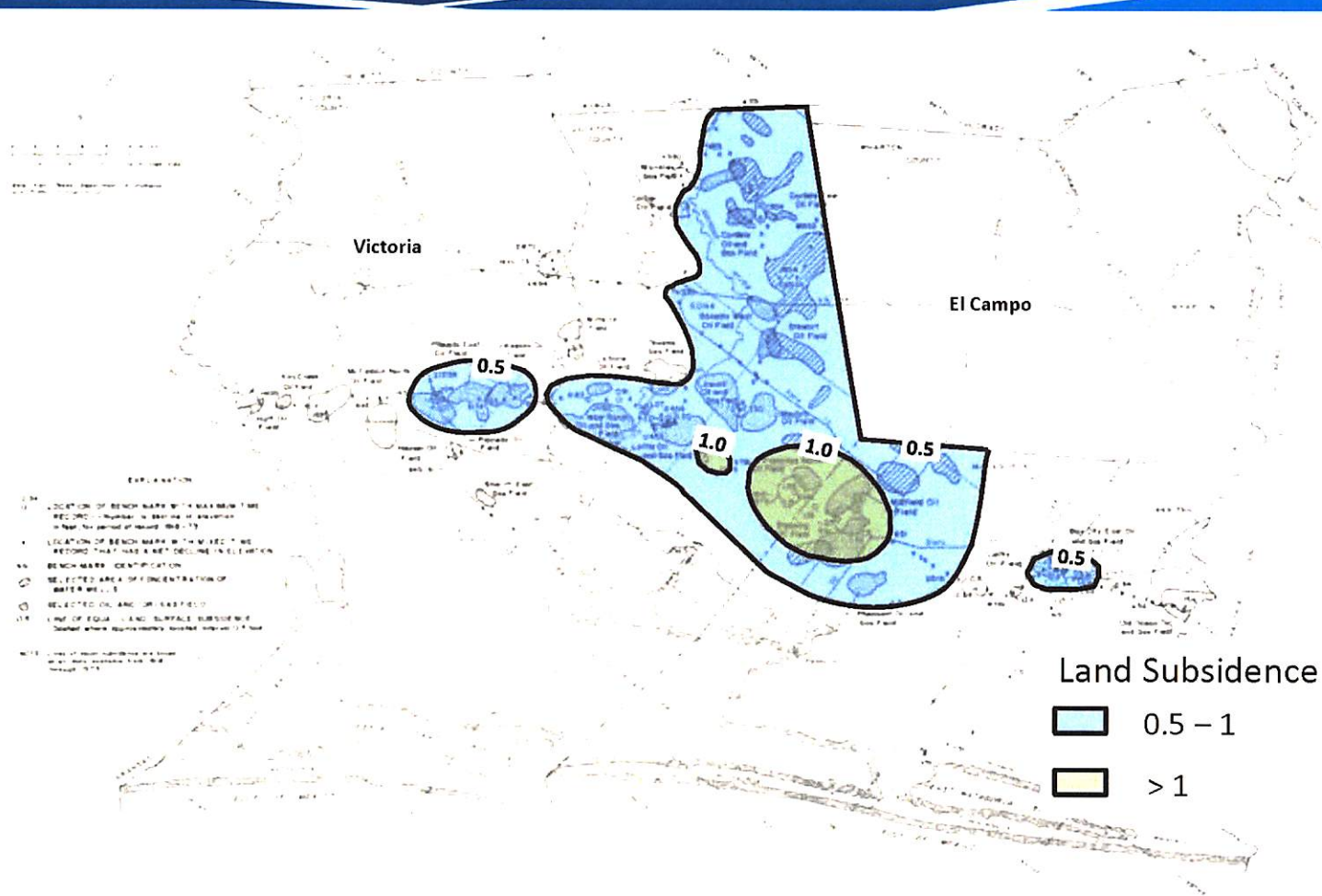
Land Subsidence (ft)

- 0.5 – 1
- > 1

Estimated Land Subsidence (Ratzlaff, 1982)

Subregion 3

Land-surface subsidence during 1918-73 in subregion 3 (Figure 6) is generally less than 0.5 foot (0.15 m). An area of subsidence of at least 0.5 foot (0.15 m) extends into Matagorda and Victoria Counties from Jackson County, with the greatest amount of subsidence, more than 1.5 feet (0.46 m), in southeastern Jackson County and northwestern Matagorda County. The principal cause for the subsidence in subregion 3 is ground-water withdrawals.

Withdrawals of oil, gas, and associated ground water have probably caused the subsidence in the areas adjacent to the oil and gas fields. The subsidence at Bay City probably is the result of withdrawal of both fresh ground water and oil, gas, and associated ground water. The subsidence in eastern Matagorda County is probably caused by withdrawals of ground water for irrigation.

The large area of subsidence in the eastern one-half of Jackson County and the northwestern part of Matagorda County, most of which occurred between 1950 and 1973, is the result of declines in water levels resulting from an increase in ground-water withdrawals for irrigation in the early 1950's (Loskot and others, 1982). The area of subsidence extending westward from Jackson County into Victoria County is also the result of an increase in ground water withdrawals for irrigation.

Land-surface subsidence in southeastern Victoria County is probably related to oil and gas production. There are very few water wells and only a small amount of ground-water withdrawal in the subsided area. Water levels in observation wells within the subsided area declined more than 1 foot (0.3 m) from 1958 to 1973 (Texas Department of Water Resources, unpublished data), but these declines were not sufficient to cause the subsidence shown for the area.

Land Subsidence (ft)
- 0.5 – 1
- > 1
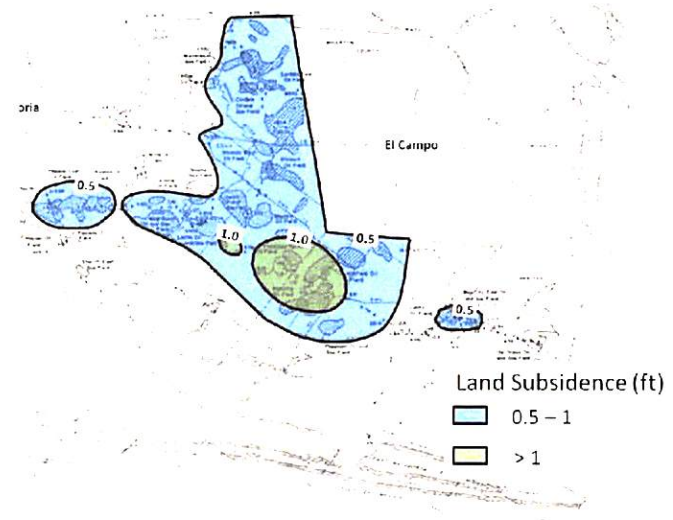
Simulated Land Subsidence by Houston Area Groundwater Model (HAGM) (1891-2009)
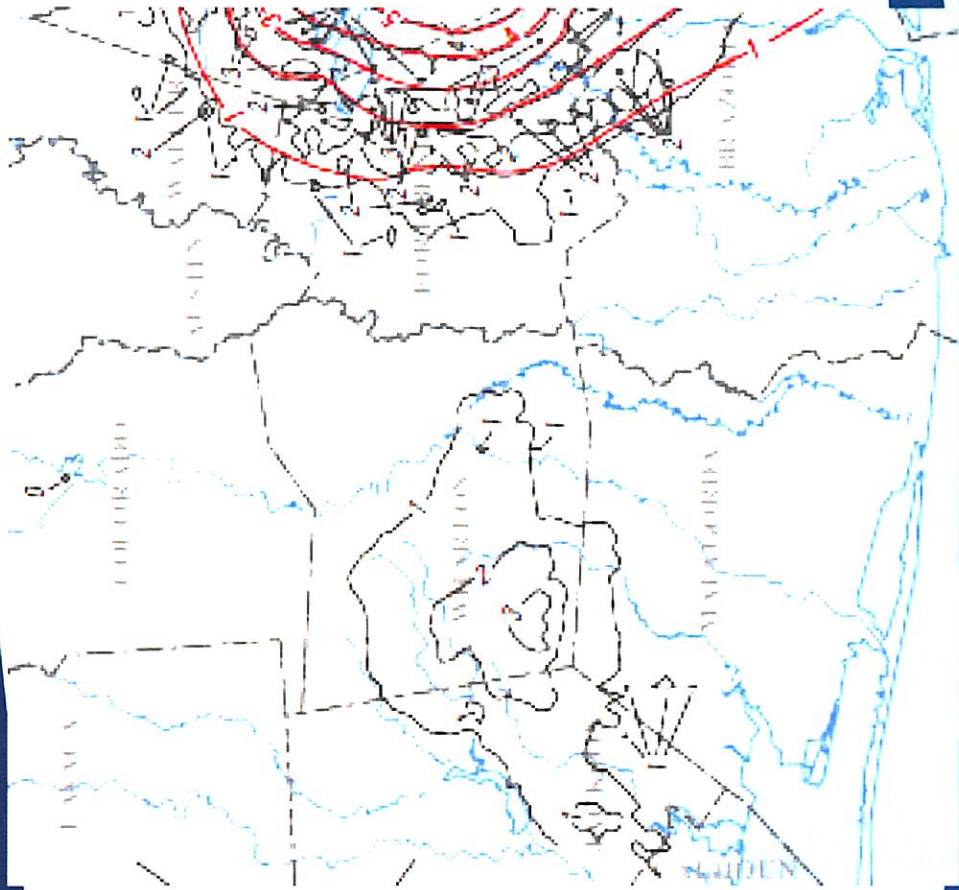
Simulated Land Subsidence by Lower Colorado River Basin (LCRB) Model
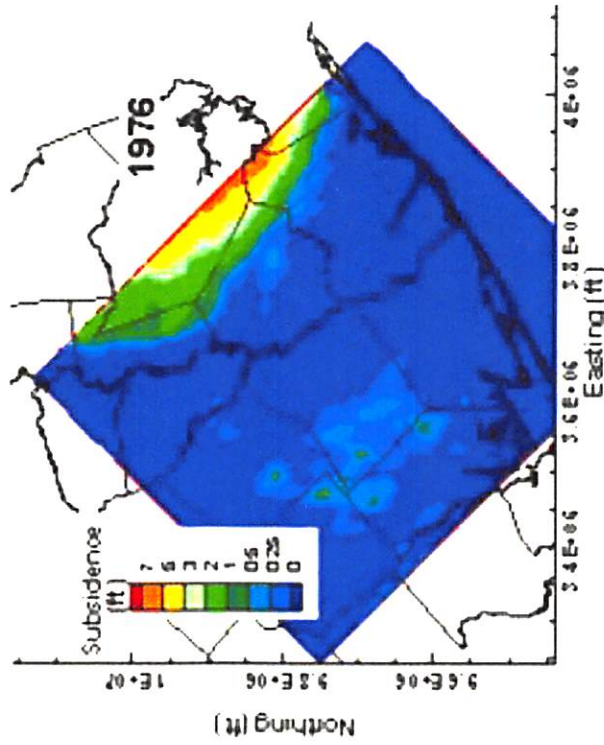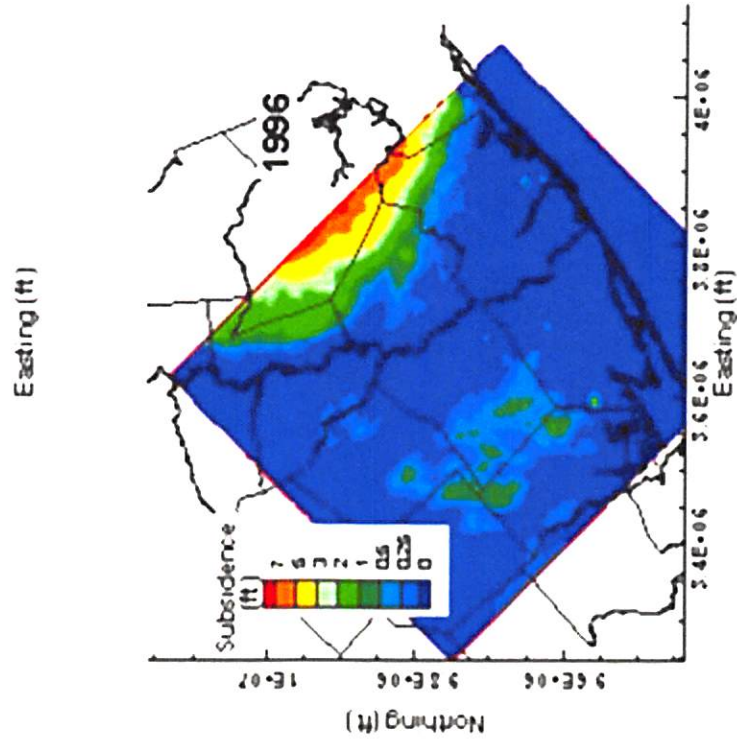
Approach for Using Topographic Data

- Land Elevation $_{(time\ 1)}$ - Land Elevation $_{(time\ 2)}$
- Assemble measurements over area and perform statistical analysis to estimate an "average" value
- Remove outliers (very high and low values) before statistical analyses
- Point measurements of Land Elevation
  - Group across decades and across 20 – 30 square mile areas to increase count
  - Calculate average difference based on values between 25% and 75% percentile
- Maps of Land Elevation
  - Old Topography Maps
    - Digitize and interpolate contour maps to generate continuous set of values
    - Sample at 500-ft spacing
  - LIDAR Maps
    - Mosiac tiles
    - Sample at 500-ft spacing
  - Group points within 1 mile square areas and then average using ESRI sofware
- Identify regions of Possible Land Subsidence

A-9

INTERA

National Geodectic Survey Permanent Identifier (PIDs) Locations

Elevation Year
- 0 - 1949
- 1950 - 1980
- 1981 - 2012

Zone
- County Boundary

0 5 10 20
Miles
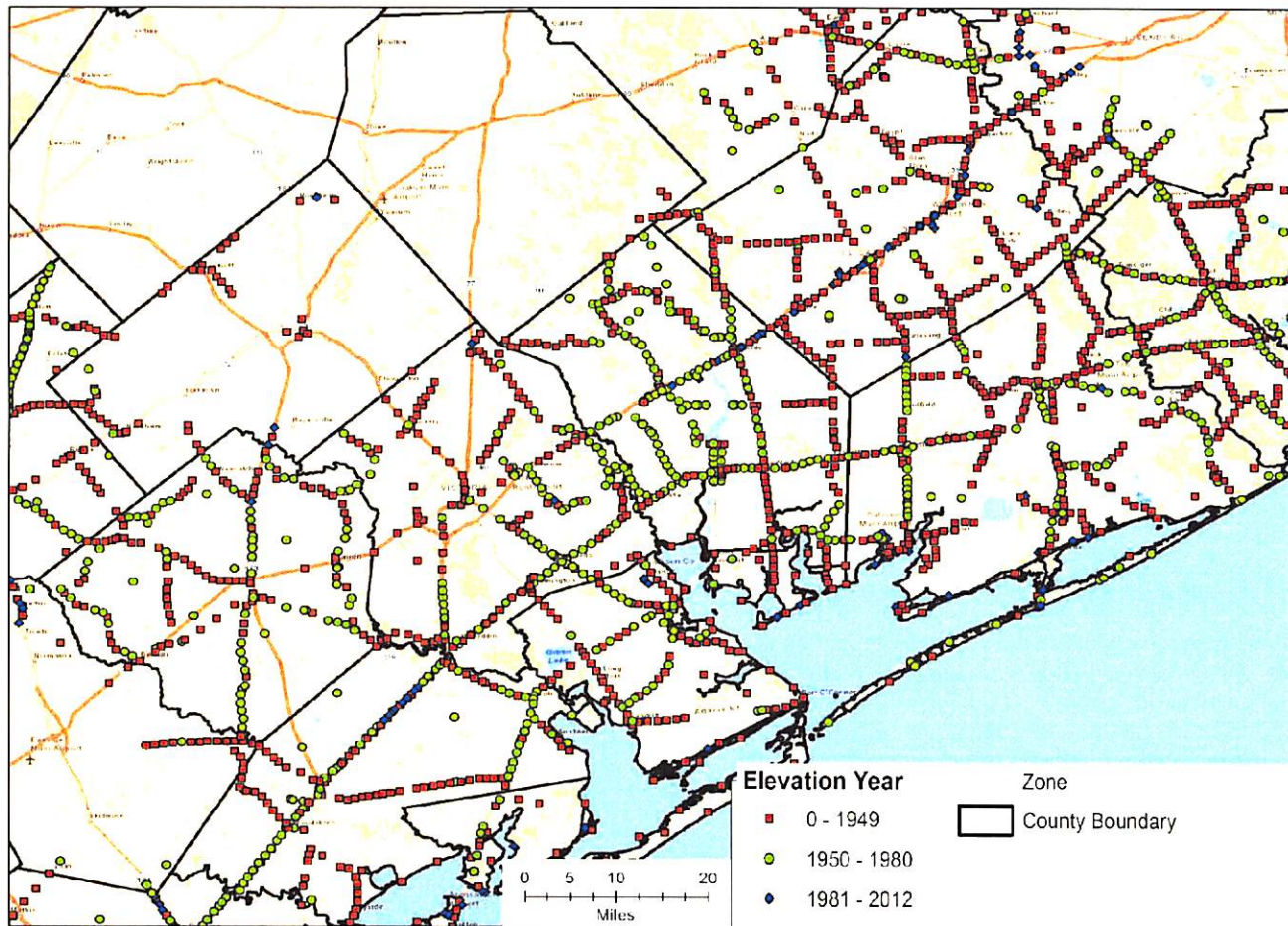
LIDAR (LIght & raDAR) Coverage
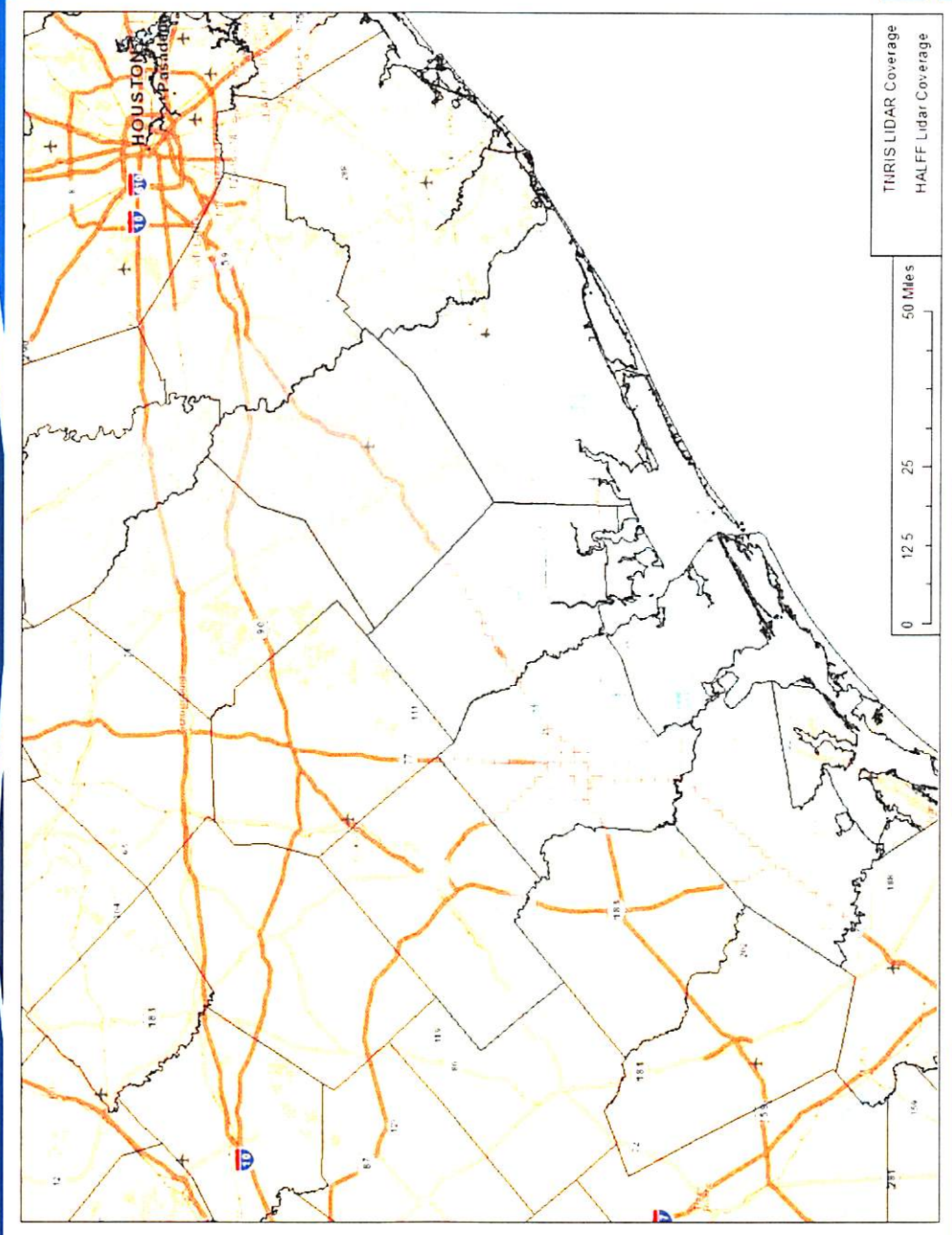
USGS Quadrangle Maps (1951 to 1962)
(5-ft to 10-ft contour interval)
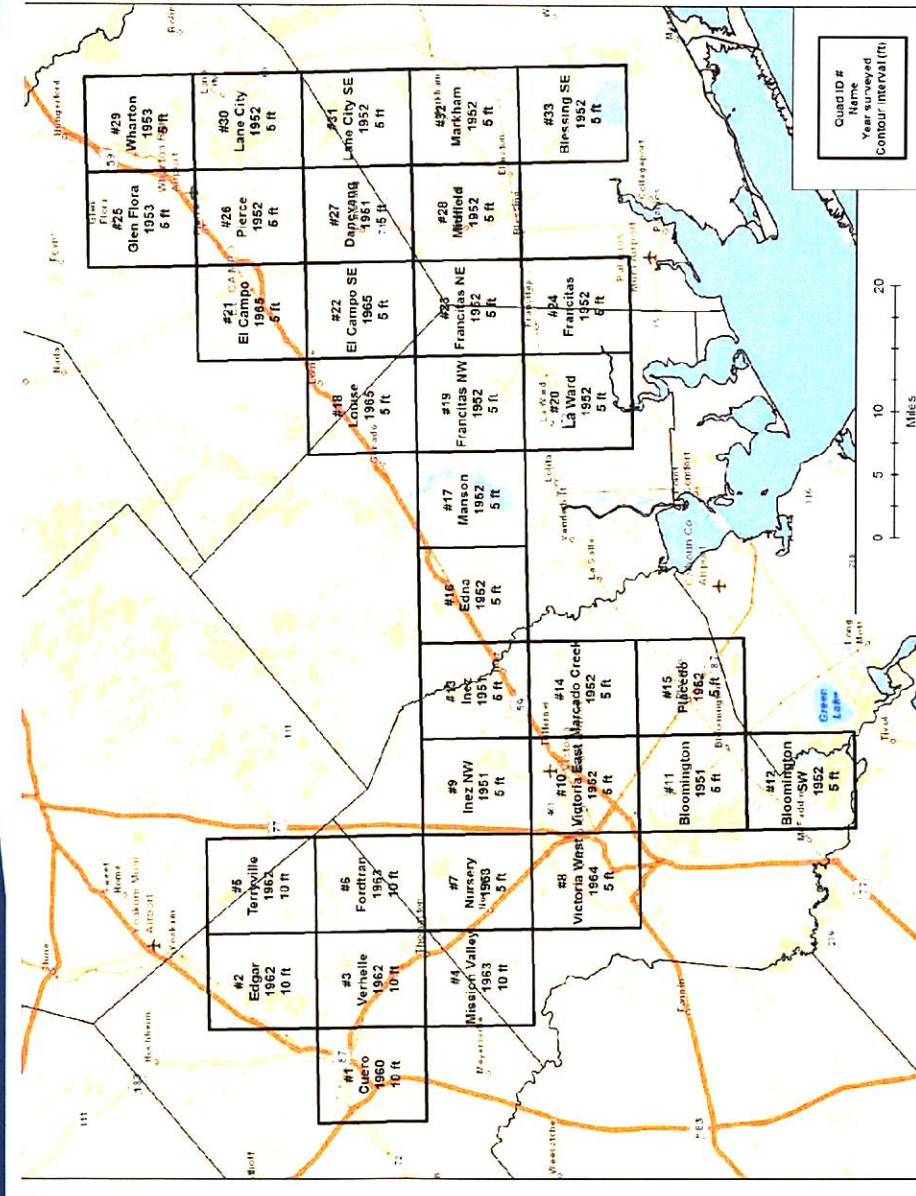
Estimated Land Subsidence based on PIDS (pre 1950s)

- Zones based on Grouping of PIDS with Similar Values
- Top Value is Weighted Average
- Bottom Value is Median
- Weighted Average based on values between 25% and 75% percentile

Preliminary Results - do not cite
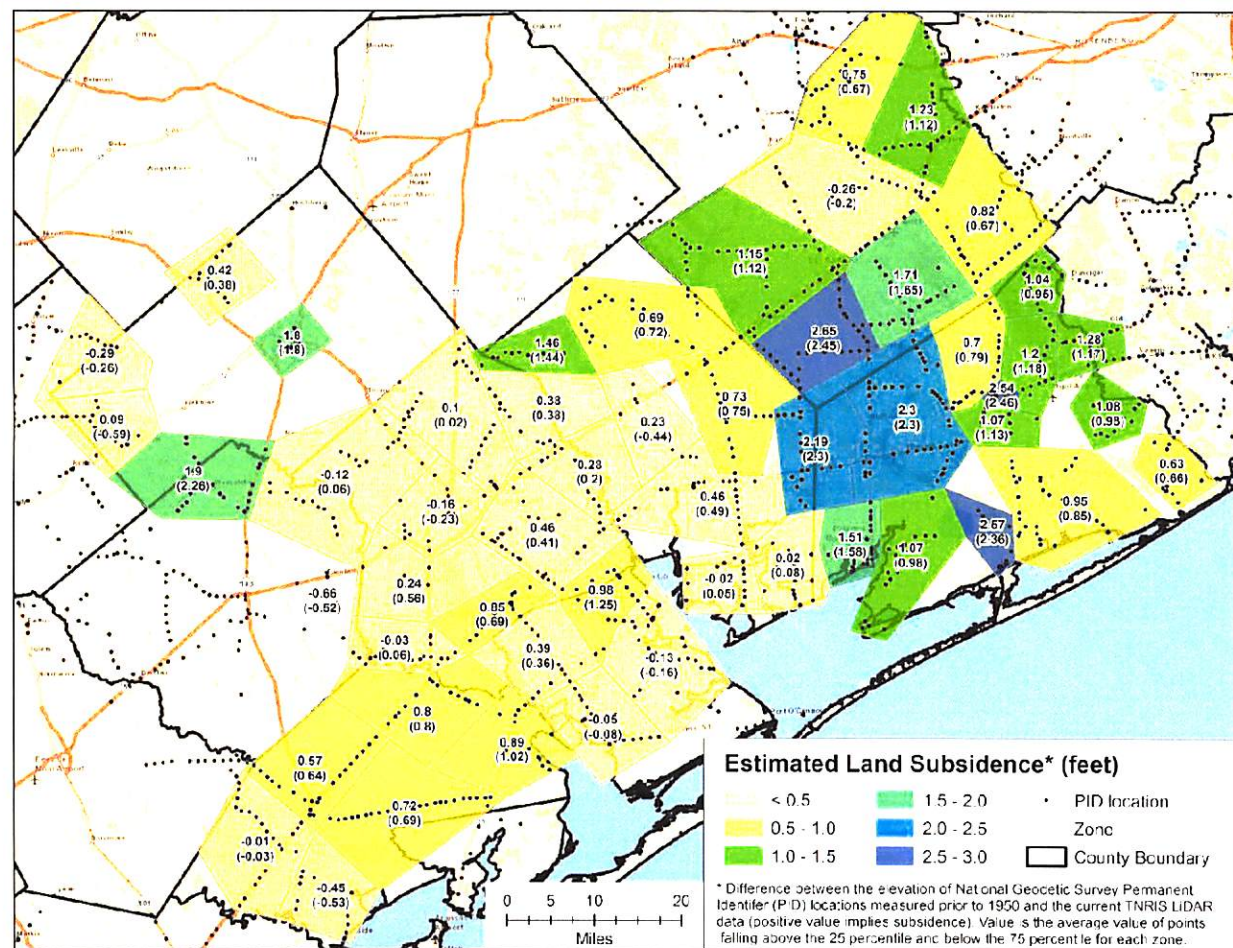
Estimated Land Subsidence based on PIDS (1950 -1980)

- Zones based on Grouping of PIDS with Similar Values
- Top Value is Weighted Average
- Bottom Value is Median
- Weighted Average based on values between 25% and 75% percentile
-

*Insufficient data is less than 5 data points

Estimated Land Subsidence* (feet)

Insufficient Data	1.0 - 1.5	PID location
< 0.5	1.5 - 2.0	Zone
0.5 - 1.0	2.0 - 2.5	County Boundary

0   5   10   20

Miles

* Difference between the elevation of National Geodetic Survey Permanent Identifier (PID) locations measured in 1950-1970 and the current TNRIS LiDAR data (positive value implies subsidence). Value is the average value of points falling above the 25 percentile and below the 75 percentile for each zone.
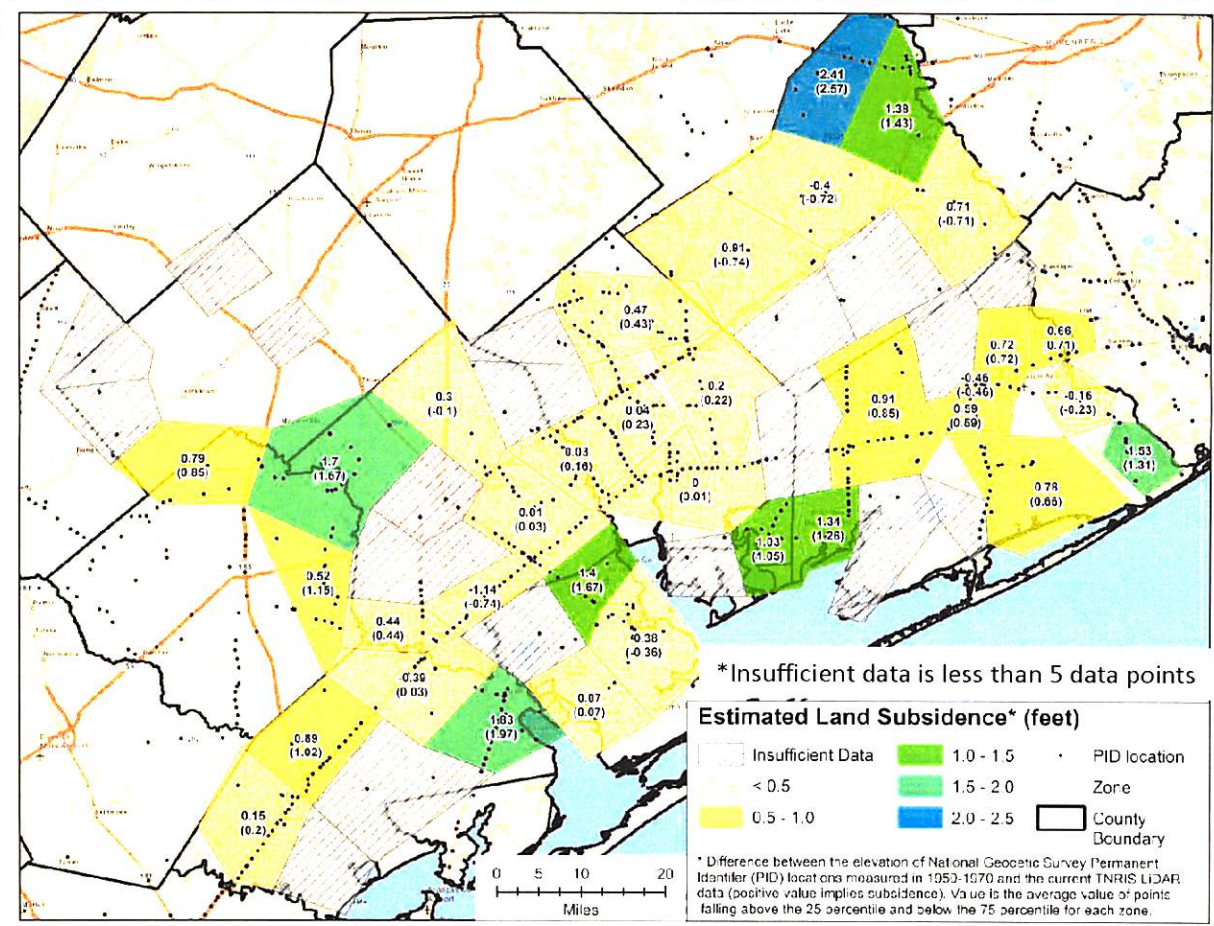
Estimated Land Subsidence Using USGS Quadrangle data and LiDAR From HALFF

Data sampled at 500 ft centers and then averaged over a 1 square mile
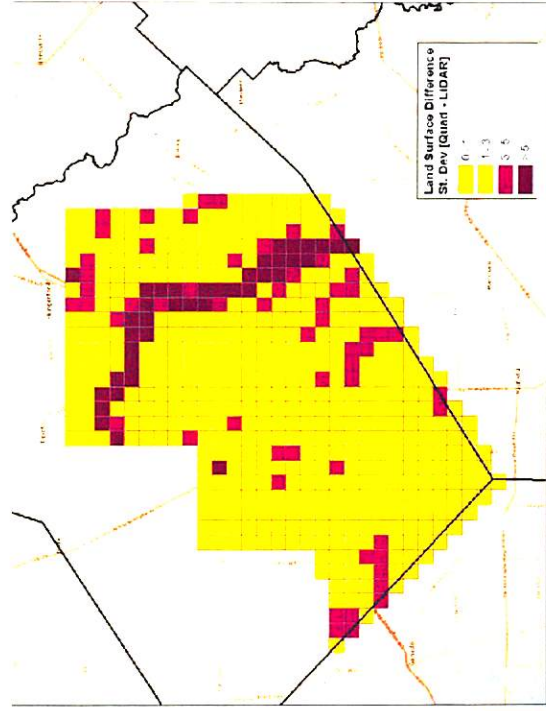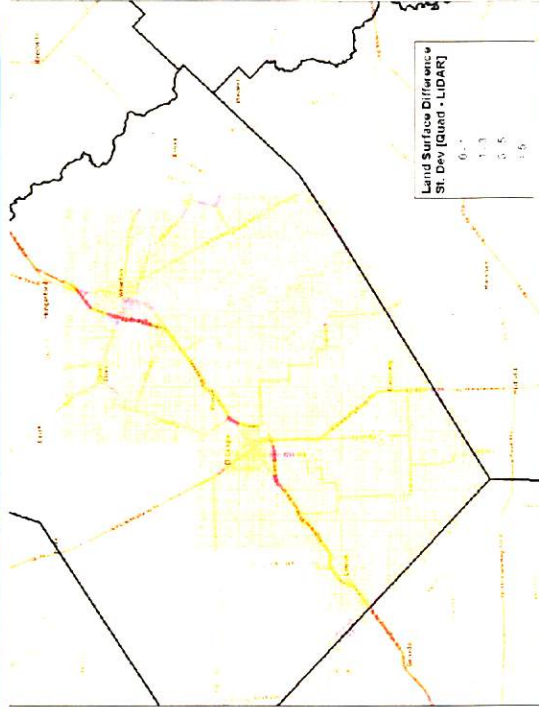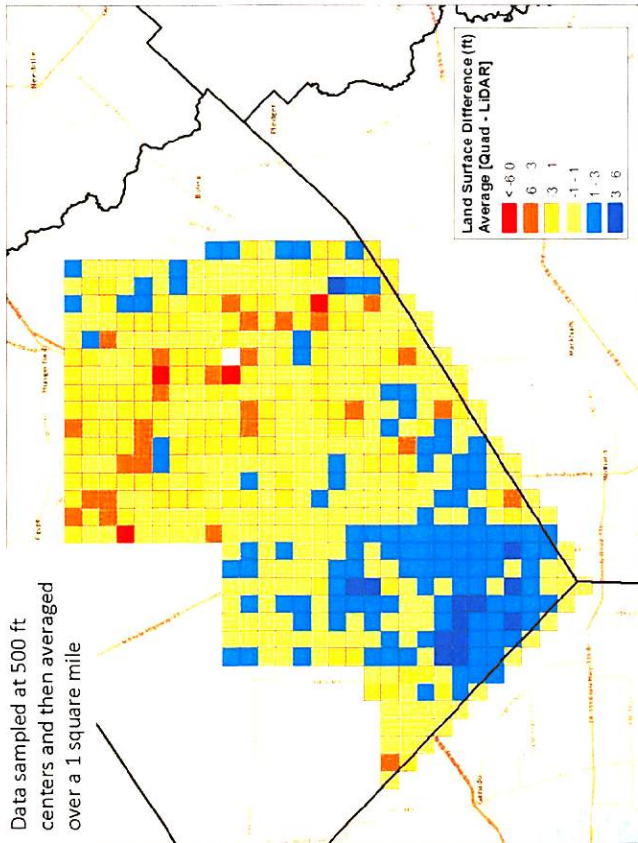
Estimated Land Subsidence Using USGS Quadrangle data and LiDAR From TNRIS

Data sampled at 500 ft centers and then averaged over a 1 square mile
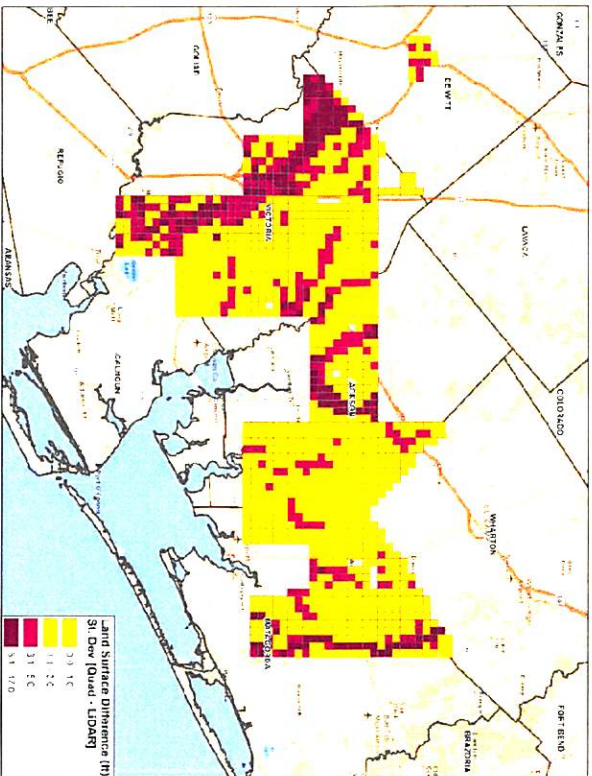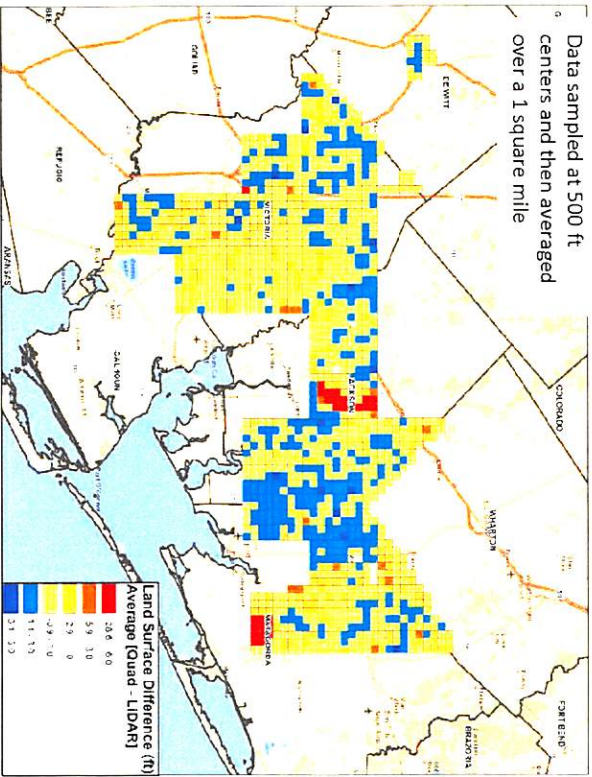
Summary

- **Land subsidence has occurred during last 70 years**

- **Analysis of PID and LIDAR data**
  - **Time period from <1950 to >2010**
  - **Most of Wharton County has experienced about 1 foot of subsidence has occurred**
  - **Maximum subsidence occurred in southwest quadrant and is about 5 ft at a point and about 2.5 feet across a the area**
  - **Error estimated at ±0.5 feet**

- **Analysis of Quadrangle and LIDAR data**
  - **Time period from 1950-1960 to > 2010**
  - **Not reliable near streams**
  - **Indicates a smaller area in Wharton has experienced subsidence than the point data – Quadrangle data may be biased low 1-2 feet**
  - **Maximum subsidence occurred in southwest quadrant and is about 5.5 ft at a point and about 2.5 feet across the area**
  - **Error estimated at ±1.5 feet in area away from streams**

Preliminary Results - do not cite

A-17

INTERA

Figure B-1   Quadrangle 1: Cuero USGS Quadrangle (1960) at 10-ft contour interval.
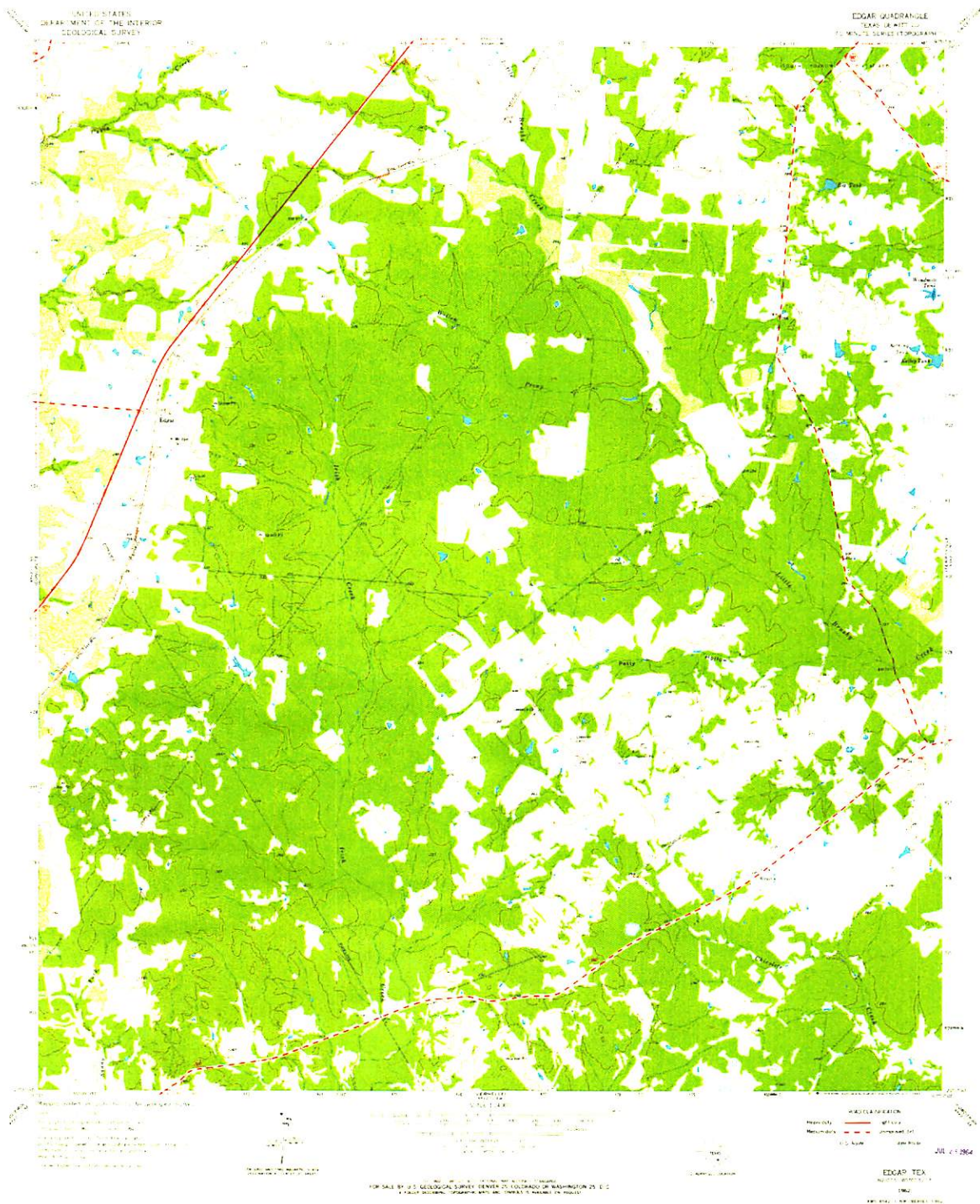
Figure B-2 Quadrangle 2: Edgar USGS Quadrangle (1962) at 10-ft contour interval.

**Figure B-3**   Quadrangle 3: Verhelle USGS Quadrangle (1962) at 10-ft contour interval.

![INTERA logo]
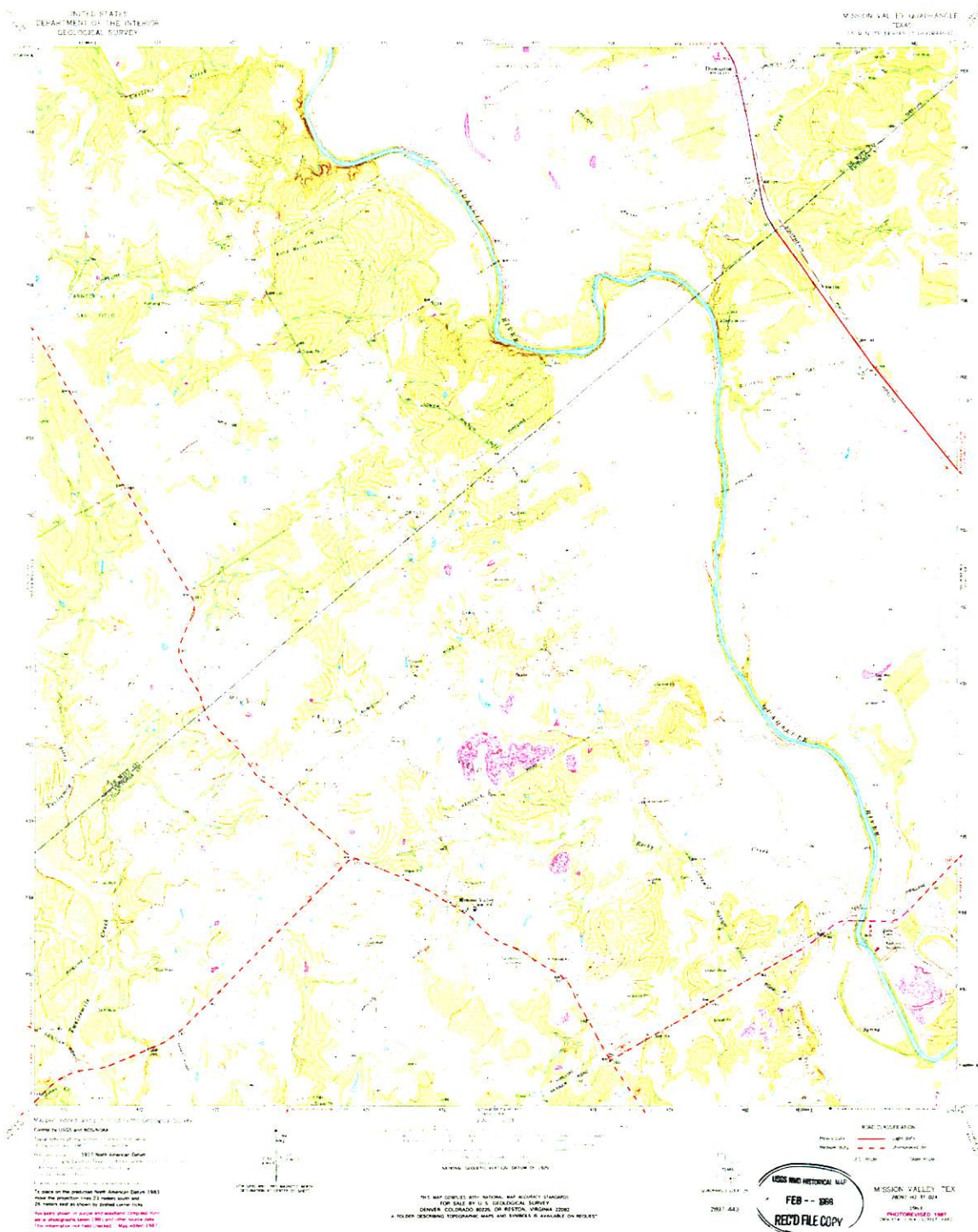
Figure B-4   Quadrangle 4: Mission Valley USGS Quadrangle (1963) at 10-ft contour interval.

Figure B-5   Quadrangle 5: Terryville USGS Quadrangle (1962) at 10-ft contour interval.

INTERRA

Figure B-6 Quadrangle B-6: Fordtran USGS Quadrangle (1963) at 10-ft contour interval.
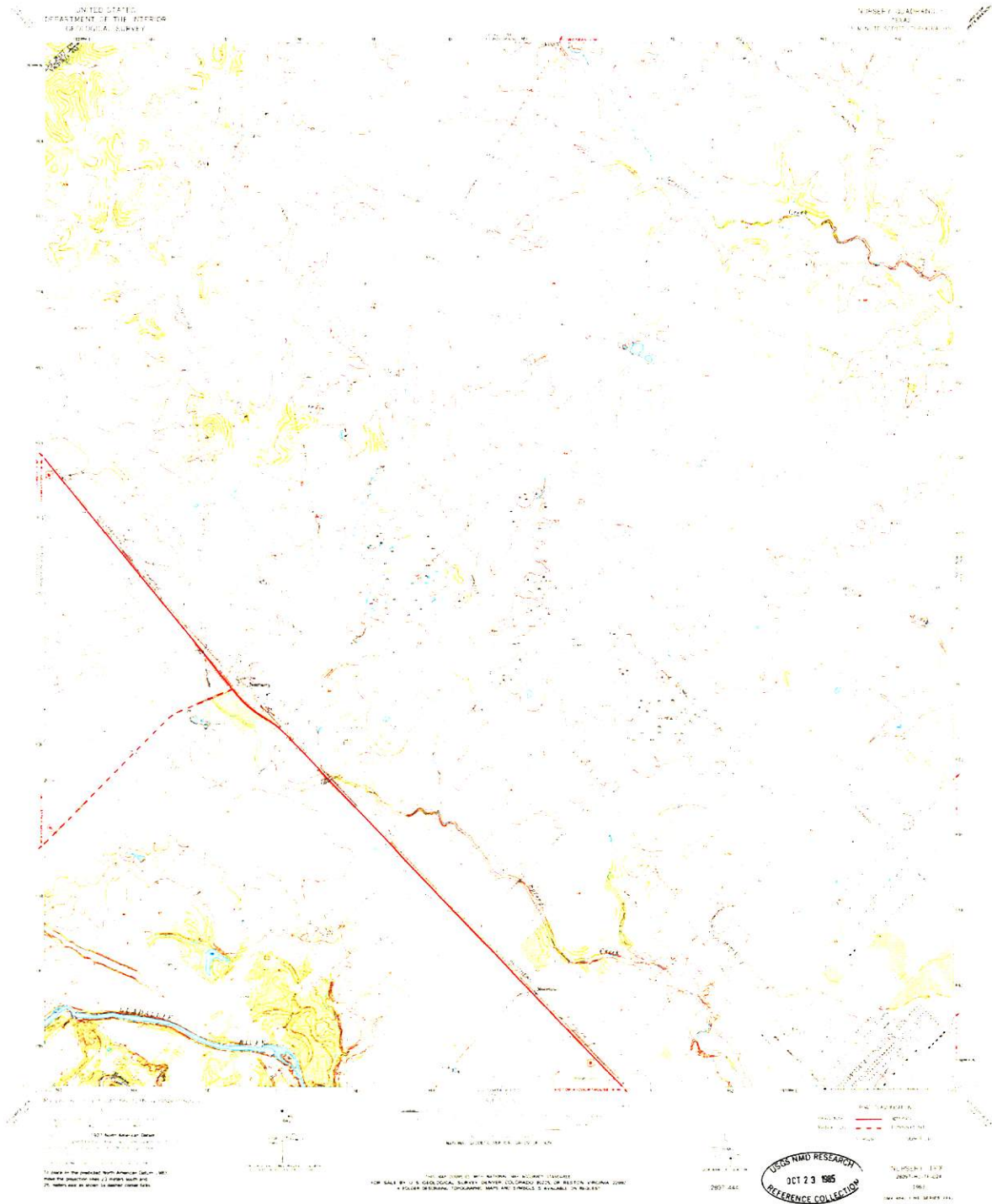
Figure B-7   Quadrangle 7: Nursery USGS Quadrangle (1963) at 5-ft contour interval.
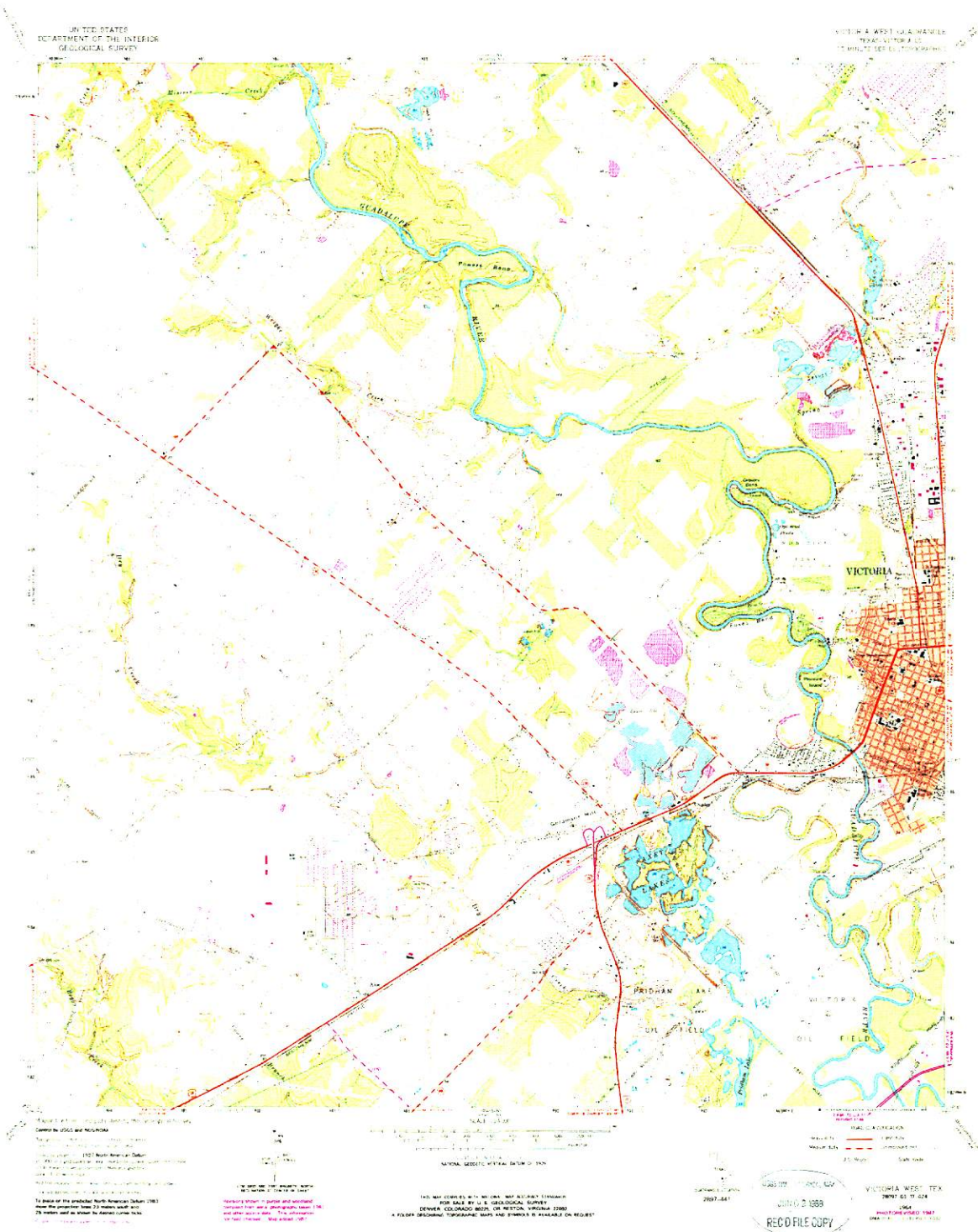
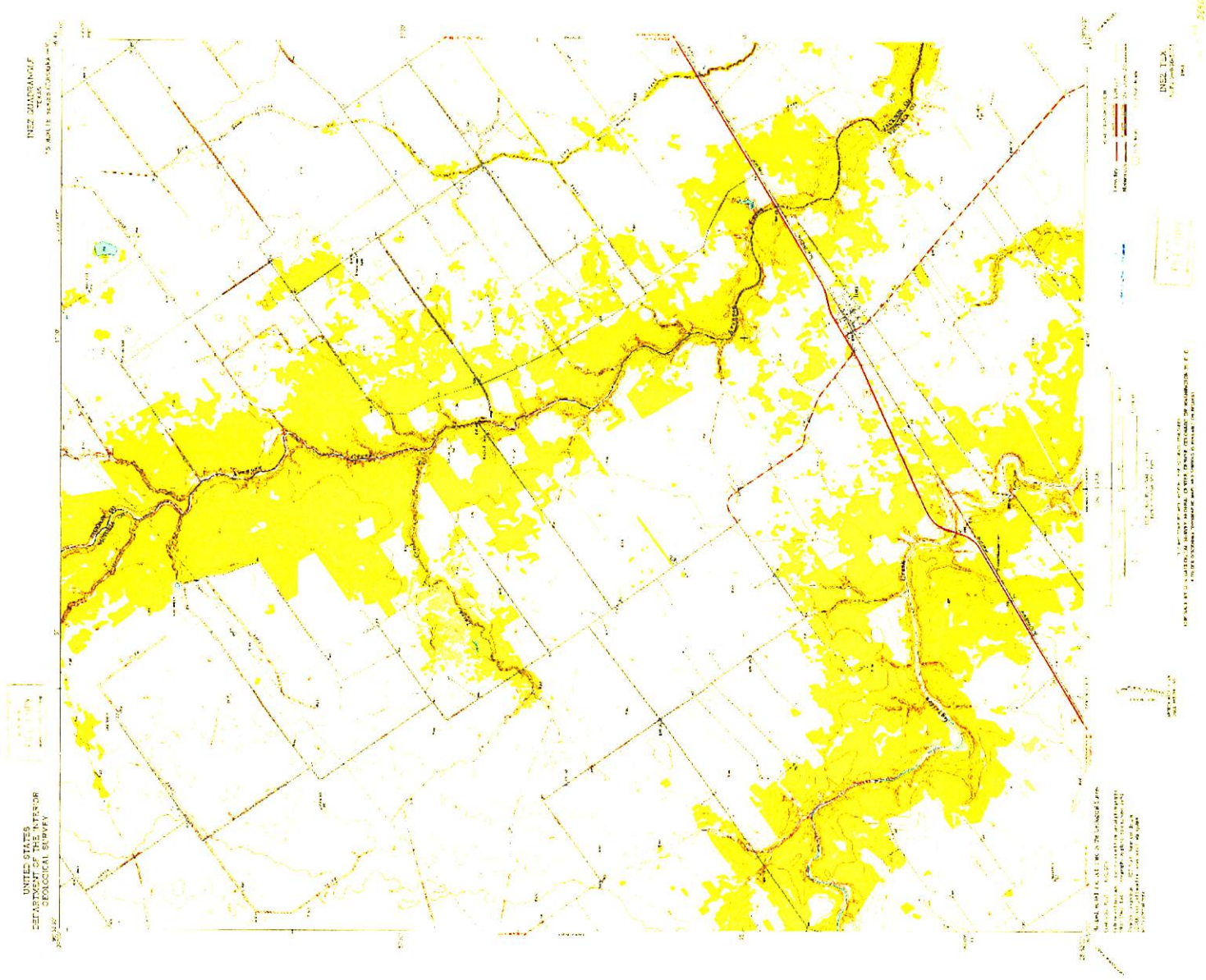**Figure B-8**   **Quadrangle 8:. Victoria W USGS Quadrangle (1964) at 5-ft contour interval.**
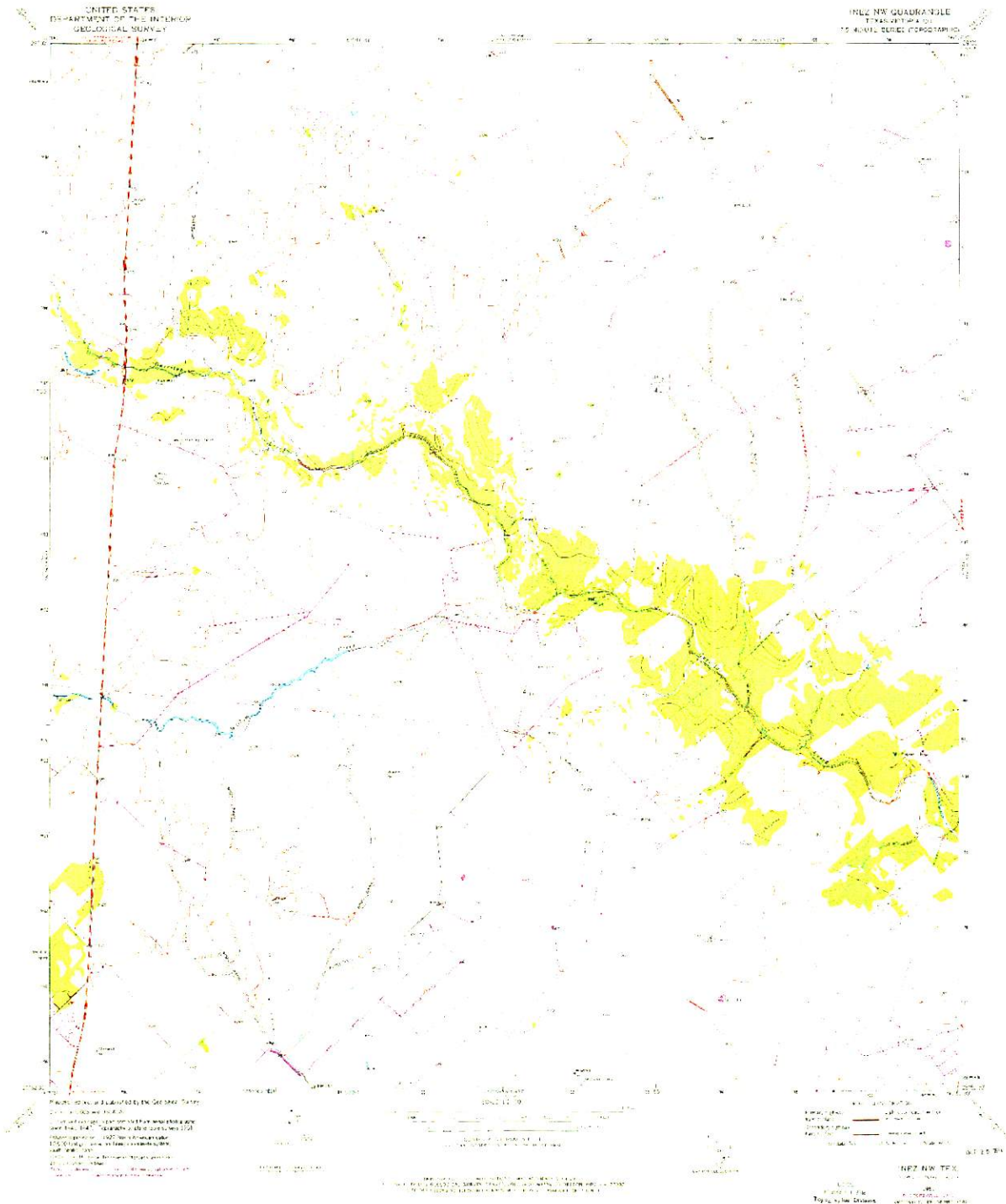
Figure B-9   Quadrangle 9: Inez NW USGS Quadrangle (1951) at 5-ft contour intervals.

Figure B-10   Quadrangle 10: Victoria E USGS Quadrangle (1952) at 5-ft contour interval.
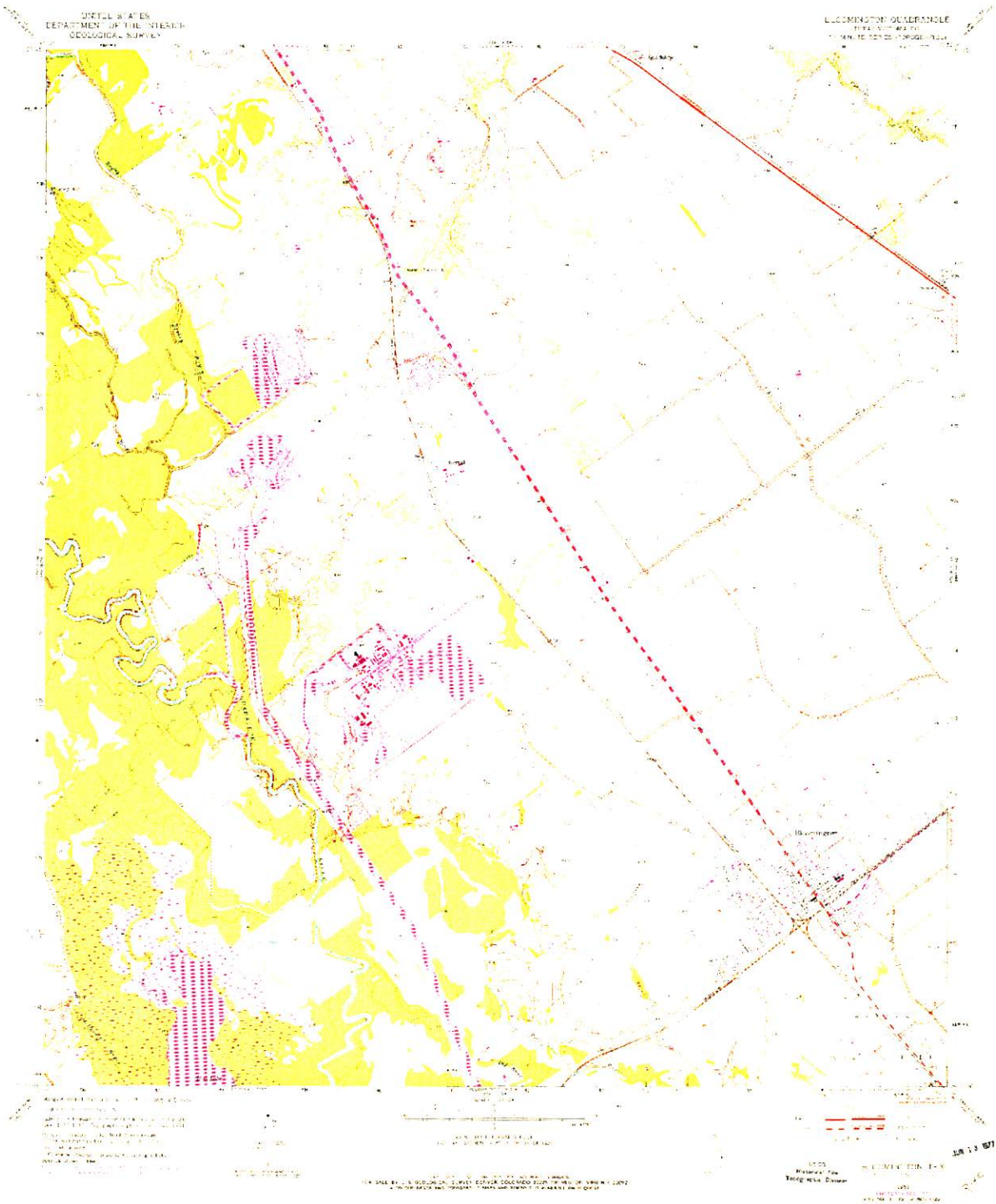
Figure B-11　　　Quadrangle 11: Bloomington NW USGS Quadrangle (1951) at 5-ft contour interval.
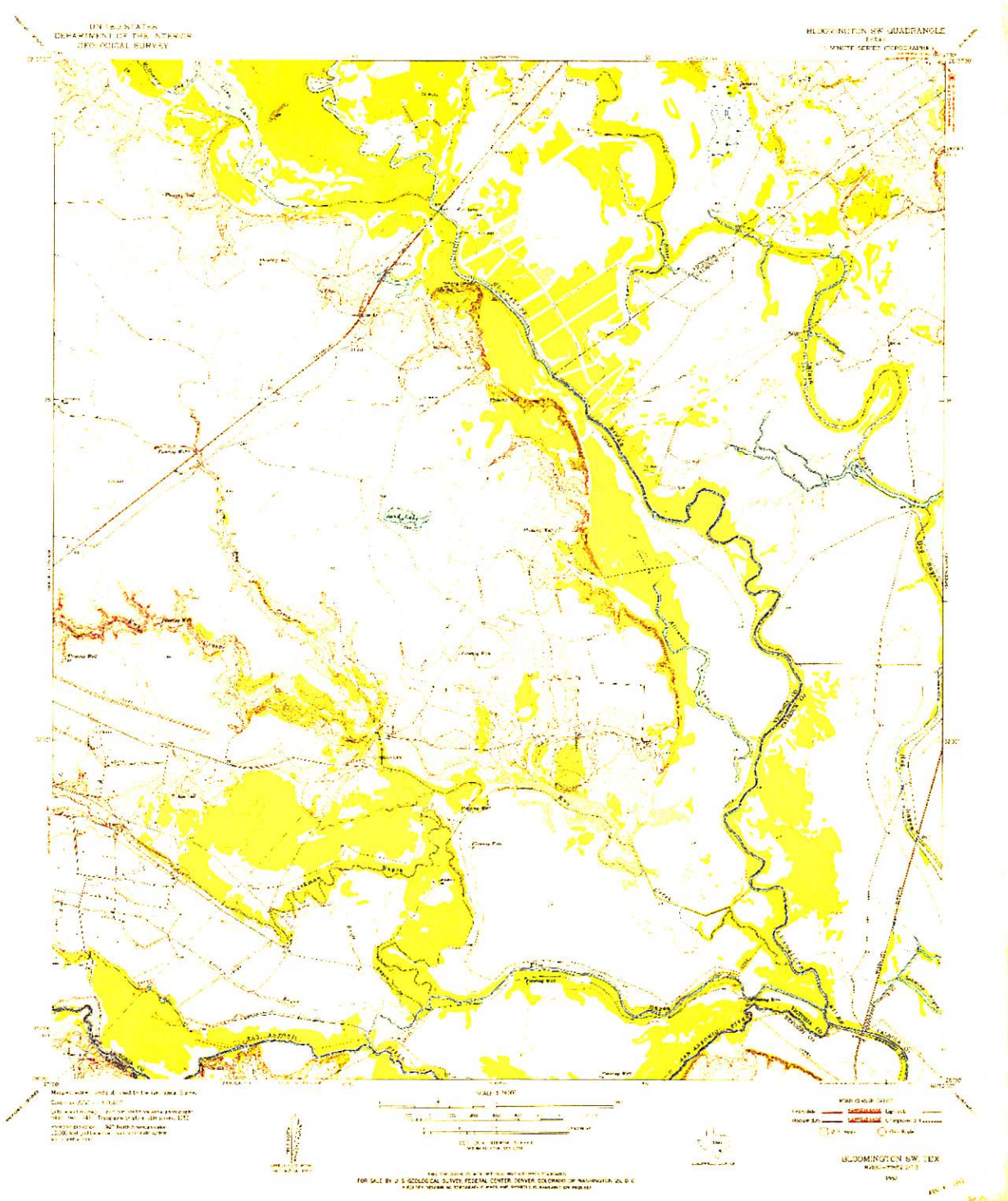
Figure B-12   Quadrangle 12: Bloomington SW USGS Quadrangle (1952) at 5-ft contour intervals.

INTERA

Figure B-13   Quadrangle 13: Inez NE USGS Quadrangle (1951) at 5-ft contour intervals.

B-14
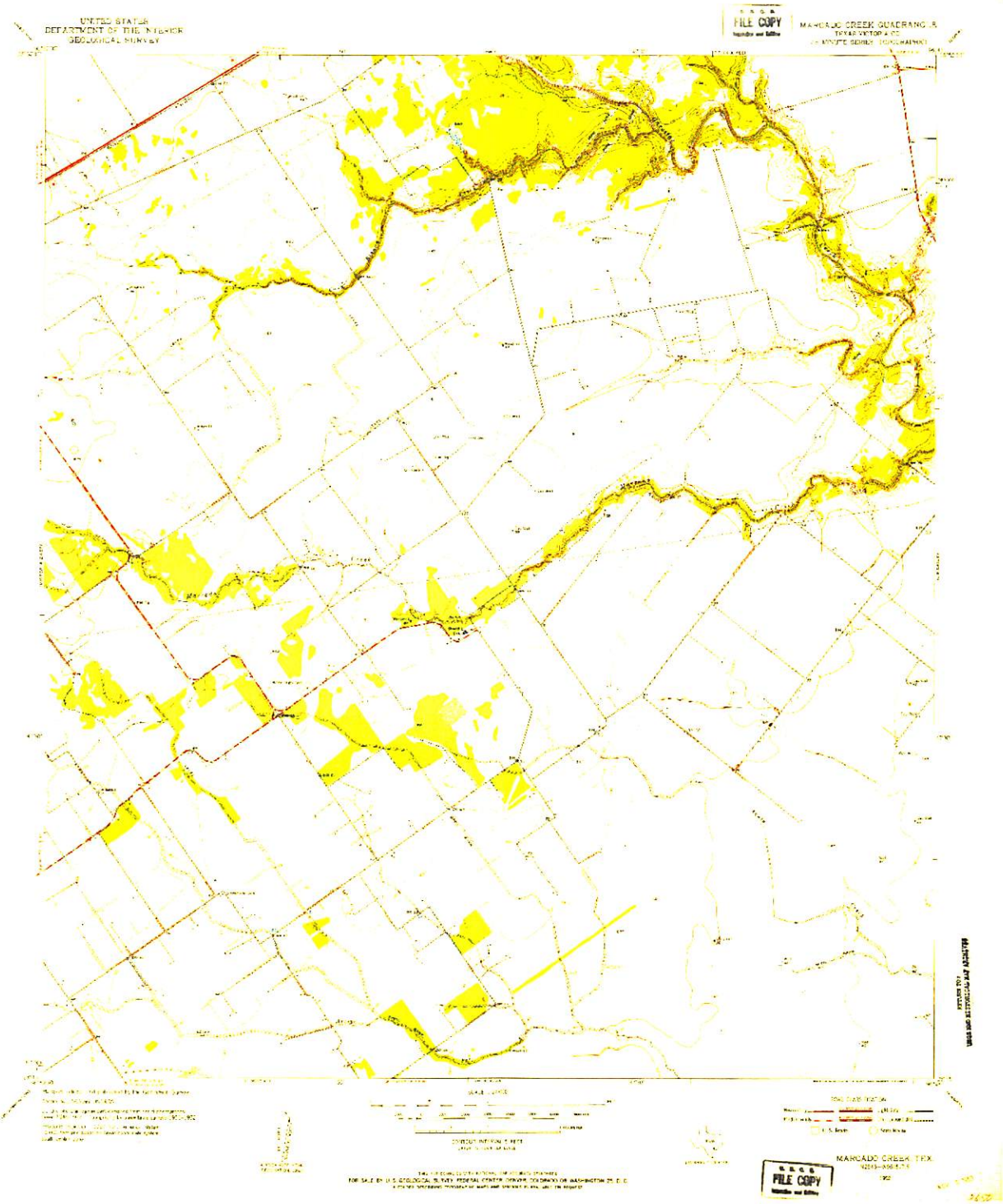
Figure B-14   Quadrangle 14: Marcado Creek USGS Quadrangle (1952) at 5-ft contour intervals.

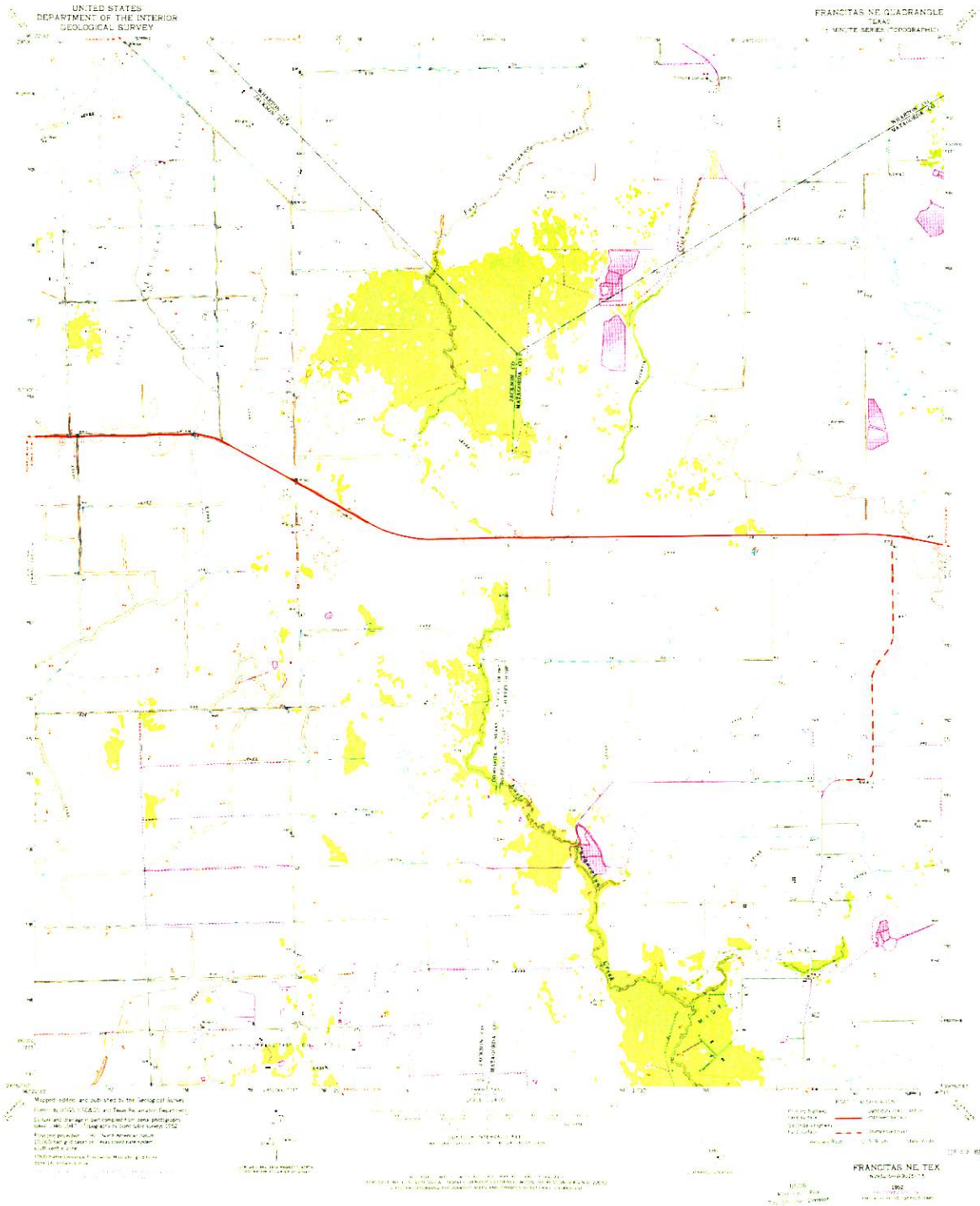Figure B-15   Quadrangle 15: Placedo USGS Quadrangle (1952) at 5-ft contour interval.
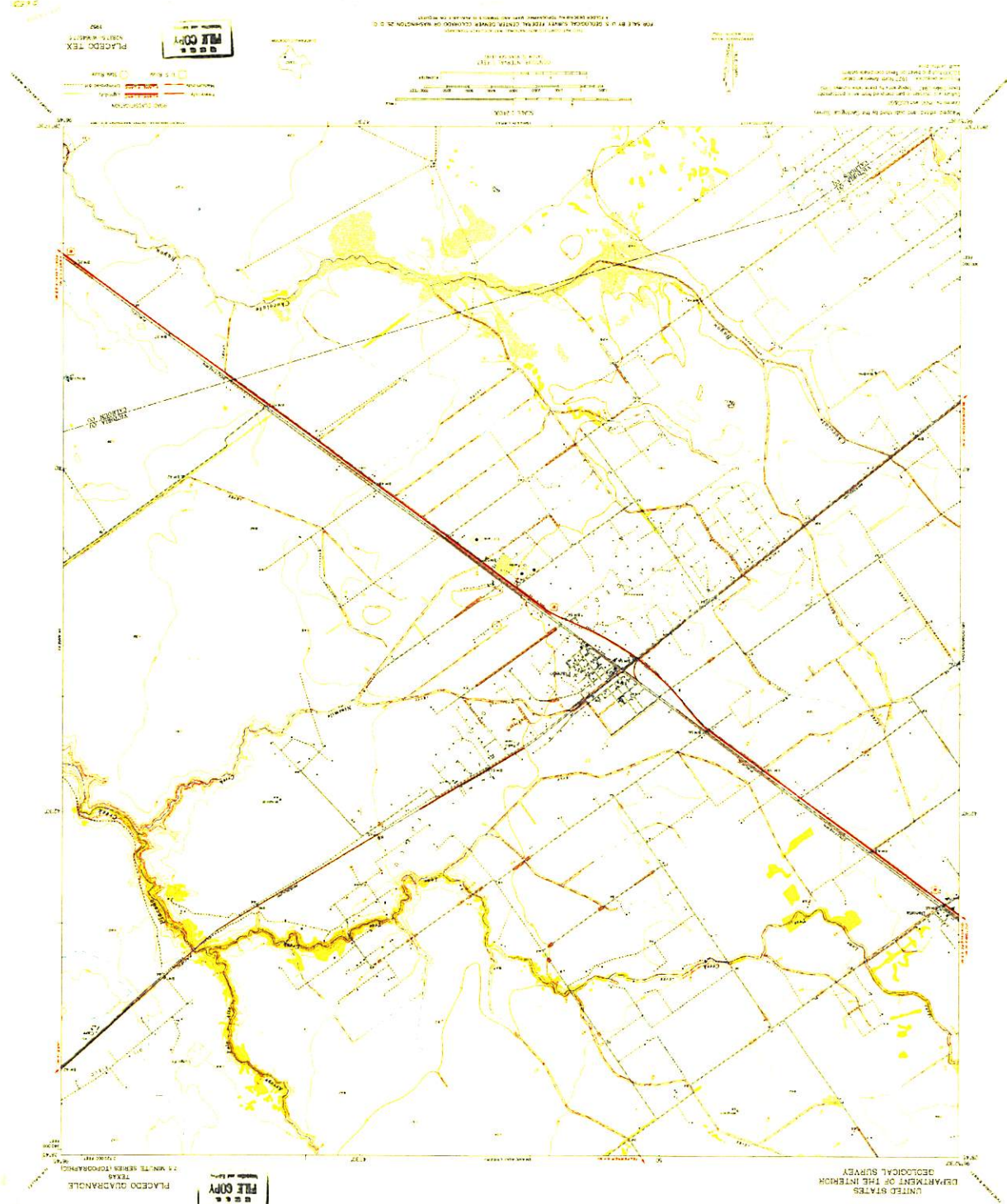
Figure B-16   Quadrangle 16: Edna USGS Quadrangle (1952) at 5-ft contour interval.

Figure B-17   Quadrangle 17: Manson USGS Quadrangle (1952) at 5-ft contour intervals.
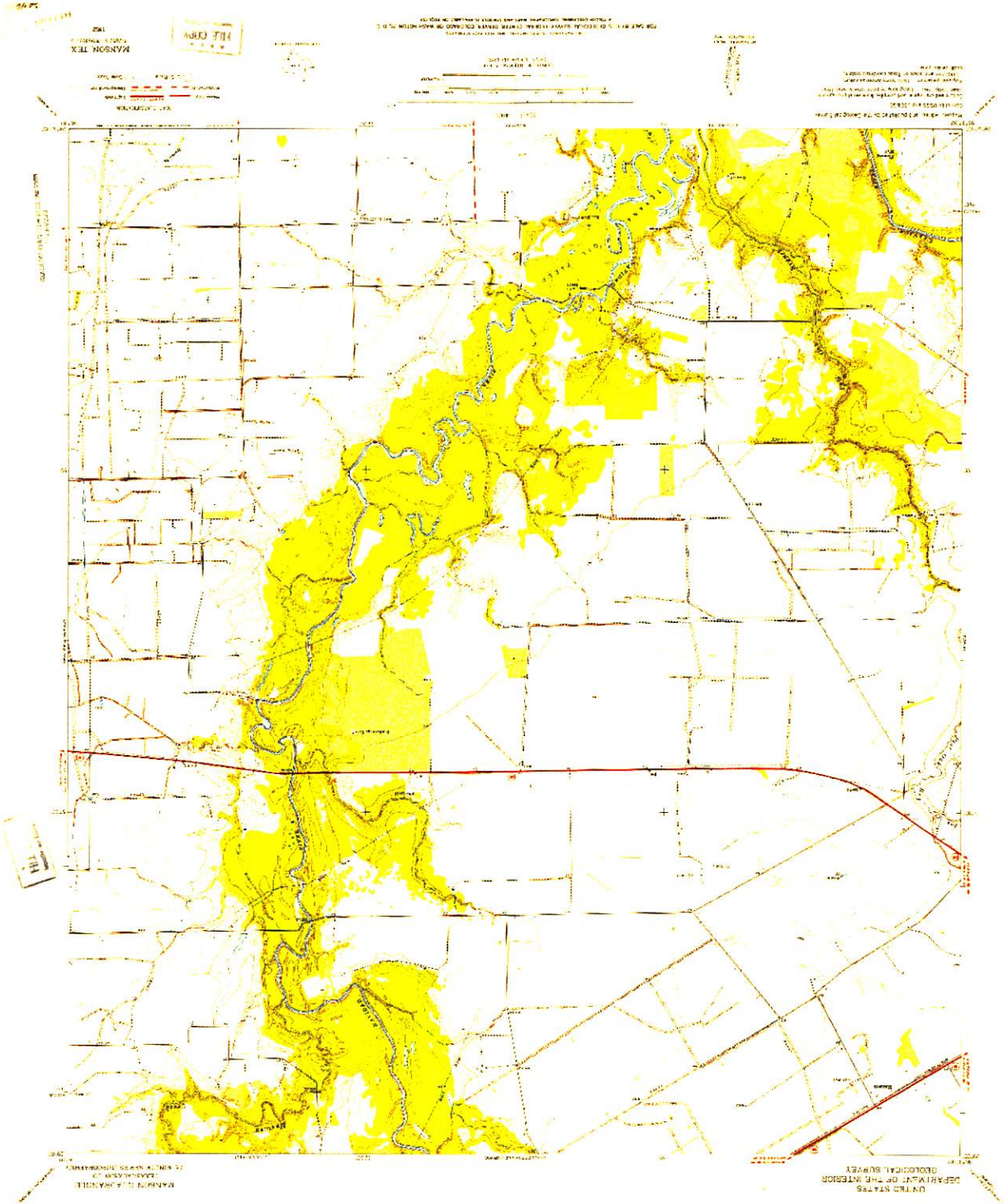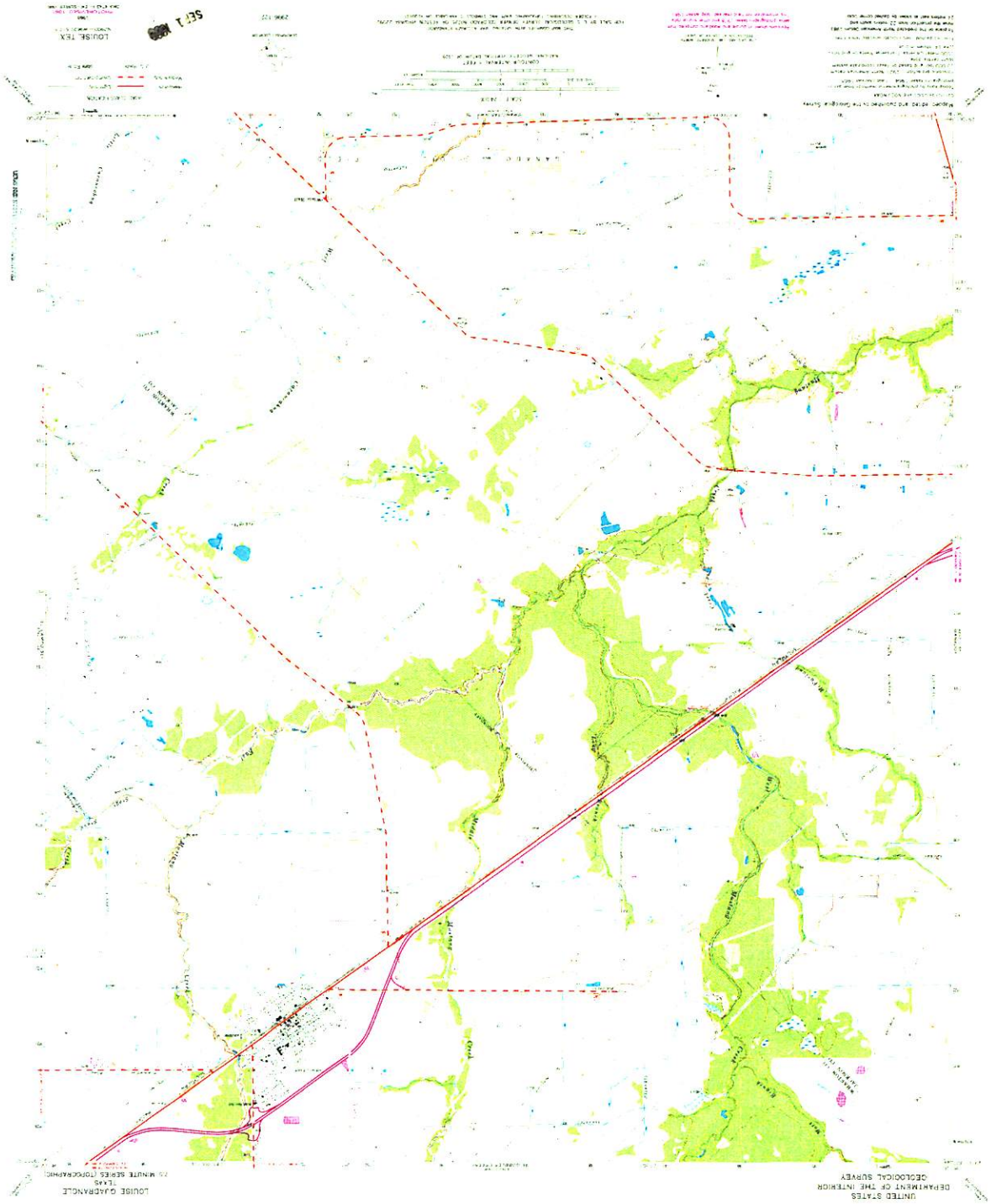
Figure B-18 Quadrangle 18: Louise USGS Quadrangle (1965) at 5-ft contour interval.

Figure B-19   Quadrangle 19: Francitas NW USGS Quadrangle (1952) at 5-ft contour interval.
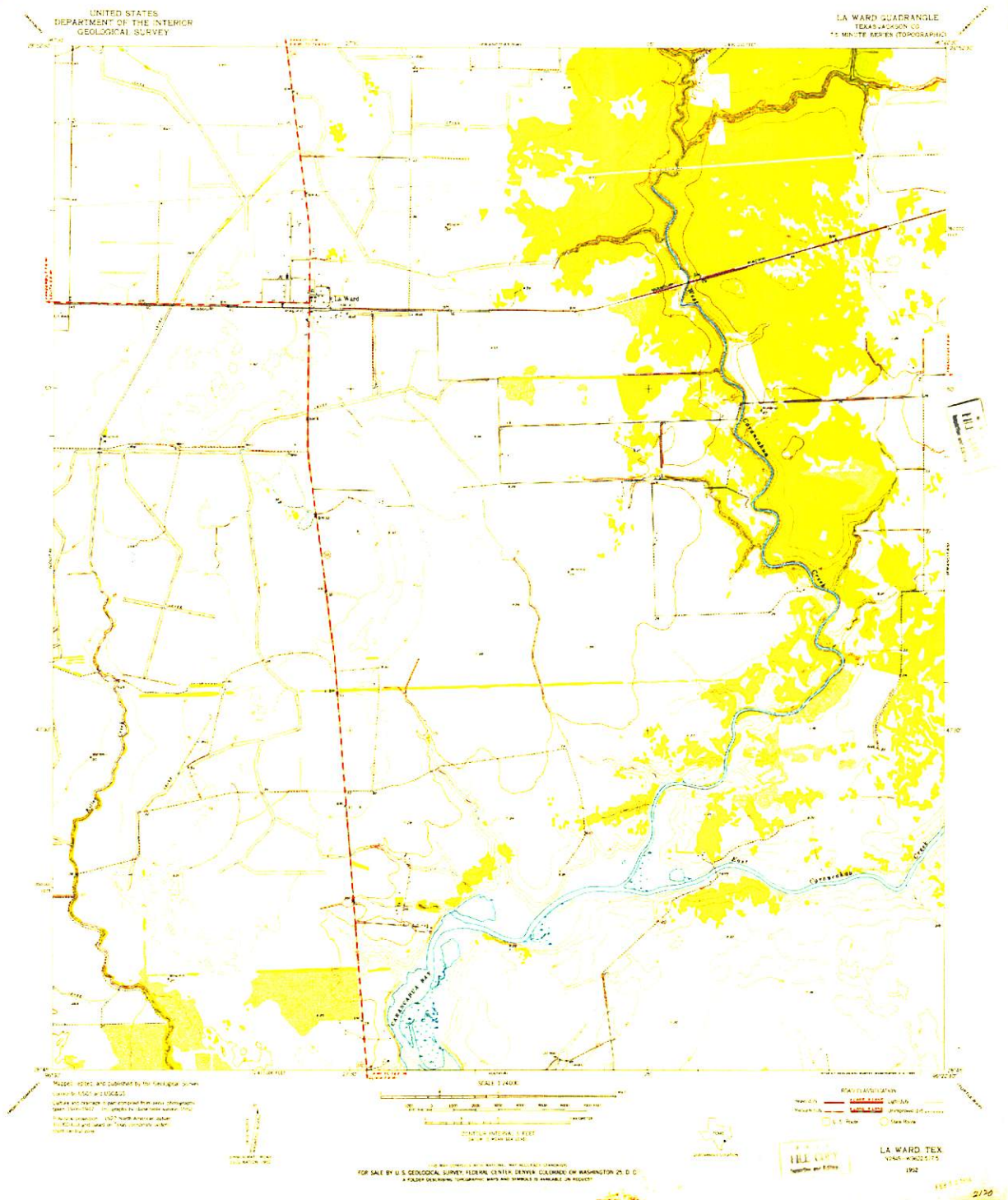
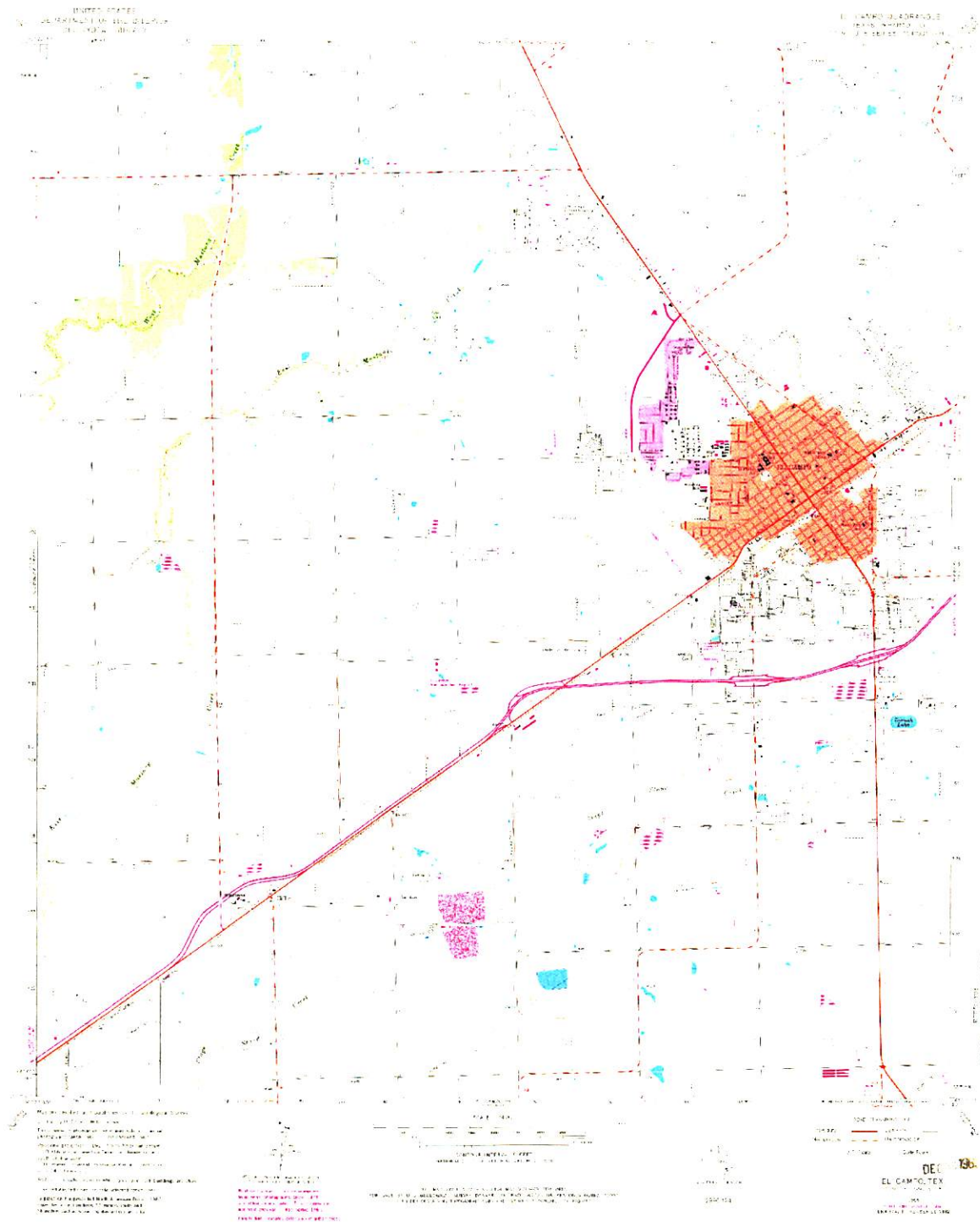**Figure B-20   Quadrangle 20: La Ward USGS Quadrangle (1952) at 5-ft contour interval.**

Figure B-21   Quadrangle 21: El Campo NE USGS Quadrangle (1965) at 5-ft contour intervals.

![INTERA]

Figure B-22   Quadrangle 22: El Campo SE USGS Quadrangle (1965) at 5-ft contour intervals.